AN ABSTRACT OF THE DISSERTATION OF

Danielle E. Marias for the degree of Doctor of Philosophy in Forest Ecosystems and Society presented on November 14, 2016.

Title: Approaches for Characterizing Plant Physiological Responses to Environmental Stress.

Abstract approved:

_____

Frederick C. Meinzer

It is uncertain how predicted changes in climate will impact vegetation responses and plant species' distributions because the physiological mechanisms underlying thresholds for damage are not well understood, and responses to stress vary by functional type and developmental stage. Thus, it is crucial to investigate physiological responses to heat and drought stress on multiple species, populations, and growth stages with diverse approaches. In this dissertation, I employ a suite of physiological and modeling methods to inform our knowledge of plant physiological responses to environmental stress in *Coffea arabica* saplings, *Pseudotsuga mensizeii* (PSME) and *Pinus ponderosa* (PIPO) seedlings, and old-growth PIPO.

In Chapter 2, I evaluate the effect of leaf age and methodology on the thermotolerance or heat tolerance of *C. arabica* leaf discs using chlorophyll fluorescence and electrolyte leakage methods. I found that mature leaves were more heat tolerant than expanding leaves, longer time between temperature exposure and measurement yielded more accurate thermotolerance assessments, and photochemistry was more heat-sensitive than cell membranes.

To complement the second chapter investigating heat stress responses on detached leaf discs, Chapter 3 examines the effect of leaf age and heat stress duration (45 min or 90 min) on whole-plant physiological responses and capacity to recover in *C. arabica* by monitoring chlorophyll fluorescence (F_V/F_M), gas exchange, and foliar non-structural carbohydrate (NSC) dynamics *in situ* in response to a simulated heat wave (49°C) in a growth chamber. I found that the 90 min treatment resulted in greater photosynthetic damage and slower recovery than the 45 min treatment, expanding leaves recovered more slowly than in mature leaves, and both heat treatments inhibited flowering. A leaf energy balance model demonstrated that heat stress would be exacerbated by drought-induced stomatal closure. Heat treatment duration significantly impacted NSC dynamics that were closely related to reproduction and repair.

Because seedling establishment governs species' distributions, and because seedlings are particularly threatened by high temperatures at the soil surface, in Chapter 4 I examined the thermotolerance and heat stress responses of PIPO and PSME seedling populations from contrasting climates. Unexpectedly, I found that PSME was more heat tolerant the PIPO. I also monitored physiological recovery after exposure to a simulated heat wave (45°C) by measuring photosynthesis, F_V/F_M, foliar NSC, and carbon stable isotope ratios (proxy for intrinsic water use efficiency, iWUE). Heat stress responses were consistent with phenotypic plasticity and reflected the conditions under which the plants were grown, while iWUE, a measure of potential drought resistance, was consistent with ecotypic differentiation and the climates from which the seedlings originated.

To investigate responses to environmental stress on larger temporal and spatial scales without the challenges of making repeated physiological measurements on old-growth trees, in Chapter 5 I used long-term trajectories of tree-ring growth and carbon and oxygen isotopes of tree-ring cellulose ($\delta^{13}C_{cell}$, and $\delta^{18}O_{cell}$) to successfully predict the stand characteristics of two sets (upland, riparian) of old-growth PIPO using the Physiological Principles in Predicting Growth (3-PG) model, the $\delta^{13}C_{cell}$ submodel, and a $\delta^{18}O_{cell}$ submodel added by me. The expanded model helped to explain physiological drivers underlying the different tree-ring growth, $\delta^{13}C_{cell}$, and $\delta^{18}O_{cell}$ trajectories measured at the upland and riparian sites. The combination of both $\delta^{18}O$ and $\delta^{13}C_{cell}$ submodels provided a useful and novel way to constrain 3-PG.

This dissertation demonstrates an innovative strategy of applying diverse approaches to understand the physiological mechanisms behind vegetation responses to environmental stress.

Approaches for Characterizing Plant Physiological Responses to Environmental Stress

by

Danielle E. Marias

A DISSERTATION

submitted to

Oregon State University

in partial fulfillment of
the requirements for the
degree of

Doctor of Philosophy

Presented November 14, 2016
Commencement June 2017

Doctor of Philosophy dissertation of Danielle E. Marias presented on November 14, 2016

APPROVED:

_____

Major Professor, representing Forest Ecosystems and Society

_____

Head of the Department of Forest Ecosystems and Society

_____

Dean of the Graduate School

I understand that my dissertation will become part of the permanent collection of Oregon State University libraries. My signature below authorizes release of my dissertation to any reader upon request.

_____

Danielle E. Marias, Author

ACKNOWLEDGEMENTS

I am incredibly grateful to so many people for their support and encouragement throughout my PhD journey. First and foremost, I thank Rick, my advisor for his guidance and support throughout my MS and PhD. His work ethic and outlook on life inspire me. I am thankful for my supportive committee members Renée Brooks, Chris Still, Dave Woodruff, and Ryan Contreras who helped me to become a better scientist. I am incredibly grateful to Ariel Muldoon for her invaluable help with statistics. I also thank the greater College of Forestry and Oregon State community, colleagues, and friends who let me discuss everything from tree responses to drought to the best skiing and mountain biking in Oregon. I am lucky to be a part of such a great community. Thank you to Vicki Tolar Burton who helped to transform my writing with her Writing 599 course in the winter of 2016. The strategies I learned were useful for writing this dissertation and will also benefit me for the rest of my life.

Friends and family near and far, thank you for keeping me smiling and supporting me through what seemed at times a never-ending journey. Mom and Dad, thank you for being my biggest fans. Don, thanks for your unending support, patience, and understanding through the ups and downs that enabled me to complete this crazy life chapter. Thanks Opie, our dog for motivating me to go outside and savor every moment.

CONTRIBUTION OF AUTHORS

In Chapters 2 and 3, Danielle E. Marias participated in the experimental design, data collection, data analyses, and writing of the manuscript. Frederick C. Meinzer participated in the experimental design, data analyses, and writing of the manuscript. Christopher Still participated in the experimental design and writing of the manuscript.

In Chapter 4, Danielle E. Marias participated in the experimental design, data collection, data analyses, and writing of the manuscript. Frederick C. Meinzer participated in the experimental design, data analyses, and writing of the manuscript. David R. Woodruff and Katherine A. McCulloh participated in the experimental design and writing of the manuscript.

In Chapter 5, Danielle E. Marias participated in the experimental design, modeling, data analyses, and writing of the manuscript. Christopher Still participated in the experimental design, modeling, data analyses, and writing of the manuscript. J. Renée Brooks participated in the data collection, data analyses, and writing of the manuscript. Youngil Kim participated in the modeling and writing of the manuscript. Frederick C. Meinzer participated in the experimental design, data analyses, and writing of the manuscript.

TABLE OF CONTENTS

TABLE OF CONTENTS (Continued)

Page

TABLE OF CONTENTS (Continued)

Page

LIST OF FIGURES

LIST OF FIGURES (Continued)

Figure Page

LIST OF FIGURES (Continued)

LIST OF TABLES

LIST OF APPENDIX FIGURES

LIST OF APPENDIX TABLES

Approaches for Characterizing Plant Physiological Responses to Environmental Stress

1. INTRODUCTION

Future climate change scenarios predict global mean surface temperature to increase, in addition to more frequent and intense high temperature and drought events (Intergovernmental Panel on Climate Change, 2014). Rising temperatures are expected to exceed current thermal limits for some plant species (O'Sullivan *et al.*, 2016). However, it is uncertain how these changes in climate will impact vegetation responses and plant species' distributions because the physiological mechanisms underlying thresholds for damage are not well understood. Predicting the consequences of these climatic changes on forest ecosystems is a major challenge for scientists (Bonan, 2008). Thus, it is crucial to investigate physiological responses to heat and drought stress to inform predictions of species distributions in response to future changes in climate.

Heat and drought stress impact plant function from the cellular to whole plant scale. Heat and drought induce cellular, enzymatic, and tissue damage, increase respiration, reduce photosynthesis, stomatal conductance, growth, and reproduction, and lead to shifts in carbohydrate dynamics, and mortality (Wahid *et al.*, 2007; Bita & Gerats, 2013; Teskey *et al.*, 2015). Therefore, monitoring these plant functions are crucial for understanding plant responses to environmental stress.

Plants exhibit many strategies to cope with increased temperature and drought which impact the ability of species to persist under different climate regimes (Walther, 2003). For example, plants mitigate heat stress through mechanisms that influence the ability to withstand and/or avoid heat stress. This includes producing heat shock proteins

that desaturate membrane lipids to maintain cell membrane integrity (Horváth *et al.*, 2012), regulating gas exchange and evaporative cooling to avoid high leaf temperatures (Tomlinson *et al.*, 2013), and shifting carbohydrate dynamics for repair, storage, metabolism, and growth (Hartmann & Trumbore, 2016). These mechanisms underlie the phenotypically plastic functional traits in response to heat and drought stress (Kerr *et al.*, 2015) that enable a species to adapt to changing climates. For example, heat tolerance measured with chlorophyll fluorescence is highly plastic (Knight & Ackerly, 2002), allowing species to acclimate to local environmental growing conditions. For species that span large geographic ranges and climates, this differential expression of physiological traits has led to the formation of distinct ecotypes within a species and thus may influence population-specific establishment within a species. Adapting to different climates via both phenotypic plasticity and ecotypic variation is advantageous because a species that can withstand a wide range of environmental conditions is likely to persist in the face of a changing climate. Therefore, examining how species and populations adjust the expression of functional traits to mitigate heat and drought stress improves our understanding of how changing climate will impact species distributions.

To further complicate predictions of responses to environmental stress, plants respond differently to heat and drought stress at different developmental stages. For example, plants employ drought resistance strategies to cope with low soil moisture but these strategies may change with age and size (Woodruff & Meinzer, 2011). Even within a growth stage, it is crucial to consider that physiological responses differ across leaf ages, especially in evergreen species that have relatively long leaf life spans (Yamada *et*

al., 1996). Therefore, efforts to examine multiple species, populations, and growth stages are crucial for addressing the challenge of predicting the consequences of future climate change on forest ecosystems.

This challenge lies not only in understanding physiological responses across species and developmental stages, but also incorporating physiological information into predictive models. Predictive vegetation models such as Dynamic Global Vegetation Models (DGVMs) are advantageous because they make predictions about larger spatial scales than physiological measurements that are often limited to the whole-plant scale. However, models like DGVMs are limited in accuracy because they lack the plant physiological data to parameterize them, and the species-specific physiological processes underlying the shifts in vegetation composition such as recruitment, competition, and tree mortality (Moorcroft 2006, Fisher *et al.* 2010). Therefore, efforts that use physiological measurements to parameterize models are critical for accurately predicting species' responses to environmental stress and shifts in climate.

In this dissertation, I employ a suite of physiological and modeling methods to inform our knowledge of plant physiological responses to environmental stress in multiple species at multiple growth stages including *Coffea arabica* saplings, *Pseudotsuga mensizeii* (PSME) and *Pinus ponderosa* (PIPO) seedlings, and old-growth PIPO. Monitoring a suite of physiological parameters with multiple approaches provides a more complete picture of how the physiological performance of *C. arabica*, PSME, and PIPO is impacted by heat and drought stress at different developmental stages.

Coffee is an important species around the globe. More than 120 million people in over 70 countries rely on the coffee economy for their livelihoods (The Climate Institute, 2016). *C. arabica* is native to Ethiopia but is now grown throughout the tropics. Its optimal mean annual temperature range is 18-24°C and it is highly sensitive to fluctuations in temperature (Camargo 2010). The tropics are extremely vulnerable to climate change because the tropics are expected to experience rising temperatures and an increased frequency of heat waves throughout the 21st century (Intergovernmental Panel on Climate Change, 2014). The amount of suitable habitat to grow *C. arabica* is predicted to significantly diminish due to changes in climate (Davis *et al.*, 2012). To inform these modeled predictions, in Chapters 2 and 3 of this dissertation, I investigate the effects of short duration heat stress on *C. arabica* saplings on detached leaf discs and whole plants. Although high temperature events are known to negatively affect photosynthetic performance, the legacy effects on the capacity to recover are largely unknown. Additionally, there is a poor understanding of the variation in heat tolerance among species (Curtis *et al.* 2014) as increasing temperatures are expected to exceed current thermal limits (O'Sullivan *et al.*, 2016).

The second chapter of this dissertation focuses on accurately quantifying high temperature tolerance or thermotolerance and thresholds to heat-induced damage on leaf discs of *C. arabica*. Different methods to measure thermotolerance, time between temperature exposure and measurement, and leaf age class complicate accurately assessing thermotolerance and thresholds to heat stress, a problem for a valuable species threatened by rising temperatures. To address this issue, I assess the thermotolerance of

C. arabica leaf discs using chlorophyll fluorescence and electrolyte leakage (Epron & Dreyer, 1992; Vilagrosa *et al.*, 2010). Although these two methods to evaluate thermotolerance are well-established, some studies suggest that these methods yield similar thermotolerance assessments (Larcher, 1995) while others find discrepancies between the methods, which may depend on species (Cunningham & Read, 2006; Xu *et al.*, 2014). However, these methods have yet to be compared in *C. arabica*. I also examine how leaf age, known to induce age-related leaf-level physiological shifts, influences assessments of thermotolerance using chlorophyll fluorescence. Finally, because the protocol for measuring thermotolerance curves with chlorophyll fluorescence is not standardized, I compare the chlorophyll fluorescence thermotolerance curves measured 15 minutes after temperature exposure with those measured 24 hours after temperature exposure. Accurately quantifying *C. arabica*'s thresholds for heat damage and understanding the differences in available techniques and methodology on leaves of different ages are crucial for predicting its fate under high temperature stress and directing management efforts.

To complement the second chapter investigating heat stress responses on detached leaf discs, the third chapter examines whole-plant responses of *C. arabica* to a simulated heat wave in a growth chamber using *in situ* measurements. Specifically, I investigate the effect of leaf age and heat stress duration on whole plant physiological responses and capacity to recover in *C. arabica* by monitoring chlorophyll fluorescence, gas exchange, and non-structural carbohydrate (NSC) dynamics *in situ*. Chlorophyll fluorescence paired with gas exchange provides multiple indicators of photosynthetic performance

throughout the treatment campaign. Leaf NSCs indicate how leaves of different ages and heat waves of different durations impact carbohydrate allocation to growth, metabolism, and storage. Shifts in NSC allocation among starch, sucrose, glucose, and fructose may indicate mechanisms to cope with and recover from heat stress (Liu & Huang, 2000). To our knowledge, no studies have examined the effects of heat stress on NSCs in *C. arabica*, an important component of understanding carbon use under changing climates. To place the results of the whole-plant growth chamber experiment in a natural field context, I complement the observed gas exchange measurements with a leaf energy balance model to estimate how a combined heat and drought scenario would impact leaf temperatures of *C. arabica*. The model enables us to incorporate our experimental observations on heat stress responses into predictions about how future climates with drought may exacerbate heat stress.

High temperatures are not only expected to increase in the tropics, but in temperate regions as well. Tree mortality has been documented worldwide and linked to increased severity and intensity of drought and high temperature stress (Allen *et al.*, 2010). Species distributions are shifting to higher elevations and latitudes at faster rates than previously reported with the greatest species range shifts found in studies showing highest levels of warming (Chen *et al.*, 2011). Given the predicted increase in global surface temperature with an increase in duration and frequency of heat waves (Intergovernmental Panel on Climate Change, 2014), and the close relationship between species' distribution patterns and climate factors (Stephenson, 1990), temperate species will be greatly impacted by warming temperatures (Walther, 2003). Tree species'

distributions can shift through shrinking the distribution via mortality and expanding the distribution via seedling establishment (Johnson *et al.*, 2011). The seedling is the developmental stage that is most vulnerable to mortality because seedlings are especially susceptible to abiotic stressors, and are particularly threatened by high temperatures at the soil surface due to the near-surface boundary layer that reduces heat loss compared to taller plants (Johnson *et al.*, 2011). In exposed microsites, this can result in high midday air temperatures at the ground surface commonly between 40°C and 50°C despite air temperature being only 25°C (Alexander, 1987; Kolb & Robberecht, 1996). Higher temperature results in greater VPD and thus transpiration and water use, causing drought stress, reduced water use efficiency (Way *et al.*, 2013a, 2013b), and fewer days to mortality (Will *et al.*, 2013). Therefore, understanding the physiological mechanisms that impact seedling establishment and seedling responses to a warmer climate is essential for more accurately predicting species distribution patterns in future warmer and drier climates (Walther, 2003; Aitken *et al.*, 2008).

Both PIPO and PSME are ecologically and economically valuable species in the Pacific Northwest and both species have large geographic ranges. It is therefore of great interest to investigate how these species will respond to heat stress. PIPO is believed to be more tolerant of heat, drought, frost, and fire than PSME. Populations within both species have been shown to display phenotypic plasticity and adapt to the current growing conditions (Koehn *et al.*, 2010; Kolb *et al.*, 2016). Both species have also demonstrated evidence for within-species ecotypes where populations from climates with contrasting temperature and precipitation regimes exhibit physiological traits reflecting

the climate of origin even when grown in the same environment (Sorensen, 1983; Perić *et al.*, 2009; Du *et al.*, 2014; Kerr *et al.*, 2015). Both phenotypic plasticity and ecotypic variation enable a species to persist under changing environmental conditions. Investigating how these drive functional trait expression is critical for understanding how these species may survive future climates. In the fourth chapter of this dissertation, I investigate the heat tolerance and effects of a simulated heat wave on the physiological recovery of two populations each of first year germinant (~7 months old) *Pseudotsuga mensizeii* (PSME) and *Pinus ponderosa* (PIPO) seedlings from contrasting climates using gas exchange, chlorophyll fluorescence, NSCs, and carbon isotope ratios. Similar to Chapters 2 and 3, chlorophyll fluorescence, gas exchange and NSCs inform the effect of heat stress on photosynthetic performance and carbon allocation. The carbon isotope ratio of leaves is a proxy for intrinsic water use efficiency and drought resistance (Jones, 2009). The comparisons between and within species shed light on species' responses to predicted increases in temperature. Examining how phenotypic plasticity and ecotypic variation drive the expression of functional traits underlying heat tolerance and drought resistance improves our understanding of how species will respond to future changes in temperature and water availability.

As trees increase in age and size, making physiological measurements, determining thresholds for stress damage, and conducting experimental manipulations become increasingly difficult. However, collecting tree cores enables us to examine the physiology of old-growth trees that have inaccessible canopies. This is because as trees mature and form growth rings, their physiological responses to environmental conditions

are recorded in each annual growth ring or tree-rings. Tree-rings are formed from C and O from the atmosphere and soil water so tree-ring widths and tree-ring C and O stable isotopes ($\delta^{13}C$ and $\delta^{18}O$) are indicators of environmental conditions and the nature of the C and O incorporated into each tree-ring each year. Therefore, tree-rings enable us to reconstruct past environmental conditions such as relative humidity and soil moisture as well as tree physiology including responses to pests and leaf-level gas exchange (McCarroll & Loader, 2004; Williams *et al.*, 2010; Brooks & Mitchell, 2011; Gessler *et al.*, 2014; Marias *et al.*, 2014; Saffell *et al.*, 2014; Voelker *et al.*, 2014; Hartl-Meier *et al.*, 2015).

To address the challenges of conducting experiments on old-growth trees and accurately estimating responses to environmental stress beyond the whole tree scale, process-based models are useful. Predictive physiological process-based vegetation models have been parameterized with tree-ring growth data to more accurately predict tree growth and productivity on larger spatial and temporal scales. The Physiological Principles in Predicting Growth or 3-PG model (Landsberg & Waring, 1997) is one such stand growth model that is based on physiological processes that calculates total carbon fixed from photosynthetically active radiation absorbed by the forest canopy and incorporates site-specific climate and stand characteristics. Because 3-PG is based on physiological principles governing C allocation, water use, and productivity, the addition of a $\delta^{13}C$ submodel improved the 3-PG model (Wei *et al.*, 2014). This suggests that the addition of tree-ring $\delta^{18}O$ will also improve 3-PG because the combination of both $\delta^{13}C$ and $\delta^{18}O$ improves estimates of leaf gas exchange responses (Scheidegger *et al.*). In

Chapter 5 of this dissertation, I incorporate a $\delta^{18}O$ submodel into 3-PG with the $\delta^{13}C$ submodel (Wei *et al.*, 2014) using tree-ring growth, $\delta^{13}C$, and $\delta^{18}O$ of old-growth (~260 yo) *Pinus ponderosa* collected from a heavily-instrumented and well-studied site by the head of the Metolius river in the Cascades of central Oregon (Law *et al.*, 2000). The addition of the tree-ring $\delta^{18}O$ submodel is novel and is expected to enhance 3-PG because the combination of both $\delta^{13}C$ and $\delta^{18}O$ provides more insight into gas exchange and water use processes. To test the expanded model, I use it to examine the physiological drivers underlying differences in observed growth between a set of upland and riparian trees. Improving process-based models such as 3-PG informs our understanding of how future changes in climate may impact the physiological responses at the stand level.

This dissertation is unique because it applies a synergy of approaches to understand physiological responses to environmental stress. The analysis of different functional types (angiosperm, conifer), developmental stage (seedling, sapling, old growth), spatial scale (cellular, leaf, whole plant, stand), temporal scale (tree-rings for the past, physiological measurements for the present, modeling for the future), and combination of physiological and modeling methods demonstrates an innovative strategy to address one of the most pressing environmental questions of this century: how will plants respond to future climate change?

1.1 References

Aitken SN, Yeaman S, Holliday JA, Wang T, Curtis-McLane S (2008) Adaptation, migration or extirpation: climate change outcomes for tree populations. *Evolutionary Applications*, **1**, 95–111.

Alexander RR (1987) *Ecology, Silviculture, and Management of the Engelmann Spruce--Subalpine Fir Type in the Central and Southern Rocky Mountains*. U.S. Dept. of Agriculture, Forest Service, 144 pp.

Allen CD, Macalady AK, Chenchouni H *et al.* (2010) A global overview of drought and heat-induced tree mortality reveals emerging climate change risks for forests. *Forest ecology and management*, **259**, 660–684.

Bita CE, Gerats T (2013) Plant tolerance to high temperature in a changing environment: scientific fundamentals and production of heat stress-tolerant crops. *Frontiers in Plant Science*, **4**.

Bonan GB (2008) *Ecological Climatology: Concepts and Applications*. Cambridge University Press, 1 p.

Brooks JR, Mitchell AK (2011) Interpreting tree responses to thinning and fertilization using tree-ring stable isotopes. *New Phytologist*, **190**, 770–782.

Chen I-C, Hill JK, Ohlemüller R, Roy DB, Thomas CD (2011) Rapid Range Shifts of Species Associated with High Levels of Climate Warming. *Science*, **333**, 1024–1026.

The Climate Institute (2016) A Brewing Storm: the climate change risks to coffee.

Cunningham SC, Read J (2006) Foliar temperature tolerance of temperate and tropical evergreen rain forest trees of Australia. *Tree Physiology*, **26**, 1435–1443.

Davis AP, Gole TW, Baena S, Moat J (2012) The impact of climate change on indigenous arabica coffee (Coffea arabica): predicting future trends and identifying priorities. *PLoS One*, **7**, e47981.

Du B, Jansen K, Junker LV *et al.* (2014) Elevated temperature differently affects foliar nitrogen partitioning in seedlings of diverse Douglas fir provenances. *Tree Physiology*, **34**, 1090–1101.

Epron D, Dreyer E (1992) Effects of severe dehydration on leaf photosynthesis in Quercus petraea (Matt.) Liebl.: photosystem II efficiency, photochemical and nonphotochemical fluorescence quenching and electrolyte leakage. *Tree Physiology*, **10**, 273–284.

Gessler A, Ferrio JP, Hommel R, Treydte K, Werner RA, Monson RK (2014) Stable isotopes in tree rings: towards a mechanistic understanding of isotope fractionation and mixing processes from the leaves to the wood. *Tree Physiology*, tpu040.

Hartl-Meier C, Zang C, Büntgen U *et al.* (2015) Uniform climate sensitivity in tree-ring stable isotopes across species and sites in a mid-latitude temperate forest. *Tree Physiology*, **35**, 4–15.

Hartmann H, Trumbore S (2016) Understanding the roles of nonstructural carbohydrates in forest trees – from what we can measure to what we want to know. *New Phytologist*, **211**, 386–403.

Horváth I, Glatz A, Nakamoto H *et al.* (2012) Heat shock response in photosynthetic organisms: Membrane and lipid connections. *Progress in Lipid Research*, **51**, 208–220.

Intergovernmental Panel on Climate Change (2014) IPCC Fifth Assessment Synthesis Report. *IPCC 5th Assessment Synthesis Report*.

Johnson DM, McCulloh KA, Reinhardt K (2011) The Earliest Stages of Tree Growth: Development, Physiology and Impacts of Microclimate. In: *Size- and Age-Related Changes in Tree Structure and Function* (eds Meinzer FC, Lachenbruch B, Dawson TE), pp. 65–87. Springer Netherlands.

Jones HG (2009) What is water use efficiency? In: Bacon M (ed) Water use efficiency in plant biology. Blackwell Publishing, Oxford, UK, pp. 27-41.

Kerr KL, Meinzer FC, McCulloh KA, Woodruff DR, Marias DE (2015) Expression of functional traits during seedling establishment in two populations of Pinus ponderosa from contrasting climates. *Tree Physiology*, **35**, 535–548.

Knight CA, Ackerly DD (2002) An ecological and evolutionary analysis of photosynthetic thermotolerance using the temperature-dependent increase in fluorescence. *Oecologia*, **130**, 505–514.

Koehn AC, McDonald GI, Turner DL, Adams DL; (2010) *Dynamic phenotypic plasticity in photosynthesis and biomass patterns in Douglas-fir seedlings*. 14 pp.

Kolb PF, Robberecht R (1996) High temperature and drought stress effects on survival of Pinus ponderosa seedlings. *Tree Physiology*, **16**, 665–672.

Kolb TE, Grady KC, McEttrick MP, Herrero A (2016) Local-Scale Drought Adaptation of Ponderosa Pine Seedlings at Habitat Ecotones. *Forest Science*.

Landsberg JJ, Waring RH (1997) A generalised model of forest productivity using simplified concepts of radiation-use efficiency, carbon balance and partitioning. *Forest Ecology and Management*, **95**, 209–228.

Larcher W (1995) Photosynthesis as a Tool for Indicating Temperature Stress Events. In: *Ecophysiology of Photosynthesis* (eds Schulze PDE-D, Caldwell PDMM), pp. 261–277. Springer Berlin Heidelberg.

Law BE, Waring . R. H., Anthoni PM, Aber JD (2000) Measurements of gross and net ecosystem productivity and water vapour exchange of a Pinus ponderosa ecosystem, and an evaluation of two generalized models. *Global Change Biology*, **6**, 155–168.

Liu X, Huang B (2000) Carbohydrate Accumulation in Relation to Heat Stress Tolerance in Two Creeping Bentgrass Cultivars. *Journal of the American Society for Horticultural Science*, **125**, 442–447.

Marias DE, Meinzer FC, Woodruff DR *et al.* (2014) Impacts of dwarf mistletoe on the physiology of host Tsuga heterophylla trees as recorded in tree-ring C and O stable isotopes. *Tree Physiology*, **34**, 595–607.

McCarroll D, Loader NJ (2004) Stable isotopes in tree rings. *Quaternary Science Reviews*, **23**, 771–801.

O'Sullivan OS, Heskel MA, Reich PB *et al.* (2016) Thermal limits of leaf metabolism across biomes. *Global Change Biology*, n/a-n/a.

Perić S, JAZBEC A, Tijardović M, Margaletić J, Ivanković M, Pilaš I, Medak J (2009) Provenance studies of Douglas fir in the locality of» Kontija «(Istria). *Periodicum biologorum*, **111**, 487–493.

Saffell BJ, Meinzer FC, Voelker SL, Shaw DC, Brooks JR, Lachenbruch B, Mckay J (2014) Tree-ring stable isotopes record the impact of a foliar fungal pathogen on CO2 assimilation and growth in Douglas-fir. *Plant, Cell & Environment*, **37**, 1536–1547.

Scheidegger Y, Saurer M, Bahn M, Siegwolf R Linking stable oxygen and carbon isotopes with stomatal conductance and photosynthetic capacity: a conceptual model. *Oecologia*, **125**, 350–357.

Sorensen FC (1983) Geographic Variation in Seedling Douglas-Fir (Pseudotsuga Menziesii) from the Western Siskiyou Mountains of Oregon. *Ecology*, **64**, 696–702.

Stephenson NL (1990) Climatic control of vegetation distribution: the role of the water balance. *American Naturalist*, 649–670.

Teskey R, Wertin T, Bauweraerts I, Ameye M, McGuire MA, Steppe K (2015) Responses of tree species to heat waves and extreme heat events. *Plant, cell & environment*, **38**, 1699–1712.

Tomlinson KW, Poorter L, Sterck FJ, Borghetti F, Ward D, de Bie S, van Langevelde F (2013) Leaf adaptations of evergreen and deciduous trees of semi-arid and humid savannas on three continents. *Journal of Ecology*, **101**, 430–440.

Vilagrosa A, Morales F, Abadía A, Bellot J, Cochard H, Gil-Pelegrin E (2010) Are symplast tolerance to intense drought conditions and xylem vulnerability to cavitation coordinated? An integrated analysis of photosynthetic, hydraulic and leaf level processes in two Mediterranean drought-resistant species. *Environmental and Experimental Botany*, **69**, 233–242.

Voelker SL, Brooks JR, Meinzer FC *et al.* (2014) Reconstructing relative humidity from plant δ18O and δD as deuterium deviations from the global meteoric water line. *Ecological Applications*, **24**, 960–975.

Wahid A, Gelani S, Ashraf M, Foolad MR (2007) Heat tolerance in plants: an overview. *Environmental and experimental botany*, **61**, 199–223.

Walther G-R (2003) Plants in a warmer world. *Perspectives in Plant Ecology, Evolution and Systematics*, **6**, 169–185.

Way DA, Domec J-C, Jackson RB (2013a) Elevated growth temperatures alter hydraulic characteristics in trembling aspen (Populus tremuloides) seedlings: implications for tree drought tolerance. *Plant, Cell & Environment*, **36**, 103–115.

Way DA, Crawley C, Sage RF (2013b) A hot and dry future: warming effects on boreal tree drought tolerance. *Tree Physiology*, **33**, 1003–1005.

Wei L, Marshall JD, Link TE *et al.* (2014) Constraining 3-PG with a new δ13C submodel: a test using the δ13C of tree rings. *Plant, Cell & Environment*, **37**, 82–100.

Will RE, Wilson SM, Zou CB, Hennessey TC (2013) Increased vapor pressure deficit due to higher temperature leads to greater transpiration and faster mortality during drought for tree seedlings common to the forest-grassland ecotone. *The New Phytologist*, **200**, 366–374.

Williams AP, Michaelsen J, Leavitt SW, Still CJ (2010) Using tree rings to predict the response of tree growth to climate change in the continental United States during the twenty-first century. *Earth Interactions*, **14**, 1–20.

Woodruff DR, Meinzer FC (2011) Water stress, shoot growth and storage of non-structural carbohydrates along a tree height gradient in a tall conifer. *Plant, cell & environment*, **34**, 1920–1930.

Xu H, Liu G, Liu G, Yan B, Duan W, Wang L, Li S (2014) Comparison of investigation methods of heat injury in grapevine (Vitis) and assessment to heat tolerance in different cultivars and species. *BMC plant biology*, **14**, 1.

Yamada M, Hidaka T, Fukamachi H (1996) Heat tolerance in leaves of tropical fruit crops as measured by chlorophyll fluorescence. *Scientia Horticulturae*, **67**, 39–48.

2. LEAF AGE AND METHODOLOGY IMPACT ASSESSMENTS OF THERMOTOLERANCE OF *COFFEA ARABICA*

Danielle E. Marias, Frederick C. Meinzer, Christopher Still

2.1 Abstract

Given future climate predictions of increased heatwaves in the tropics, suitable habitat to grow ecologically, economically, and socially valuable *Coffea arabica* L. is threatened. Accurate assessments of high temperature tolerance or thermotolerance are critical for understanding *C. arabica* responses to increased temperature. Thermotolerance curves of *C. arabica* leaf discs were constructed by measuring chlorophyll fluorescence (ratio of variable to maximum fluorescence, F_V/F_M; minimum fluorescence, F_O) across three leaf age classes and two recovery times (15 min, 24 h) after 15 min exposure to temperatures from 25-58°C. Thermotolerance measured with electrolyte leakage after 20 min at 25-65°C was compared with F_V/F_M thermotolerance curves. The temperature corresponding to 50% damage (T_{50}) was 49.0°C and 58.6°C for the chlorophyll fluorescence and electrolyte leakage methods, respectively. The critical temperature at which the F_O rise began on F_O-temperature curves (T_{crit}) was 46.0°C. We found that the 24 h recovery time yielded more accurate estimates of T_{50}, and that thermotolerance based on T_{crit} increased with leaf age. Differences between the fluorescence and electrolyte leakage methods showed that photosystem II processes were more sensitive to temperatures above 40°C than cell membrane stability.

2.2 Introduction

The shade-adapted species *C. arabica* originated from Ethiopia and is now grown in 80 countries on four continents in the inter-tropical zone between 20-25°N in Hawaii and 24°S in Brazil (DaMatta & Ramalho, 2006). Mature *C. arabica*'s optimal mean

annual temperature range is 18-24º (Camargo, 1985; Teketay, 1999). However, *C. arabica* grows best in tropical regions that are ecologically sensitive to climate variability (Seddon *et al.*, 2016) and prone to seasonal drought (DaMatta & Ramalho, 2006). *C. arabica* is also often grown under full sunlight where leaf temperatures are often 15-20°C greater than air temperature (Butler, 1977; Alvim & Kozlowski, 2013), especially in outer canopy leaves (DaMatta, 2004). Furthermore, the frequency and intensity of heat waves in the tropics are expected to increase through the 21st century (Cramer *et al.*, 2001; Corlett, 2011; Diffenbaugh & Scherer, 2011). Given these potential threats to *C. arabica* performance, production (Craparo *et al.*, 2015), and suitable habitat (Davis *et al.*, 2012), as well as the limited existing data on thermotolerances of tropical species (Corlett, 2011), it is vital to accurately quantify the thermotolerance of *C. arabica* to help predict and improve our understanding of its physiological responses to increasing temperatures.

High temperature stress impacts many components of plant function including growth, phenology, membrane integrity and fluidity, photosynthesis, respiration, and enzyme activity, all of which may differ in temperature responses (Bita & Gerats, 2013; Teskey *et al.*, 2015). To assess plant responses to increasing temperature, thermotolerance curves are constructed by measuring plant functions following exposure to a series of increasing temperatures to reveal thresholds and parameters that are used to quantify and compare thermotolerance (Larcher, 1995). Plant functions often used to construct thermotolerance curves include photosynthesis (Larcher, 1995) and photorespiration (O'Sullivan *et al.*, 2013) while other studies use proxies for plant

functions such as visible foliar damage for tissue death, permanent damage, or mortality (Bilger *et al.*, 1984; Cunningham & Read, 2006), electrolyte leakage for cell membrane stability (Whitlow *et al.*, 1992; Ismail & Hall, 1999; Bajji *et al.*, 2002), and chlorophyll fluorescence for photochemistry, electron transport, and photosynthetic performance (Schreiber & Berry, 1977; Loik & Harte, 1996; Maxwell & Johnson, 2000; Knight & Ackerly, 2002; Krause *et al.*, 2010). Measurements of these plant function proxies or indicators are often simplified by conducting them on leaf discs rather than intact leaves attached to a plant. Although diverse plant functions have been used to assess thermotolerance, each plant function or proxy may differ in its response to increased temperature, influencing assessments of overall thermotolerance.

Electrolyte leakage, an indicator of cell membrane integrity, is widely used to assess tolerance of heat and other stresses because it is inexpensive, non-destructive of whole plants, and suitable for analyzing a large number of samples (Flint *et al.*, 1967; Whitlow *et al.*, 1992; Bajji *et al.*, 2002). An increase in ion leakage with increasing stress is used as an indicator of irreversible or permanent tissue damage, an approach similar to that of assessing visible leaf damage (Bilger *et al.*, 1984; Cunningham & Read, 2006). In *C. arabica*, electrolyte leakage has been used to evaluate low temperature tolerance (Campos *et al.*, 2003) and leakage after exposure to 40°C, 50°C, and 57°C (Gascó *et al.*, 2004), but not across a wide range of small temperature increments to generate thermotolerance parameters for quantitative comparisons.

Chlorophyll fluorescence has also been widely used to evaluate thermotolerance because it is rapid, non-invasive, and provides information about photosynthetic

functions including electron transport, photosystem I (PSI) and photosystem II (PSII) activity, and thus photosynthetic performance (Krause & Weis, 1984; Bilger *et al.*, 1987; Schreiber *et al.*, 1995; Maxwell & Johnson, 2000; Baker & Rosenqvist, 2004; Misra *et al.*, 2012). It is also closely correlated with thermotolerance evaluated with visible leaf damage assessments (Lindgren & Hällgren, 1993; Larcher, 1995; Binder & Fielder, 1996) and used to assess permanent tissue damage (Krause *et al.*, 2010). Heat stress can reduce photosynthetic performance by destroying PSII reaction centers, disrupting electron transport, increasing membrane fluidity, causing dissociation of primary electron acceptors Q_A and Q_B, and separating the light-harvesting complex from PSII reaction centers (Maxwell & Johnson, 2000; Zhang *et al.*, 2012). These events can be detected by chlorophyll fluorescence emission. Although chlorophyll fluorescence has been applied to *C. arabica* to investigate the effect of nitrogen nutrition on high light acclimation (Ramalho *et al.*, 2000), seasonal photoprotective mechanisms in a field experiment (Chaves *et al.*, 2007), low temperature responses (Ramalho *et al.*, 2003; Partelli *et al.*, 2009; Batista-Santos *et al.*, 2011), and the combined influence of elevated CO_2 and temperature (Rodrigues *et al.*, 2016), chlorophyll fluorescence has not been used to measure leaf age-related differences in high temperature tolerance nor compared with other methods to measure thermotolerance.

Given the relatively long life span of up to 510 days reported for *C. arabica*'s evergreen leaves (Vasudeva & Gopal, 1975), and its specific temperature requirements at different ontogenetic stages such as germination, seedling establishment, branch formation, and floral bud and fruit initiation (DaMatta & Ramalho, 2006),

thermotolerance likely changes with leaf age in *C. arabica.* Consistent with this expectation, based on chlorophyll fluorescence, (Yamada *et al.*, 1996) found that 3.5-month-old leaves of 23 tropical fruit-bearing species were more heat tolerant than 2.5-month-old leaves, suggesting that leaf ageing and life span are related to photosynthetic thermotolerance (Zhang *et al.*, 2012). In addition to leaf age, another variable that influences assessments of thermotolerance is the measurement protocol used, particularly the time between temperature exposure and when measurements are made. Krause *et al.* (2010) investigated recovery time after temperature exposure in tropical, mature *Ficus insipida* trees and found that a 24 h recovery time yielded more accurate measures of thermotolerance using chlorophyll fluorescence than a 15 min recovery time. It is unknown how leaf age, the type of method used, and measurement protocol influence assessments of thermotolerance parameters in *C. arabica.* To fill this gap, we quantified thermotolerance curves of *C. arabica* across a wide range of temperatures in three leaf age classes, using chlorophyll fluorescence and electrolyte leakage methods, and two recovery times after temperature exposure. We addressed the following hypotheses: 1) older leaves are more heat tolerant than younger leaves, 2) a 24 h recovery time results in more accurate thermotolerance assessments than a 15 min recovery time, and 3) photochemistry assessed from chlorophyll fluorescence will be more sensitive to increasing temperature than membrane damage assessed from electrolyte leakage.

2.3 Materials & Methods

Plant material

C. arabica (Eritrean Mokka) plants of about ~6-9 months in age, obtained from the Hawaii Agriculture Research Center in January 2014, were grown in a peat-perlite-pumice growing mix (Sunshine LA4 P) in 9.63 L pots in a greenhouse in Corvallis, Oregon (44.5667°N, 123.2833°W). Supplemental metal halide and high pressure sodium lighting (400 watts) was used to maintain a 12-hour photoperiod during the fall and winter months. Measurements were made in May 2014 when average daytime temperature was 24.0°C and average nighttime temperature was 19.7°C, relative humidity ranged from 42-65%, and average daily maximum photosynthetically active radiation (PAR) was 424 µmol m^{-2} s^{-1}; and in May 2015 when average daytime temperature was 22.9°C and average nighttime temperature was 19.5°C, relative humidity ranged from 53-67%, and average daily maximum PAR was 623 µmol m^{-2} s^{-1}. Plants were watered to field capacity three times per week and fertilized once every two weeks (Miracle-Gro All-Purpose Liquid Plant Food, 12%N, 4%P_2O_5, 8%K_2O all season formula). *C. arabica* is a tropical evergreen species that continually produces new flushes of leaves year-round. Leaf age class (expanding, fully expanded, mature) was determined by visually dividing a plagiotropic branch into thirds where leaf age sequence increased from the outermost leaves to the base of the branch (e.g. (Wright *et al.*, 2006). Leaves in the outer third were the youngest and still expanding (expanding), leaves in the middle third were expanded (fully expanded), and leaves in the inner third were the oldest, fully expanded, and mature (mature) (similar to Wright *et al.* 2006). All leaf age classes showed net CO_2 uptake (data not shown).

Chlorophyll fluorescence: Theory

Common chlorophyll fluorescence parameters used to characterize responses to increasing temperature are minimum fluorescence (F_O), and the ratio of variable fluorescence to maximum fluorescence (F_V/F_M). Chlorophyll fluorescence symbols used are in the convention of Maxwell and Johnson (2000). F_O measures the minimum fluorescence emitted by dark-adapted leaves, where F_O is lowest when all PSII reaction centers are open to accept electrons (all primary acceptors are oxidized), indicating maximum photosynthetic efficiency. F_O versus temperature (F_O-T) curves are commonly used to compare photosynthetic thermotolerance across species, phenology, and climates (Schreiber & Berry, 1977; Smillie & Nott, 1979; Valladares & Pearcy, 1997; Knight & Ackerly, 2002; Weng & Lai, 2005; Zhang *et al.*, 2012). As temperature increases, F_O increases, indicating a greater proportion of closed PSII reaction centers and thus lower photosynthetic efficiency. The temperature at which the temperature-induced Fo rise begins (T_{crit}) on the F_O-T curve correlates well with the relative heat sensitivity of photosynthesis, the temperature at which net CO_2 assimilation declines (Downton *et al.*, 1984), irreversible decreased quantum yield of CO_2 fixation (Schreiber & Berry, 1977), irreversible damage to leaf tissue (Bilger *et al.*, 1984), and thylakoid membrane fluidity (Tovuu *et al.*, 2013).

F_V/F_M measures the maximum quantum efficiency of PSII photochemistry (Genty *et al.*, 1989) and is calculated as:

$$\frac{F_V}{F_M} = \frac{F_M - F_O}{F_M} = 1 - \frac{F_O}{F_M} \quad (1)$$

Therefore, F_V/F_M decreases if F_O increases and/or F_V decreases (caused by an increase in F_O and/or decrease in F_M), both of which indicate stress-induced changes to photochemistry (Schreiber & Berry, 1977; Ilík *et al.*, 2003). While an increase in F_O indicates PSII inactivation or damage, a decrease in F_V (caused by an increase in F_O and/or decrease in F_M) indicates damage to the oxygen evolving complex and water splitting system that disrupts electron donation to PSII reaction centers (Yamashita & Butler, 1968; Weis & Berry, 1987; Bolhar-Nordenkampf *et al.*, 1989; Havaux, 1993; Yamada *et al.*, 1996). F_V/F_M is also affected by the efficiency of non-photochemical quenching that is linearly related to nonradiative (heat) dissipation of excitation energy. A decline in F_V/F_M caused by an increase in F_O may also indicate photodamage, while a decline in F_V/F_M caused by a decrease in F_M is often related to an increase in zeaxanthin, heat dissipation, and photoinhibition, a thylakoid process that protects against destructive dissipation of excess excitation energy (Demmig *et al.*, 1987; Krause, 1988; Maxwell & Johnson, 2000). Thermotolerance curves assessed using F_V/F_M have been widely used to evaluate thermotolerance with F_V/F_M typically declining around 40ºC (Krause *et al.*, 2010; Teskey *et al.*, 2015).

Chlorophyll fluorescence: Measurements

In May 2014, one 2.54 cm^2 leaf disc was collected with a 1.8-cm-diameter borer from each of three randomly selected leaves within each age class from each of six plants prior to dawn to ensure sufficient dark-adaptation time (Willits & Peet, 2001). Dark-adapted leaf discs were placed in closed plastic bags and immersed in a preheated water

bath (General Purpose Aquabath Model 2343, Thermo Fisher Scientific, Marietta, OH, USA) at each temperature (25˚C, 28˚C, 31˚C, 34˚C, 37˚C, 40˚C, 43˚C, 46˚C, 49˚C, 52˚C, 55˚C, 58˚C) for 15 min at each temperature. Different sets of leaf discs were exposed to each temperature. A fine-wire thermocouple in each plastic bag recorded that discs reached each desired temperature within 1 min. Chlorophyll fluorescence was measured at room temperature with a portable pulse-amplitude modulated chlorophyll fluorometer (Mini-PAM, Heinz Walz GmbH, Germany) 15 min and 24 h after exposure to each temperature. Untreated leaf discs without heating served as controls. During recovery times, leaf discs were stored in the dark on petri dishes with moist filter paper.

To measure F_O, a measuring light (red light-emitting diode, 650 nm, 0.15 µmol m^{-2} s^{-1} PAR) with a pulse-width of 3 µs was turned on at a pulse modulation frequency of 0.6 kHz to induce the minimal level of fluorescence (F_O). We did not observe irregular F_O increases at relatively low heating temperatures due to anaerobiosis so did not wrap leaf discs in Miracloth as in Krause *et al*. (2010). The Schreiber and Berry (1977) method uses continuous heating as F_O is measured. A drawback of this method is the continuous additional heat exposure time so F_O was measured on leaf discs at each temperature to isolate the effect of a single temperature without the confounding effects of previous temperature exposure (e.g. Cunningham and Read 2006; Krause *et al*. 2010). This is especially important because thermal acclimation to high temperatures and subsequent changes to thermotolerance can occur on relatively short timescales (Yordanov *et al.*, 1995). F_V/F_M was then determined by applying a 0.8 s saturating pulse of white light, which transiently closed all PSII reaction centers (and prevented any photochemical

processes from occurring), minimized heat dissipation (since leaves were dark-adapted), and induced maximum fluorescence (F_M) and variable fluorescence (F_V). F_V/F_M was calculated as in Equation 1 (Genty *et al.*, 1989). F_V/F_M is a reliable measure of the potential quantum yield of PSII and is lowered by factors that cause inhibition of PSII reaction centers and increase non-radiative (heat) dissipation.

Electrolyte leakage

In May 2015, one mature fully expanded leaf (mature age class) was collected before dawn from each of five plants. Two discs from each leaf were placed in 6 mL of deionized H_2O in 15 mL polycarbonate tubes. Samples were infiltrated under vacuum for 15 min. Tubes were heated for 20 min in a preheated water bath at each desired temperature (30˚C, 35˚C, 40˚C, 45˚C, 50˚C, 55˚C, 60˚C, 65˚C). Different sets of leaf discs were exposed to each temperature. Tubes were shaken for 1.5 h and the conductivity of the water in each tube was measured with a conductivity meter (Product catalog number 89094-958, VWR International, Radnor, PA, USA). Tubes were then heated for 20 min in a 100˚C water bath and shaken again for 1.5 h. The final conductivity of the solution represented electrolyte leakage of completely killed leaf tissue. Percent electrolyte leakage or percent damage was calculated as:

$$\%\ electrolyte\ leakage = \frac{Conductivity\ after\ exposure\ to\ temperature\ (°C)}{Conductivity\ after\ exposure\ to\ 100°C}\ x\ 100 \qquad (2)$$

To determine whether the one-year difference in dates on which each method was used to measure thermotolerance curves affected results (F_V/F_M and electrolyte leakage methods were conducted on different plants one year apart, May 2014 and May 2015,

respectively), three mature fully expanded leaves of the mature age class from each of five plants were collected at pre-dawn on the same day in December 2015. Chlorophyll fluorescence (one disc per leaf) and electrolyte leakage (two discs per leaf) methods were used to measure F_V/F_M and percent damage after discs were exposed to 50ºC, the temperature at which differences between methods were greatest.

Statistical Analysis

To directly compare the thermotolerance curves measured with F_V/F_M and electrolyte leakage, F_V/F_M values were normalized and converted to a percent scale so that the F_V/F_M value of the untreated (control) group was considered 100% (no damage). Percent electrolyte leakage values were normalized so that percent electrolyte leakage values at the minimum percent electrolyte leakage (at 40˚C for all replicates) was considered 0% (no damage). For ease of comparison with the F_V/F_M thermotolerance curves, the percent electrolyte leakage axis (y-axis) is inverted for all figures. Thermotolerance curves assessed with F_V/F_M and electrolyte leakage were determined from third order sigmoidal functions fitted to the data:

$$f = a/(1 + exp(-(x - x_0)/b) \quad (3)$$

where f is percent of untreated (control) F_V/F_M or percent electrolyte leakage, x is the treatment temperature, and a, x_0, and b are fitting parameters. From this equation, T_{50} of F_V/F_M is the temperature that caused a 50% reduction in untreated (control) F_V/Fm. T_{50} of electrolyte leakage is the temperature that caused a 50% increase in minimum percent electrolyte leakage or percent damage.

Due to the differences in temperatures at which F_V/F_M and electrolyte leakage were measured (every 3˚C and 5˚C, respectively), Equation 3 was rearranged and used to estimate F_V/F_M percent values at the same temperatures as those used to construct the electrolyte leakage curves (every 5˚C vs every 3˚C). This allowed percent values derived from each method to be directly compared at each temperature.

T_{crit} is the temperature at which F_O begins to rise in response to increasing temperature and was determined from the intersection of two regression lines extrapolated from the slow- and fast-rising portions of the F_O -T curve (Schreiber and Berry 1977).

To account for the same individual plants being measured repeatedly, a two-way repeated measures analysis of variance (ANOVA) extra sum of squares F-test was used to determine whether there was a significant interaction effect between the main effects of leaf age and recovery time on F_V/F_M values of control (untreated) leaf discs, T_{50}, and T_{crit}. A one-way ANOVA was used to compare mean F_V/F_M of all three age classes at each temperature. To isolate which group(s) differed from the others, the Tukey test was used as an all-pairwise multiple comparisons procedure (the Holm-Sidak test was also conducted and yielded the same results). The Shapiro-Wilk procedure tested for normality and the Brown-Forsythe procedure tested for equal variance.

Simple linear regression was used to compare T_{crit} and T_{50}. To compare the F_V/F_M and electrolyte leakage methods, a two-sample t-test compared mean T_{50} derived from each method as well as mean percent F_V/F_M and mean percent electrolyte leakage at each temperature. Statistical analyses were conducted in SigmaPlot 13.0 (Systat Software, San

Jose, CA, USA) and R version 3.2.3 (2015-12-10, The R Foundation for Statistical Computing). Error bars represent one standard error (SE).

2.4 Results

Untreated (control) mean F_V/F_M values ranged 0.715-0.728 for the 15 min recovery time and 0.725-0.736 for the 24 h recovery time. Control mean F_V/F_M did not significantly differ among leaf age classes (F=2.470, P=0.134) but the 24 h mean F_V/F_M of all age classes combined was 0.0151 greater than after the 15 min recovery (F= 24.807, P= 0.004). F_V/F_M declined with increasing temperature above 40˚C for both recovery times and all age classes (Figure 2.1). After 15 min of recovery, mean F_V/F_M significantly differed among age classes at 46˚C, 49˚C, and 52˚C; all age classes significantly differed at 49°C while mean F_V/F_M of the mature age class was significantly greater than that of the expanding age class at 46°C and 52°C (Figure 2.1A, P<0.05). In contrast, after the 24 h recovery, mean F_V/F_M of the mature age class was significantly greater than the expanding and fully expanded age classes only at 49˚C (Figure 2.1B, P<0.05).

There was a marginally significant interaction between recovery time and leaf age on T_{50} (F=3.952, P = 0.054). After 15 min of recovery, mean T_{50} differed significantly among all three ages classes, with T_{50} increasing with leaf age (P<0.05, Table 2.1). The greatest difference in mean T_{50} (5.3°C, P<0.001) occurred between the mature and expanding age classes. Mean T_{50} of the mature age class was 3.2°C greater than that of the fully expanded age class (P=0.002) and T_{50} of the fully expanded age class was 2.1°C

greater than that of the expanding age class (P=0.043). After 24 h of recovery, T_{50} also increased with increasing leaf age but differences were not significant between any age class (P>0.05, Table 2.1). Within age classes, only the expanding age class showed a significant increase in T_{50} with recovery time (P=0.025).

For all age classes, F_O began to rise at ~43˚C (Figure 2.2). There was a statistically significant interaction between recovery time and leaf age on mean T_{crit} (F=8.596, P = 0.007). Mean T_{crit} of the mature age class was significantly greater than that of the expanding and fully expanded age classes at both the 15 min and 24 h recovery times (Table 2.1). The difference in mean T_{crit} between the mature and expanding age classes was 2.0°C after 15 min of recovery (P<0.001) and 3.3°C after 24 h of recovery (P<0.001). The difference in mean T_{crit} between the mature and fully expanded age classes was 1.4°C in the 15 min recovery time (P=0.001) and 3.1°C in the 24 h recovery time (P<0.001). T_{crit} did not differ significantly between the fully expanded and expanding age class for either recovery time (P>0.05) and mean T_{crit} did not significantly differ between recovery times for any age class (P>0.05).

T_{crit} derived from F_O-T thermotolerance curves (Figure 2.2) was significantly related to T_{50} derived from the F_V/F_M thermotolerance curves (Figure 2.1) across all three age classes for both the 15 min and 24 h recovery times (P<0.001, R^2=0.69; P=0.003, R^2= 0.43, Figure 2.3). Relationships were not significant within each age class (P>0.05).

Because T_{50} derived from F_V/F_M thermotolerance curves of the mature age class did not significantly change with recovery time, the F_V/F_M thermotolerance curve of the mature age class measured after the 24 h recovery time was compared with the

electrolyte leakage method. Between 40ºC and 65ºC, percent increase in electrolyte leakage was significantly smaller than the percent decline in F_V/F_M (Figure 2.4, $P<0.05$). With increasing temperature, percent F_V/F_M declined above 40ºC while percent electrolyte leakage did not increase until a threshold of ~50ºC was reached. T_{50} from the electrolyte leakage thermotolerance curve (58.6 ± 0.9ºC) was significantly greater than T_{50} from the F_V/F_M thermotolerance curve (49.0 ± 0.5ºC; $P <0.001$; Table 2.1).

By assessing Fv/Fm and electrolyte leakage on the same day on the same leaves from the same individuals, we observed no effect of the one-year difference in measurement dates on which each method was originally applied; percent of initial F_V/F_M was still significantly lower than percent damage using the electrolyte leakage method (Figure 2.5).

2.5 Discussion

Understanding how estimates of thermotolerance in *C. arabica* are influenced by leaf age, recovery time, and assessment method is critical given the ecological, economic, and social value of *C. arabica* and grim predictions of complete loss of suitable habitat by 2050 (Davis *et al.*, 2012). The mean F_V/F_M value of untreated leaf discs 0.72-0.74), was similar to previously reported values for *C. arabica* under controlled conditions (0.75-0.78, (Rodrigues *et al.*, 2016). Consistent with reports for other species, F_V/F_M of *C. arabica* began to decline significantly above 40ºC (Loik & Harte, 1996; Krause *et al.*, 2010), indicating a reduction in maximum quantum efficiency of PSII photochemistry

due to high temperature stress (Maxwell & Johnson, 2000). Generally, damage to PSII is reversible at temperatures below 40ºC (Teskey *et al.*, 2015).

Significant differences in T_{50} among all leaf age classes at 15 min but not 24 h after treatment demonstrates how the time between treatment temperature exposure and measurement influences apparent thermotolerance and interpretations of T_{50}. T_{50} of the expanding age class significantly increased after 24 h of recovery, while T_{50} of the fully expanded and mature age classes did not significantly change between recovery times, suggesting that older *C. arabica* leaves are more resistant to temperature-induced damage (Zhang *et al.*, 2012). Interestingly, the significant increase in T_{50} of expanding leaves between recovery times (Krause *et al.*, 2010) from 44.8°C to 47.0°C (Table 2.1) contrasts with the generalization that damage to PSII is only reversible at temperatures below 40°C, emphasizing the importance of considering study species and temperature exposure duration (Teskey *et al.*, 2015). The increase in T_{50} of the expanding age class between recovery times also decreased the range of T_{50} across leaf age classes after the 24 h recovery (~47-49°C) compared to the 15 min recovery (~45-50°C), suggesting that allowing 24 h recovery may reduce leaf age-related variation in thermotolerance curves measured with F_V/Fm. Consistent with this, F_V/F_M significantly differed among age classes at 46°C, 49°C, and 52°C after 15 min recovery, but differed only at 49°C after 24 h of recovery. This suggests that the 24 h recovery time more accurately assessed T_{50}, consistent with the results of Krause *et al.* (2010). In contrast, recovery time did not significantly affect age-related patterns of T_{crit} as T_{crit} of the mature age class was significantly greater than that of the expanding and fully expanded age classes for both

recovery times, suggesting that T_{crit} may be less affected by recovery time and therefore a more robust measure of photosynthetic thermotolerance than T_{50}.

Our results are consistent with the hypothesis that older leaves have greater photosynthetic thermotolerance than younger leaves, an evolutionary adaptation that would protect older leaves from irreversible damage (Yamada *et al.*, 1996). Zhang *et al*. (2012) also found that leaf lifespan was positively related to T_{crit}, suggesting that longer persistence is related to greater photosynthetic thermotolerance. T_{crit} was also greater in leaves of mature *Ficus insipida* Willd. trees than in leaves of *F. insipida* seedlings (Krause *et al.*, 2010). The differences in T_{crit} and T_{50} among leaf age classes may also reflect age-related changes such as shifts in the xanthophyll cycle-associated energy dissipation (Demmig-Adams *et al.*, 1994; Tegischer *et al.*, 2002). Due to the evolutionary tradeoff between metabolism and persistence that governs many leaf traits related to leaf age including specific leaf area, leaf nitrogen, photosynthetic capacity, maintenance respiration, and photosynthetic capacity per unit leaf nitrogen (Poorter & Bongers, 2006; Bonan, 2008), it is not surprising that thermotolerance also varies with leaf age.

The range of T_{crit} observed in *C. arabica* (42.7-46.0°C) falls within the broad range of values (35-48˚C) reported for other tropical species (Weng & Lai, 2005). In addition to our results showing that leaf age significantly influences T_{crit} in *C. arabica*, other studies show that T_{crit} is highly plastic (Knight & Ackerly, 2002) and influenced by environmental conditions such as ambient temperature and drought (Schreiber & Berry, 1977; Ghouil *et al.*, 2003; Daas *et al.*, 2008). For instance, T_{crit} was greater in summer than winter for temperate, tropical, CAM, and C4 species (Weng & Lai, 2005), T_{crit} of

desert and coastal species was greater when measured in the field (Knight & Ackerly, 2002), and T_{crit} of tropical plants was greater than that of alpine plants (Smillie & Nott, 1979).

Generally T_{50} derived from F_V/F_M thermotolerance curves was greater than T_{crit} derived from F_O-T curves (Table 2.1), consistent with the relationship between T_{50} and T_{crit} observed in *Eucalyptus* trees (Lin, 2012), implying that significant damage to photochemistry occurs prior to a 50% reduction in F_V/F_M. The significant relationships between T_{crit} and T_{50} across all leaf age classes for both recovery times (Figure 2.3) are consistent with previous observations that T_{crit} was significantly related to other measures of thermotolerance, including the temperature at which net CO_2 assimilation declines (Downton *et al.*, 1984), temperature thresholds for irreversible decreases in the quantum yield of CO_2 fixation (Schreiber & Berry, 1977), and temperature thresholds for irreversible tissue damage (Bilger *et al.*, 1984). The significant relationship between T_{crit} and T_{50} in *C. arabica* across but not within leaf age classes suggests that considerations of leaf age are important when assessing thermotolerance, and sampling a range of leaf ages would yield the most representative thermotolerance measurements.

Although this is not the first time chlorophyll fluorescence or electrolyte leakage methods have been applied in some way to *C. arabica* (DaMatta *et al.*, 1997; Campos *et al.*, 2003; Gascó *et al.*, 2004; Silva *et al.*, 2004; Netto *et al.*, 2005; Chaves *et al.*, 2007), to our knowledge this is the first study to directly quantify and compare thermotolerance assessments using both methods in *C. arabica*. The comparison of the electrolyte leakage and chlorophyll fluorescence methods used to measure thermotolerance curves (Figure

2.4) showed that F_V/F_M was more sensitive to increasing temperature than electrolyte leakage, likely because the photosynthetic apparatus is more sensitive to high temperature stress than cell membranes (Bjorkman *et al.*, 1975; DaMatta & Ramalho, 2006). (Xu *et al.*, 2014) also found that F_V/F_M was more sensitive to heat stress than electrolyte leakage methods in grapevine (*Vitis*). In our study, F_V/F_M declined >40 °C, whereas electrolyte leakage increased >50 °C, consistent with (Gascó *et al.*, 2004) who showed that exposing *C. arabica* shoots to 40°C and 50°C for one hour did not cause a significant increase in electrolyte leakage, although electrolyte leakage and leaf hydraulic conductance both markedly increased when shoots were exposed to 57°C, indicating extensive disruption of membranes.

F_V/F_M measures the maximum efficiency of photochemistry while electrolyte leakage measures irreversible tissue damage, similar to assessments of visible leaf damage (Cunningham & Read, 2006) and leaf tissue necrosis (Bilger *et al.*, 1984). (Cunningham & Read, 2006) found that F_V/F_M had a lower threshold for temperature-induced damage than visible damage in five of eight species in their study (two of four tropical species; three of four temperate species), also suggesting that damage to PSII and the thylakoid membrane occurs at lower temperatures than permanent damage to cell membranes (Levitt, 1980; Anderson *et al.*, 1997). This contrasts with studies that found close correlations between chlorophyll fluorescence and visible damage assessments (Lindgren & Hällgren, 1993; Larcher, 1995; Binder & Fielder, 1996; Liu & Huang, 2000). In further contrast to our results, (Bibi *et al.*, 2008) found that membrane leakage was more sensitive to temperature than F_V/F_M or photosynthesis in cotton, and (Epron &

Dreyer, 1992) found that electrolyte leakage was more sensitive to drought stress than F_V/F_M in *Quercus petraea*, which was attributed to F_V/F_M being less sensitive to drought and only declining when drought becomes severe (Way *et al.*, 2013). These discrepancies among studies may be related to differences in species, experimental setup, environmental conditions, and type of stress investigated. Other studies that have used both F_V/F_M and electrolyte leakage methods to assess thermotolerance did not directly compare methods (Loik & Harte, 1996; Yang *et al.*, 1996). The mixed results when evaluating thermotolerance using chlorophyll fluorescence and tissue damage methods demonstrate that although methods to quantify thermotolerance are often related, response to temperature varies across plant functions (Teskey *et al.*, 2015) and leaf age (Table 2.1). This highlights the complexity of evaluating thermotolerance and the importance of considering the methodology, type of plant function, and leaf developmental stage when assessing thermotolerance. Our results also confirmed that significant differences in assessments of thermotolerance between the F_V/F_M and electrolyte leakage methods (Figure 2.5) were not affected by measurement date, demonstrating each method's high repeatability on mature fully expanded leaves (Xu *et al.*, 2014) and the greater high temperature sensitivity of PSII than cell membrane integrity.

Conclusions

Given future climate predictions of increasingly severe heatwaves, accurately quantifying thermotolerance of *Coffea arabica* is crucial. In this study, we investigated

how leaf age, experimental protocol, and method employed influenced thermotolerance assessments. We found that mature leaves were more heat tolerant than expanding leaves, waiting 24 h after temperature exposure yielded more accurate thermotolerance assessments than 15 min, and photochemistry was more heat sensitive than cell membranes. These factors should be considered when predicting plant responses to heat stress.

Although limited to potted *C. arabica* plants in a greenhouse, this study has implications for how thermotolerance of *C. arabica* is measured because leaf age and methodology influenced thermotolerance assessments and interpretations. In addition, thermotolerance evaluations are also influenced by drought (Way *et al.*, 2013; Teskey *et al.*, 2015), light intensity (Berry & Bjorkman, 1980; Buchner *et al.*, 2013), and duration and intensity of heat treatment (Colombo & Timmer, 1992). Considerations of thermotolerance methods, environmental conditions, and experimental setup are critical to accurately understand how species such as *C. arabica* respond to increased temperature.

2.6 Acknowledgements

This work was supported by the NSF Graduate Research Fellowship Program and NSF grant IOS 11-46746. We are grateful to the OSU Greenhouse Operations staff for their assistance with the maintenance of our plant material.

2.7 References

Alvim P de T, Kozlowski TT (2013) *Ecophysiology of Tropical Crops*. Elsevier, 517 pp.

Anderson JM, Park Y, Chow W (1997) Photoinactivation and photoprotection of photosystem II in nature. *Physiologia Plantarum*, **100**, 214–223.

Bajji M, Kinet J-M, Lutts S (2002) The use of the electrolyte leakage method for assessing cell membrane stability as a water stress tolerance test in durum wheat. *Plant Growth Regulation*, **36**, 61–70.

Baker NR, Rosenqvist E (2004) Applications of chlorophyll fluorescence can improve crop production strategies: an examination of future possibilities. *Journal of Experimental Botany*, **55**, 1607–1621.

Batista-Santos P, Lidon FC, Fortunato A *et al.* (2011) The impact of cold on photosynthesis in genotypes of Coffea spp.—Photosystem sensitivity, photoprotective mechanisms and gene expression. *Journal of Plant Physiology*, **168**, 792–806.

Berry J, Bjorkman O (1980) Photosynthetic response and adaptation to temperature in higher plants. *Annual Review of Plant Physiology*, **31**, 491–543.

Bibi A, Oosterhuis D, Gonias E (2008) Photosynthesis, quantum yield of photosystem II and membrane leakage as affected by high temperatures in cotton genotypes. *Journal of Cotton Science*.

Bilger H-W, Schreiber U, Lange OL (1984) Determination of leaf heat resistance: comparative investigation of chlorophyll fluorescence changes and tissue necrosis methods. *Oecologia*, **63**, 256–262.

Bilger W, Schreiber U, Lange OL (1987) Chlorophyll fluorescence as an indicator of heat induced limitation of photosynthesis in Arbutus unedo L. In: *Plant Response to Stress* (eds Tenhunen JD, Catarino FM, Lange OL, Oechel WC), pp. 391–399. Springer Berlin Heidelberg.

Binder WD, Fielder P (1996) Chlorophyll fluorescence as an indicator of frost hardiness in white spruce seedlings from different latitudes. *New Forests*, **11**, 233–253.

Bita C, Gerats T (2013) Plant tolerance to high temperature in a changing environment: scientific fundamentals and production of heat stress-tolerant crops. *Crop Science and Horticulture*, **4**, 273.

Bjorkman O, Mooney HA, Ehleringer J (1975) Photosynthetic responses of plants from habitats with contrasting thermal environments. *Carnegie Inst. Wash. Yearbook*, **74**, 743–748.

Bolhar-Nordenkampf H, Long S, Baker N, Oquist G, Schreiber U, Lechner E (1989) Chlorophyll fluorescence as a probe of the photosynthetic competence of leaves in the field: a review of current instrumentation. *Functional Ecology*, 497–514.

Bonan GB (2008) *Ecological Climatology: Concepts and Applications*. Cambridge University Press, 1 p.

Buchner O, Karadar M, Bauer I, Neuner G (2013) A novel system for in situ determination of heat tolerance of plants: first results on alpine dwarf shrubs. *Plant Methods*, **9**, 7.

Butler DR (1977) Coffee Leaf Temperatures in a Tropical Environment. *Acta Botanica Neerlandica*, **26**, 129–140.

Camargo AP (1985) Florescimento e frutificação de café arábica nas diferentes regiões cafeeiras do Brasil. *Pesquisa Agropecuária Brasileira*, **20**, 831–839.

Campos PS, nia Quartin V, chicho Ramalho J, Nunes MA (2003) Electrolyte leakage and lipid degradation account for cold sensitivity in leaves ofCoffea sp. plants. *Journal of plant physiology*, **160**, 283–292.

Chaves ARM, Ten-Caten A, Pinheiro HA, Ribeiro A, DaMatta FM (2007) Seasonal changes in photoprotective mechanisms of leaves from shaded and unshaded field-grown coffee (Coffea arabica L.) trees. *Trees*, **22**, 351–361.

Colombo S, Timmer V (1992) Limits of Tolerance to High-Temperatures Causing Direct and Indirect Damage to Black Spruce. *Tree Physiology*, **11**, 95–104.

Corlett RT (2011) Impacts of warming on tropical lowland rainforests. *Trends in Ecology & Evolution*, **26**, 606–613.

Cramer W, Bondeau A, Woodward FI *et al.* (2001) Global response of terrestrial ecosystem structure and function to CO2 and climate change: results from six dynamic global vegetation models. *Global Change Biology*, **7**, 357–373.

Craparo ACW, Van Asten PJA, Läderach P, Jassogne LTP, Grab SW (2015) Coffea arabica yields decline in Tanzania due to climate change: Global implications. *Agricultural and Forest Meteorology*, **207**, 1–10.

Cunningham SC, Read J (2006) Foliar temperature tolerance of temperate and tropical evergreen rain forest trees of Australia. *Tree Physiology*, **26**, 1435–1443.

Daas C, Montpied P, Hanchi B, Dreyer E (2008) Responses of photosynthesis to high temperatures in oak saplings assessed by chlorophyll-a fluorescence: inter-specific diversity and temperature-induced plasticity. *Annals of Forest Science*, **65**, 1.

DaMatta FM (2004) Ecophysiological constraints on the production of shaded and unshaded coffee: a review. *Field Crops Research*, **86**, 99–114.

DaMatta FM, Ramalho JDC (2006) Impacts of drought and temperature stress on coffee physiology and production: a review. *Brazilian Journal of Plant Physiology*, **18**, 55–81.

DaMatta FM, Maestri M, Mosquim PR, Barros RS (1997) Photosynthesis in coffee (Coffea arabica and C. canephora) as affected by winter and summer conditions. *Plant Science*, **128**, 43–50.

Davis AP, Gole TW, Baena S, Moat J (2012) The impact of climate change on indigenous arabica coffee (Coffea arabica): predicting future trends and identifying priorities. *PLoS One*, **7**, e47981.

Demmig B, Winter K, Krüger A, Czygan FC (1987) Photoinhibition and zeaxanthin formation in intact leaves : a possible role of the xanthophyll cycle in the dissipation of excess light energy. *Plant Physiology*, **84**, 218–224.

Demmig-Adams B, Adams III WW, Foyer C, Mullineaux P (1994) Light stress and photoprotection related to the xanthophyll cycle. *Causes of photooxidative stress and amelioration of defense systems in plants.*, 105–126.

Diffenbaugh NS, Scherer M (2011) Observational and model evidence of global emergence of permanent, unprecedented heat in the 20th and 21st centuries. *Climatic Change*, **107**, 615–624.

Downton WJS, Berry JA, Seemann JR (1984) Tolerance of photosynthesis to high temperature in desert plants. *Plant Physiology*, **74**, 786–790.

Epron D, Dreyer E (1992) Effects of severe dehydration on leaf photosynthesis in Quercus petraea (Matt.) Liebl.: photosystem II efficiency, photochemical and nonphotochemical fluorescence quenching and electrolyte leakage. *Tree Physiology*, **10**, 273–284.

Flint H, Boyce B, Beattie D (1967) Index of injury-a useful expression of freezing injury to plant tissues as determined by the electrolytic method. *Canadian Journal of Plant Science*, **47**, 229–230.

Gascó A, Nardini A, Salleo S (2004) Resistance to water flow through leaves of Coffea arabica is dominated by extra-vascular tissues. *Functional Plant Biology*, **31**, 1161–1168.

Genty B, Briantais J-M, Baker NR (1989) The relationship between the quantum yield of photosynthetic electron transport and quenching of chlorophyll fluorescence. *Biochimica et Biophysica Acta (BBA)-General Subjects*, **990**, 87–92.

Ghouil H, Montpied P, Epron D, Ksontini M, Hanchi B, Dreyer E (2003) Thermal optima of photosynthetic functions and thermostability of photochemistry in cork oak seedlings. *Tree Physiology*, **23**, 1031–1039.

Havaux M (1993) Characterization of thermal damage to the photosynthetic electron transport system in potato leaves. *Plant Science*, **94**, 19–33.

Ilík P, Kouřil R, Kruk J, Myśliwa-Kurdziel B, Popelková H, Strzałka K, Nauš J (2003) Origin of chlorophyll fluorescence in plants at 55–75 C. *Photochemistry and photobiology*, **77**, 68–76.

Ismail AM, Hall AE (1999) Reproductive-Stage Heat Tolerance, Leaf Membrane Thermostability and Plant Morphology in Cowpea. *Crop Science*, **39**, 1762.

Knight CA, Ackerly DD (2002) An ecological and evolutionary analysis of photosynthetic thermotolerance using the temperature-dependent increase in fluorescence. *Oecologia*, **130**, 505–514.

Krause GH (1988) Photoinhibition of photosynthesis. An evaluation of damaging and protective mechanisms. *Physiologia Plantarum*, **74**.

Krause GH, Weis E (1984) Chlorophyll fluorescence as a tool in plant physiology. *Photosynthesis Research*, **5**, 139–157.

Krause GH, Winter K, Krause B, Jahns P, García M, Aranda J, Virgo A (2010) High-temperature tolerance of a tropical tree, Ficus insipida: methodological reassessment and climate change considerations. *Functional Plant Biology*, **37**, 890–900.

Larcher W (1995) Photosynthesis as a Tool for Indicating Temperature Stress Events. In: *Ecophysiology of Photosynthesis* (eds Schulze PDE-D, Caldwell PDMM), pp. 261–277. Springer Berlin Heidelberg.

Levitt J (1980) Response of plants to environmental stresses. *Water, radiation, salt and other stresses*, **2**.

Lin Y-S (2012) *How will Eucalyptus tree species respond to global climate change? A comparison of temperature responses of photosynthesis. PhD Dissertation.* PhD Dissertation, Hawkesbury Institute for the Environment University of Western Sydney, 1-186 pp.

Lindgren K, Hällgren J-E (1993) Cold acclimation of Pinus contorta and Pinus sylvestris assessed by chlorophyll fluorescence. *Tree Physiology*, **13**, 97–106.

Liu X, Huang B (2000) Heat Stress Injury in Relation to Membrane Lipid Peroxidation in Creeping Bentgrass. *Crop Science*, **40**, 503.

Loik ME, Harte J (1996) High-temperature tolerance of Artemisia tridentata and Potentilla gracilis under a climate change manipulation. *Oecologia*, **108**, 224–231.

Maxwell K, Johnson GN (2000) Chlorophyll fluorescence—a practical guide. *Journal of experimental botany*, **51**, 659–668.

Misra AN, Misra M, Singh R (2012) *Chlorophyll fluorescence in plant biology*. INTECH Open Access Publisher.

Netto AT, Campostrini E, de Oliveira JG, Bressan-Smith RE (2005) Photosynthetic pigments, nitrogen, chlorophyll a fluorescence and SPAD-502 readings in coffee leaves. *Scientia Horticulturae*, **104**, 199–209.

O'Sullivan OS, Weerasinghe KWLK, Evans JR, Egerton JJG, Tjoelker MG, Atkin OK (2013) High-resolution temperature responses of leaf respiration in snow gum (Eucalyptus pauciflora) reveal high-temperature limits to respiratory function. *Plant, Cell & Environment*, **36**, 1268–1284.

Partelli FL, Vieira HD, Viana AP, Batista-Santos P, Rodrigues AP, Leitão AE, Ramalho JC (2009) Low temperature impact on photosynthetic parameters of coffee genotypes. *Pesquisa Agropecuária Brasileira*, **44**, 1404–1415.

Poorter L, Bongers F (2006) Leaf Traits Are Good Predictors of Plant Performance Across 53 Rain Forest Species. *Ecology*, **87**, 1733–1743.

Ramalho JC, Pons TL, Groeneveld HW, Azinheira HG, Nunes MA (2000) Photosynthetic acclimation to high light conditions in mature leaves of Coffea arabica L.: role of xanthophylls, quenching mechanisms and nitrogen nutrition. *Functional Plant Biology*, **27**, 43–51.

Ramalho JC, Quartin VL, Leitão E, Campos PS, Carelli MLC, Fahl JI, Nunes MA (2003) Cold Acclimation Ability and Photosynthesis among Species of the Tropical Coffea Genus. *Plant Biology*, **5**, 631–641.

Rodrigues WP, Martins MQ, Fortunato AS *et al.* (2016) Long-term elevated air [CO2] strengthens photosynthetic functioning and mitigates the impact of supra-optimal temperatures in tropical Coffea arabica and C. canephora species. *Global change biology*, **22**, 415–431.

Schreiber U, Berry JA (1977) Heat-induced changes of chlorophyll fluorescence in intact leaves correlated with damage of the photosynthetic apparatus. *Planta*, **136**, 233–238.

Schreiber U, Bilger W, Neubauer C (1995) Chlorophyll Fluorescence as a Nonintrusive Indicator for Rapid Assessment of In Vivo Photosynthesis. In: *Ecophysiology of*

Photosynthesis (eds Schulze PDE-D, Caldwell PDMM), pp. 49–70. Springer Berlin Heidelberg.

Seddon AWR, Macias-Fauria M, Long PR, Benz D, Willis KJ (2016) Sensitivity of global terrestrial ecosystems to climate variability. *Nature*.

Silva EA, DaMatta FM, Ducatti C, Regazzi AJ, Barros RS (2004) Seasonal changes in vegetative growth and photosynthesis of Arabica coffee trees. *Field Crops Research*, **89**, 349–357.

Smillie RM, Nott R (1979) Heat injury in leaves of alpine, temperate and tropical plants. *Australian Journal of Plant Physiology*, **6**, 135–141.

Tegischer K, Tausz M, Wieser G, Grill D (2002) Tree- and needle-age-dependent variations in antioxidants and photoprotective pigments in Norway spruce needles at the alpine timberline. *Tree Physiology*, **22**, 591–596.

Teketay D (1999) History, botany and ecological requirements of coffee. *Walia*, **20**, 28–50.

Teskey R, Wertin T, Bauweraerts I, Ameye M, Mcguire MA, Steppe K (2015) Responses of tree species to heat waves and extreme heat events. *Plant, Cell & Environment*, **38**, 1699–1712.

Tovuu A, Zulfugarov IS, Lee C-H (2013) Correlations between the temperature dependence of chlorophyll fluorescence and the fluidity of thylakoid membranes. *Physiologia Plantarum*, **147**, 409–416.

Valladares F, Pearcy R (1997) Interactions between water stress, sun-shade acclimation, heat tolerance and photoinhibition in the sclerophyll Heteromeles arbutifolia. *Plant, Cell & Environment*, **20**, 25–36.

Vasudeva N, Gopal NH (1975) Studies on leaf growth, 5: The life-span of coffee leaves in South India. *Indian Coffee (India)*, 171–174.

Way DA, Crawley C, Sage RF (2013) A hot and dry future: warming effects on boreal tree drought tolerance. *Tree Physiology*, **33**, 1003–1005.

Weis E, Berry JA (1987) Quantum efficiency of photosystem II in relation to "energy"-dependent quenching of chlorophyll fluorescence. *Biochimica et Biophysica Acta (BBA)-Bioenergetics*, **894**, 198–208.

Weng J-H, Lai M-F (2005) Estimating heat tolerance among plant species by two chlorophyll fluorescence parameters. *Photosynthetica*, **43**, 439–444.

Whitlow TH, Bassuk NL, Ranney TG, Reichert DL (1992) An Improved Method for Using Electrolyte Leakage to Assess Membrane Competence in Plant Tissues. *Plant Physiology*, **98**, 198–205.

Willits D, Peet M (2001) Measurement of chlorophyll fluorescence as a heat stress indicator in tomato: laboratory and greenhouse comparisons. *Journal of the American Society for Horticultural Science*, **126**, 188–194.

Wright IJ, Leishman MR, Read C, Westoby M (2006) Gradients of light availability and leaf traits with leaf age and canopy position in 28 Australian shrubs and trees. *Functional Plant Biology*, **33**, 407–419.

Xu H, Liu G, Liu G, Yan B, Duan W, Wang L, Li S (2014) Comparison of investigation methods of heat injury in grapevine (Vitis) and assessment to heat tolerance in different cultivars and species. *BMC plant biology*, **14**, 1.

Yamada M, Hidaka T, Fukamachi H (1996) Heat tolerance in leaves of tropical fruit crops as measured by chlorophyll fluorescence. *Scientia Horticulturae*, **67**, 39–48.

Yamashita T, Butler WL (1968) Photoreduction and Photophosphorylation with Tris-Washed Chloroplasts. *Plant Physiology*, **43**, 1978–1986.

Yang G, Rhodes D, Joly R (1996) Effects of High Temperature on Membrane Stability and Chlorophyll Fluorescence in Glycinebetaine-Deficient and Glycinebetaine-Containing Maize Lines. *Functional Plant Biology*, **23**, 437–443.

Yordanov I, Goltsev V, Tsonev T, Kruleva L (1995) Thermal acclimation of the photosynthetic apparatus depending on temperature and duration of treatment. *Bulg. J. Plant Physiol*, **21**, 12–28.

Zhang J-L, Poorter L, Hao G-Y, Cao K-F (2012) Photosynthetic thermotolerance of woody savanna species in China is correlated with leaf life span. *Annals of Botany*, **110**, 1027–1033.

2.8 Figures & Tables

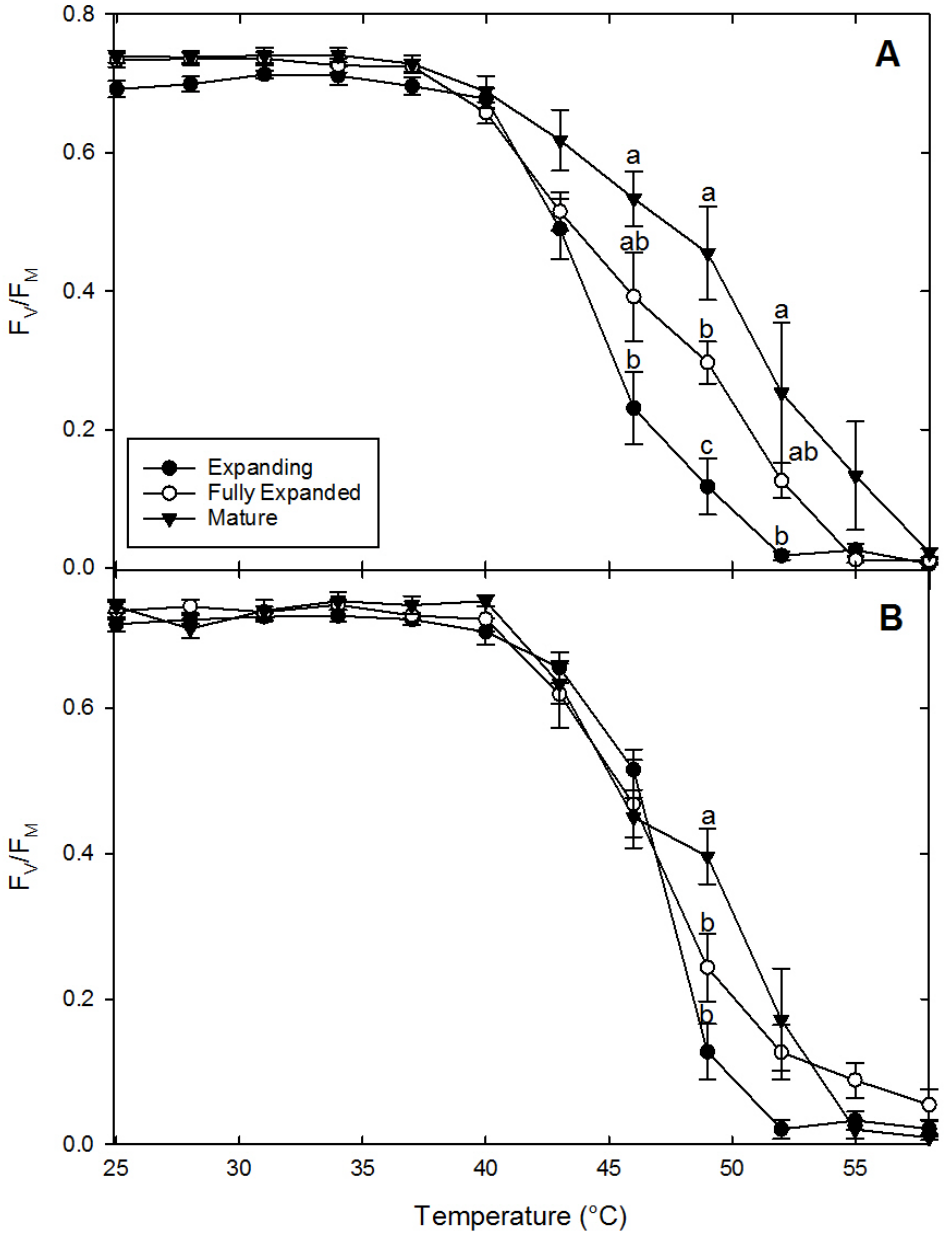

Figure 2.1 Thermotolerance curves measured with F_V/F_M as a function of temperature of three leaf age classes (expanding, fully expanded, mature) of *C. arabica* measured 15 min after temperature exposure (A) and 24 h after temperature exposure (B). Letters represent significant differences among leaf age classes at each temperature ($P<0.05$). N=6. Error bars represent SE.

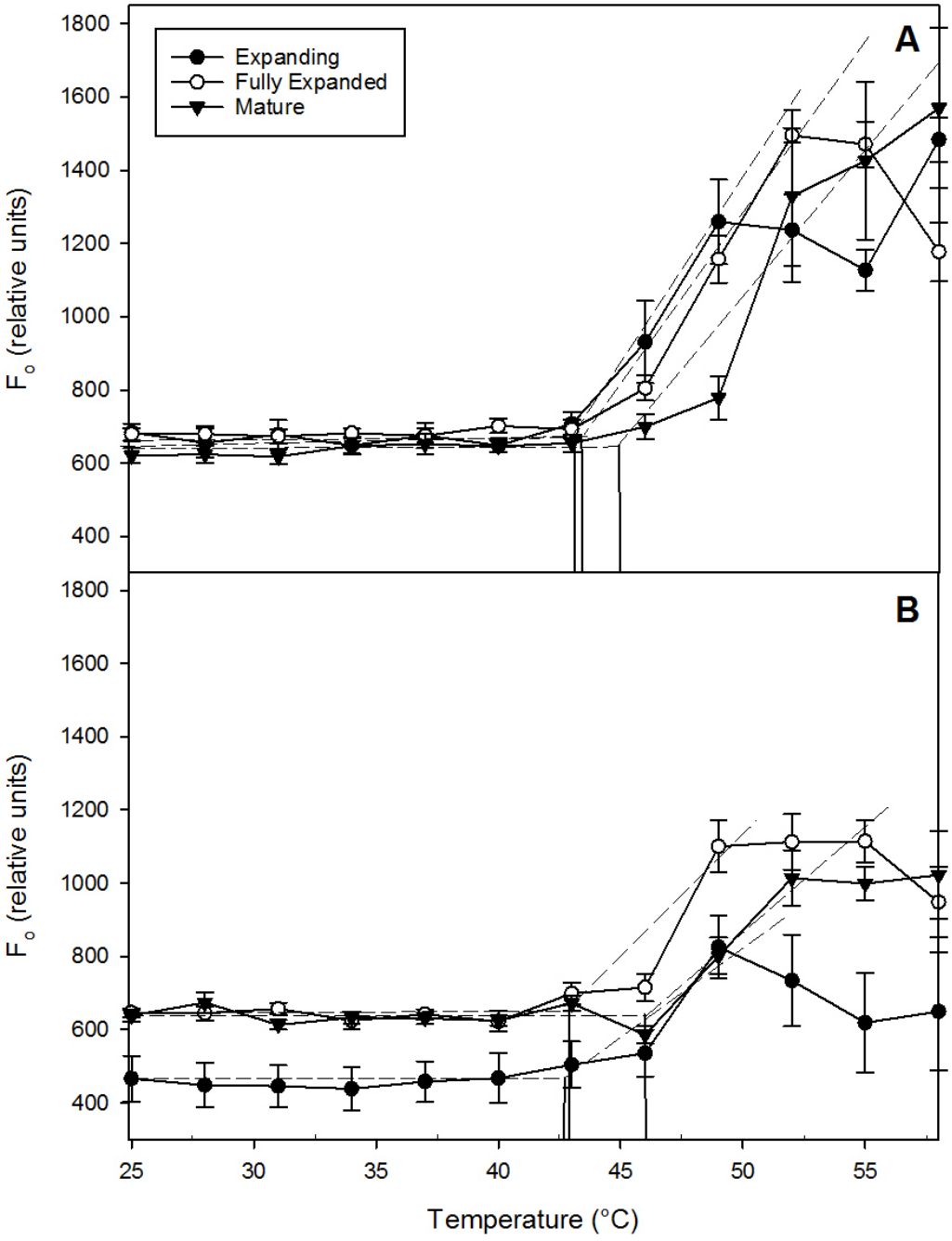

Figure 2.2 Thermotolerance curves measured with F_O as a function of temperature of three leaf age classes (expanding, fully expanded, mature) of *C. arabica* measured 15 min after temperature exposure (A) and 24 h after temperature exposure (B).

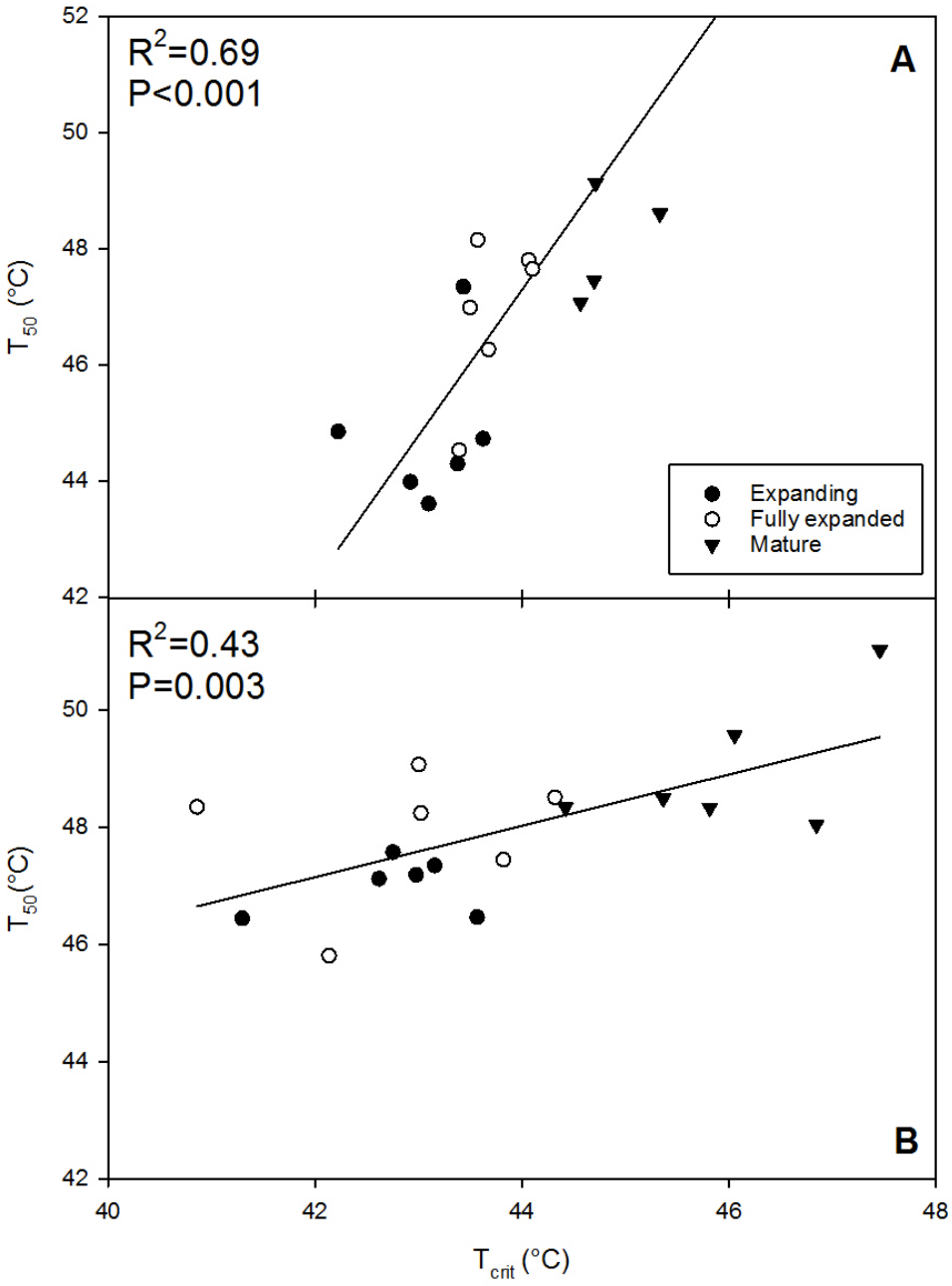

Figure 2.3 Relationship between T_{crit} derived from F_O-T thermotolerance curves and T_{50} derived from F_V/F_M thermotolerance curves for all age classes (expanding, fully expanded, mature) measured 15 min after temperature exposure (A) and 24 h after temperature exposure (B). N=6. Each point is an individual plant. Equation of regression line: y= -63.20 + 2.51x (A) and y=28.767 + 0.438x (B). Non-significant regression lines within each age class are not shown.

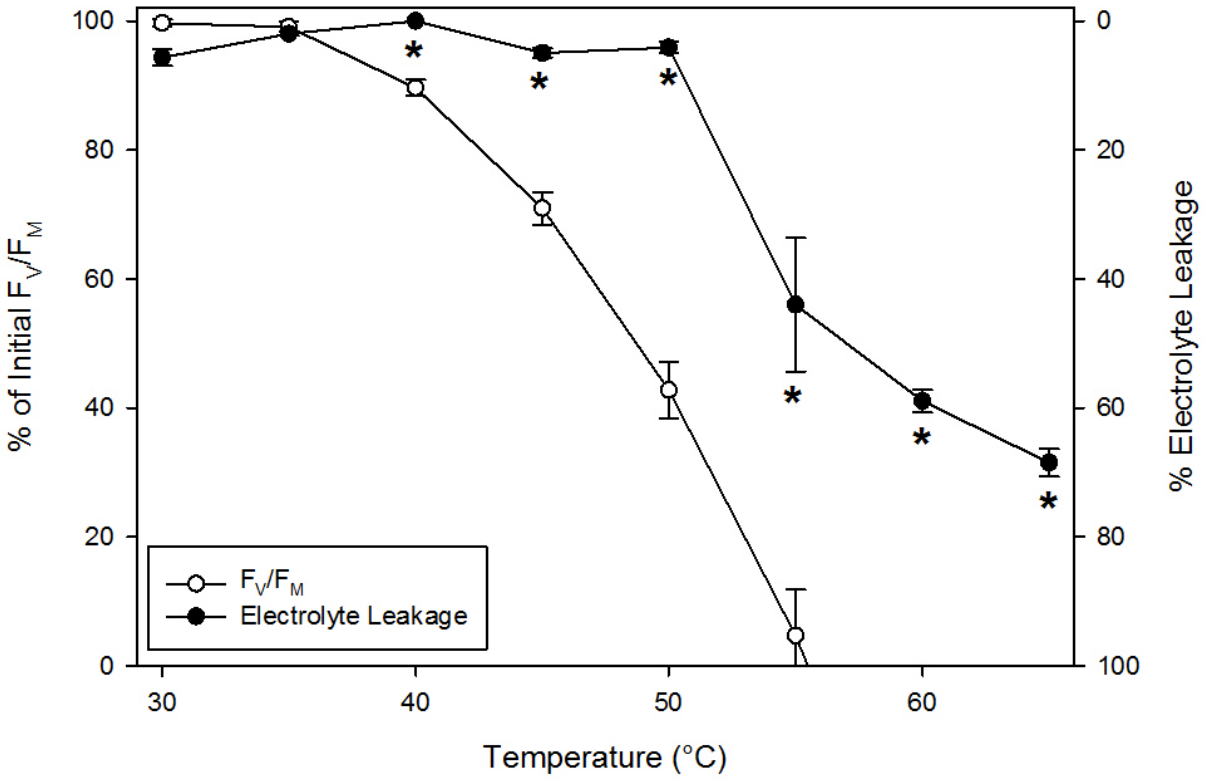

Figure 2.4 Thermotolerance curves measured with percent electrolyte leakage and percent F_V/F_M. Percent F_V/F_M data points were estimated from third order sigmoidal functions (Equation 3) fitted to the F_V/F_M thermotolerance curve for the mature age class after the 24 h recovery time. Percent F_V/F_M was normalized so untreated (control) F_V/F_M was 100% (no damage). Percent electrolyte leakage was normalized so minimum percent electrolyte leakage was 0% (no damage). Percent electrolyte leakage axis is inverted for easier comparison of curves. Asterisks represent $P<0.05$. N=5-6.

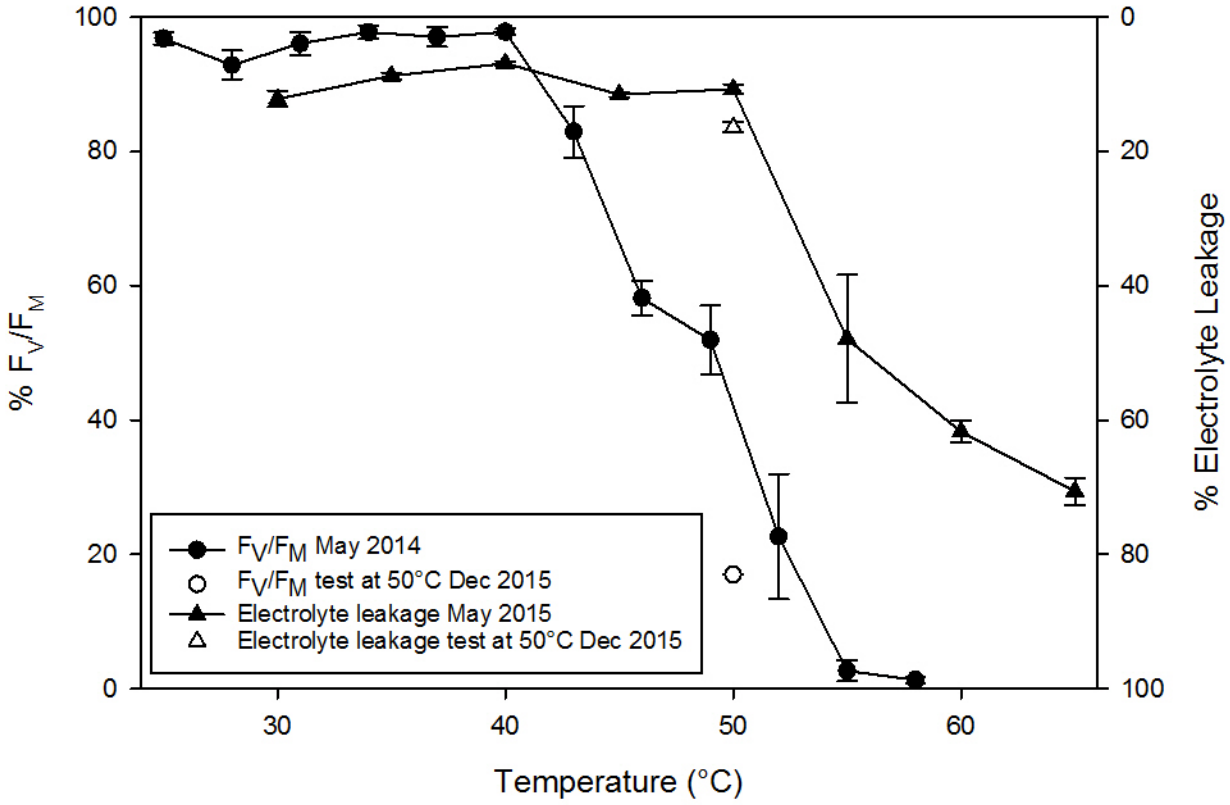

Figure 2.5 Thermotolerance curves measured with non-normalized F_V/F_M in May 2014 (closed circles) and non-normalized electrolyte leakage in May 2015 (closed triangles) compared with mean percent F_V/F_M and mean percent electrolyte leakage values at 50°C assessed on the same individuals (N=5) on the same day in December 2015 (open circle, open triangle, respectively). Percent F_V/F_M and percent electrolyte leakage values at 50°C significantly differed ($P<0.05$) and were consistent with the original F_V/F_M and electrolyte leakage thermotolerance curves measured in May 2014 and May 2015. This demonstrated that timing of when the method was conducted does not affect the observed differences between methods. Error bars represent SE. Percent electrolyte leakage axis is inverted for easier comparison of curves.

Table 2.1 Thermotolerance parameters (°C) derived from curves of F_V/F_M, electrolyte leakage, and F_O as a function of treatment temperature for 15 min and 24 h recovery times of three age classes (expanding, fully expanded, mature).

	Expanding	**Fully expanded**	**Mature**
T_{50} (F_V/F_M) 15 min	44.8 ± 0.5 Aa	46.9 ± 0.6 Ab	50.1 ± 1.3 Ac
T_{50} (F_V/F_M) 24 h	47.0 ± 0.2 Ba	47.9 ± 0.5 Aa	49.0 ± 0.5 Aa
T_{50} (electrolyte leakage)	-	-	58.6 ± 0.9
T_{crit} (F_O) 15 min	43.1 ± 0.2 Aa	43.7 ± 0.1 Aa	45.1 ± 0.3 Ab
T_{crit} (F_O) 24 h	42.7 ± 0.3 Aa	42.9 ± 0.5 Aa	46.0 ± 0.4 Ab

Uppercase letters indicate significant differences between recovery times within each age class ($P<0.05$). Lowercase letters indicate significant differences among age classes within each recovery time ($P<0.05$). Means ± SE.

3. IMPACTS OF LEAF AGE AND HEAT STRESS DURATION ON PHOTOSYNTHETIC GAS EXCHANGE AND FOLIAR NON-STRUCTURAL CARBOHYDRATES IN *COFFEA ARABICA*

Danielle E. Marias, Frederick C. Meinzer, Christopher Still

3.1 Abstract

Given future climate predictions of increased temperature, and frequency and intensity of heat waves in the tropics, suitable habitat to grow ecologically, economically, and socially valuable *Coffea arabica* is severely threatened. We investigated how leaf age and heat stress duration impact recovery from heat stress in *C. arabica*. Treated plants were heated in a growth chamber at 49°C for 45 or 90 min. Physiological recovery was monitored *in situ* using gas exchange, chlorophyll fluorescence (the ratio of variable to maximum fluorescence, F_V/F_M), and leaf non-structural carbohydrate (NSC) on mature and expanding leaves before and 2, 15, 25, and 50 days after treatment. Regardless of leaf age, the 90 min treatment resulted in greater F_V/F_M reduction two days after treatment and slower recovery than the 45 min treatment. In both treatments, photosynthesis of expanding leaves recovered more slowly than in mature leaves. Stomatal conductance (g_s) decreased in expanding leaves but did not change in mature leaves. These responses led to reduced intrinsic water use efficiency with increasing heat stress duration in both age classes. Based on a leaf energy balance model, aftereffects of heat stress would be exacerbated by increases in leaf temperature at low g_s under full sunlight where *C. arabica* is often grown, but also under partial sunlight. Starch and total NSC content of the 45 min group significantly decreased two days after treatment, then accumulated 15 and 25 days after treatment coinciding with recovery of photosynthesis and F_V/F_M. In contrast, sucrose of the 90 min group accumulated at day 2 suggesting that phloem transport was inhibited. Both treatment group responses contrasted with control plant total NSC and starch, which declined with time associated with subsequent flower and

fruit production. No treated plants produced flowers or fruits, suggesting that short duration heat stress can lead to crop failure.

3.2 Introduction

Climate models predict an increasing frequency and intensity of heat waves and high temperature events throughout the 21st century (Cramer *et al.*, 2001; Diffenbaugh & Scherer, 2011; IPCC, 2014) that are expected to influence plant species' distributions, productivity, and carbon balance, although the physiological impacts remain unclear. Heat waves are increasing under both drier and wetter conditions (Hao *et al.*, 2013). In contrast to drought, much less is known about physiological responses to heat stress (Barnabás *et al.*, 2008; Ruan *et al.*, 2010). This, along with the need to isolate the effects of heat and drought stress to understand the interactions between the two on plant physiological responses (Sevanto & Dickman, 2015), make studies on the physiological impacts of heat stress essential. Tropical species are particularly vulnerable to heat stress because of the higher radiation load, the increase in heat wave intensity and frequency expected in the tropics (Corlett, 2011), and the narrower distribution of temperatures typically experienced compared to extra-tropical species (Battisti & Naylor, 2009).

The tropics support important agricultural crops such as coffee. Global coffee consumption continues to increase; over 9 billion kg of coffee were consumed worldwide in 2014 (ICO, 2016). *Coffea arabica* L. leads the world coffee trade and provides ~65% of commercial production (ICO, 2016). *C. arabica* is a shade-adapted evergreen species that originated in Ethiopia and is now grown in 80 countries on four continents in the inter-tropical zone between 20-25ºN in Hawaii and 24ºS in Brazil (DaMatta & Ramalho,

2006). *C. arabica* is highly sensitive to fluctuations in temperature (Silva *et al.*, 2004; Camargo, 2010) with an optimal mean annual temperature range of 18-24ºC (Camargo, 1985; Teketay, 1999). An increase in the frequency and intensity of heat waves in the tropics would severely threaten suitable habitat to grow *C. arabica* (DaMatta & Ramalho, 2006; Camargo, 2010; Davis *et al.*, 2012; Bunn *et al.*, 2014; Craparo *et al.*, 2015). Therefore, it is crucial to quantify its physiological responses to and ability to recover from heat stress (Martins *et al.*, 2014, 2016; Rodrigues *et al.*, 2016).

Examining the impacts of heat stress on plant carbon utilization is critical for understanding plant responses to changes in climate and potential feedbacks between vegetation and climate. Heat stress affects plant physiology from the cellular to whole plant scales, inducing shifts in the allocation of assimilated carbon/photosynthate to repair and recovery processes. At the cellular and organelle levels, high temperatures can damage photosystem II (PSII) photochemistry and electron transport; reduce thylakoid membrane fluidity, RUBISCO activity, and cell membrane stability; and induce heat shock protein expression and the production of reactive oxygen species (ROS) (Wahid *et al.*, 2007; Teskey *et al.*, 2015). At the leaf level, high temperature stress reduces photosynthesis, increases photorespiration and dark (mitochondrial) respiration, and influences water relations and stomatal conductance (Wahid *et al.*, 2007). At the whole plant level, heat stress impacts leaf area, leaf abscission, visible foliar damage (Cunningham & Read, 2006), budburst, growth, mortality, and reproduction (Teskey *et al.*, 2015). In response to high temperature stress, plants use assimilated carbon/photosynthate to produce compounds used for repair, defense, and physiological recovery such as primary and secondary metabolites, antioxidants, osmolytes, and

phytohormones (Bita & Gerats, 2013). However, we have limited knowledge of how plant carbon allocation is altered in response to heat stress.

Non-structural carbohydrates (NSCs) traditionally include starch and free sugars (sucrose, glucose, and fructose) and are involved in growth, storage, reproduction, metabolism, and repair (Kozlowski, 1992). Although NSCs play a role in plant responses to environmental stress (Dietze *et al.*, 2014) and it is understood that high temperature shifts carbon metabolism enzymes, starch accumulation, and sucrose synthesis (Ruan *et al.*, 2010; Bita & Gerats, 2013), the role of NSCs in the response to and recovery from heat stress is poorly understood due to conflicting results (Génard *et al.*, 2008; Sala *et al.*, 2012). For example, NSCs may increase in response to heat stress because NSCs are used for repair and damage prevention (Roitsch & González, 2004; Couée *et al.*, 2006; Sugio *et al.*, 2009; Sevanto & Dickman, 2015), and therefore are associated with heat stress tolerance (Liu & Huang, 2000; Niinemets, 2010). In contrast, leaf NSCs have also been shown to decrease in response to heat stress due to reduced carbon gain and assimilation (i.e. decreased supply) by inhibited photosynthesis and stomatal conductance (Zhao *et al.*, 2013), and/or increased utilization (i.e. increased demand) by increased respiration and metabolic maintenance (Duan *et al.*, 2013).

These divergent observations of NSC responses to heat stress may be due to variation in the severity of the heat stress, which influences the extent of damage and the capacity to recover. Based on the findings of Bauweraerts *et al.* (2013, 2014), episodic heat wave events produced more stress than a constant increase in temperature, emphasizing the importance of considering duration and intensity of heat stress when predicting plant responses and the capacity to recover. Heat stress severity is a function

of intensity (exposure temperature) and duration of exposure (Colombo & Timmer, 1992). Bauweraerts *et al.* (2014) found that growth of *Quercus* seedlings increased in a +6ºC treatment but decreased in a +12ºC treatment. Therefore, it is expected that NSC dynamics would also be influenced by heat stress severity, although this remains unknown. Given that even short heat events can have substantial impacts on carbon gain (Filewod & Thomas, 2014), the predicted fluctuations in the duration of summer heat waves (Della-Marta *et al.*, 2007), and the paucity of studies manipulating heat stress duration, research on the effects of heat stress duration on physiological recovery and NSC dynamics is needed. NSC dynamics in *C. arabica* are tightly linked to sink demand from vegetative and reproductive growth (Génard *et al.*, 2008; Chaves *et al.*, 2012; Ramalho *et al.*, 2013), and many studies have investigated whether NSC levels regulate *C. arabica* photosynthesis (Vaast *et al.*, 2005; Franck *et al.*, 2006; Ronchi *et al.*, 2006; Batista *et al.*, 2011; DaMatta *et al.*, 2016). However, to our knowledge no study has investigated the impacts of heat stress-induced reductions in photosynthesis as a cause rather than a consequence of NSC dynamics in *C. arabica*.

Previous work has shown that thermotolerance of tropical species measured with chlorophyll fluorescence increases with leaf age, an evolutionary adaptation to protect older and longer-lived foliage from irreversible damage (Yamada *et al.*, 1996; Zhang *et al.*, 2012). This pattern was also observed on detached *C. arabica* leaf discs (Marias *et al.*, 2016). Because NSCs have been linked to heat stress responses and heat tolerance (Liu & Huang, 2000), NSCs may influence the ability of plants to avoid permanent damage, to tolerate heat stress, and/or to recover from heat stress. Therefore, leaf age-related differences in thermotolerance and the ability to recover from heat stress may be

related to NSC dynamics (Filewod & Thomas, 2014; Teskey *et al.*, 2015). However, this has not been investigated in *C. arabica* plants *in situ*.

The goal of this study was to investigate how leaf age and heat stress duration influence NSC dynamics and physiological responses to and recovery from heat stress in *C. arabica*. We exposed treated plants to a simulated sudden heat wave at 49ºC in a growth chamber for two different heat stress durations (45 min, 90 min) and monitored physiological responses and recovery in expanding and mature leaves for 50 days after treatment using gas exchange, chlorophyll fluorescence, and leaf NSCs. Because *C. arabica* is grown in both sun and shade (DaMatta *et al.*, 2007) and to put this study in the context of a combined heat and drought scenario, we used a leaf energy balance model to investigate the effects of reduced stomatal conductance on leaf temperature in partial and full sun conditions. We hypothesized that 1) mature leaves would exhibit less physiological damage and/or faster recovery than expanding leaves, and 2) the 90 min heat stress duration would result in greater physiological damage and/or slower recovery than the 45 min heat stress duration.

3.3 Materials & Methods

Plant material

Coffea arabica L. (Eritrean Mokka) plants about 6-9 months old, obtained from the Hawaii Agriculture Research Center in January 2014, were grown in a peat-perlite-pumice growing mix (Sunshine LA4P) in 9.6 L pots in a greenhouse in Corvallis, Oregon. Supplemental metal halide and high-pressure sodium lighting (400 watts) was used to maintain a 12-hour photoperiod during fall and winter months. The first round of

experiments began 21 July 2014 and the second round began 19 August 2014. Plants were ~1 m tall. During the sampling rounds, average daytime temperature was 23.5ºC, average nighttime temperature 18.1ºC, average daytime relative humidity 64%, average nighttime relative humidity 79%, and average daily maximum photosynthetically active radiation (PAR) was 325 µmol m^{-2} s^{-1}. Due to controlled greenhouse conditions, temperature, relative humidity, and PAR did not substantially differ between rounds (Appendix Table 3.1, Appendix Figure 3.1). Plants were kept well-watered and fertilized once every two weeks (Miracle-Gro All-Purpose Liquid Plant Food, 12%N, 4%P_2O_5, 8%K_2O).

C. arabica is a tropical evergreen species that continually produces new flushes of leaves year-round. Leaf age class (expanding, mature) was determined by visually dividing a mid-canopy plagiotropic branch into thirds where leaf age sequence increased from the outermost leaves to the base of the branch (e.g. Wright *et al.* 2006). Leaves in the outer third were the youngest and still expanding (expanding) and leaves in the inner third were the oldest, fully expanded, and mature (mature). Mean photosynthesis values were 6.3 µmol m^{-2} s^{-1} and 7.0 µmol m^{-2} s^{-1} for expanding and mature leaves, respectively, consistent with previously reported values for *C. arabica* (DaMatta *et al.*, 2007).

Heat stress duration treatments

Plants were exposed to 49ºC in a growth chamber (Model I-35LVL, Percival, Boone, IA) that accommodated two plants at a time and was equipped with cool white lighting (PAR=25 µmol m^{-2} s^{-1}). The treatment temperature of 49°C was selected based on the temperature at which a 50% reduction in initial chlorophyll fluorescence occurred

(49.0 ± 0.5°C) on *C. arabica* leaf discs (Marias *et al.*, 2016). Preliminary experiments at other temperatures also showed that 49°C induced enough heat stress to be damaging without completely scorching/killing leaves, allowing us to monitor recovery. Plants were watered to drainage directly before treatment to avoid drought effects and to buffer changes in soil temperature during treatment. Fine-wire thermocouples measured air, leaf, and soil (~10 cm depth) temperatures during treatment exposure (Appendix Figure 3.2). Pots were completely wrapped with reflective bubble wrap to isolate the soil and roots from heat exposure. This prevented soil temperatures from exceeding 30ºC (Appendix Figure 3.2), which is realistic for soil temperatures in summer (Zheng *et al.*, 1993). Two plants were heated for 45 min and two different plants were heated for 90 min on the same day in two experimental rounds: one on 21 July 2014 and one on 19 August 2014 (N=2 per round). Control (0 min) plants were not exposed to a temperature treatment (N=4 per round). Rounds were combined (N=4 for treated plants, N=8 for controls) because environmental conditions (Appendix Figure 3.1, Appendix Table 3.1) and physiological measurements did not differ between rounds. The growth chamber did not have the capability to adjust light levels. Although light can influence chlorophyll fluorescence (Ludlow, 1987; Buchner *et al.*, 2013), we assumed that the low light levels for the 45 min or 90 min treatment duration did not substantially influence results. Photosynthesis, chlorophyll fluorescence, and foliar NSC content were monitored in control and treated plants prior to treatment (day 0) and 2, 15, 25, and 50 days after treatment. Three leaves per leaf age class per individual plant were marked for re-sampling. When leaf drop occurred, an intact leaf was selected and marked for re-sampling for the remainder of the experiment.

Photosynthesis and stomatal conductance measurements

Photosynthesis and stomatal conductance were measured in the morning during active gas exchange (before afternoon stomatal closure occured) between 0700-1000 h (dawn was ~0500 h) on 1-3 marked leaves per leaf age class per individual plant using a portable photosynthesis system (LI-6400, Li-Cor, Lincoln, NE, USA). The ratio of photosynthesis to stomatal conductance (A/g_s), an estimate of intrinsic water use efficiency (i*WUE,* Jones, 2009) was calculated. In the cuvette, PAR was set to 500 µmol m^{-2} s^{-1}, leaf temperature was set to 25°C, [CO_2] sample was set to 400 µmol mol^{-1} (to represent ambient atmospheric [CO_2]), and flow rate was set to 500 µmol s^{-1}. Day 0 photosynthesis values were estimated from photosynthesis-intercellular CO_2 (C_i) curves. To compare intrinsic photosynthesis at the ambient atmospheric [CO_2] of 400 µmol mol^{-1}, photosynthesis was estimated at the average C_i value of the control (0 min) group averaged over all sampling days, which was 246 µmol mol^{-1} for expanding leaves and 254 µmol mol^{-1} for mature leaves.

Chlorophyll fluorescence measurements

Chlorophyll fluorescence was measured on 1-3 marked leaves per leaf age class per individual plant at ambient temperature with a portable pulse-amplitude modulated chlorophyll fluorometer (Mini-PAM, Heinz Walz Gmbh, Germany) at predawn to ensure leaves were dark-adapted. Chlorophyll fluorescence was measured as the ratio of variable to maximum fluorescence (F_V/F_M) in the convention of Maxwell & Johnson (2000).

F_V/F_M measures the maximum quantum efficiency of PSII photochemistry (Genty *et al.*, 1989) and is calculated as:

$$\frac{F_V}{F_M} = \frac{F_M - F_O}{F_M} = 1 - \frac{F_O}{F_M} \quad (1)$$

A measuring light (red light-emitting diode, 650 nm, 0.15 µmol m^{-2} s^{-1} PAR) with a pulse-width of 3 µs was turned on at a pulse modulation frequency of 0.6 kHz to induce the minimal level of fluorescence (F_O). F_V/F_M was then determined by applying a 0.8 s saturating pulse of white light (18000 µmol photons m^{-2} s^{-1} PAR), which transiently closed all PSII reaction centers (preventing any photochemical processes from occurring), minimized heat dissipation (since leaves were dark-adapted), and induced maximum and variable fluorescence.

Non-structural carbohydrate (NSC) analysis

One leaf per age class per individual plant was collected early morning (directly after F_V/F_M measurements were made) on each sampling date, immediately put on ice in a cooler, and transported to the nearby laboratory where samples were microwaved for 90 s to stop all enzymatic activity and oven-dried at 75ºC. Samples were stored in a freezer before being ground to a fine powder. Leaf samples were analyzed for content of total NSC, starch, sucrose, and glucose + fructose as described by Woodruff & Meinzer (2011). Water was added to the powdered samples and NSC was extracted from the solutions by heating them in steam for 1.5 h. The concentration of free glucose + fructose was determined photometrically on a 96-well microplate photometer (Multiskan FC, Thermo Scientific, Waltham, MA, USA) after enzymatic conversion of glucose +

fructose to gluconate-6-phosphate. Samples were hydrolyzed by enzymatic treatment: invertase for sucrose and amyloglucosidase for total NSC. Photometric analysis was based on absorbance of samples at 340 nm in solution with reference to the absorbance of a glucose reference solution. Total NSC was calculated as the sum of starch, sucrose, and glucose + fructose. NSC values (mg g^{-1} dry weight) are presented in figures as % dry weight.

Leaf energy balance model

A simple leaf energy balance model created by Kevin Tu (http://landflux.org/Tools.php) was used to estimate the effect of shifts in stomatal conductance (g_s) on leaf temperature (T_{leaf}). The modified leaf energy balance equation from Sridhar & Elliott (2002), Monteith & Unsworth (2007), and Jones (2013) is described in detail in Appendices and Appendix Table 3.1. To investigate the effect of changes in g_s at representative heat wave temperatures potentially experienced by *C. arabica* in the tropics, air temperatures (T_{air}) of 35°C, 40°C, and 45°C were used in the model. The range of g_s values used was 0-0.15 mol m^{-2} s^{-1}, similar to that observed in this study as well as previously reported values for field grown *C. arabica* (Meinzer *et al.*, 1990; Gutierrez & Meinzer, 1994; Silva *et al.*, 2004). Environmental and leaf parameters were set to represent conditions experienced by *C. arabica* in the tropics: short wave radiation (SWR) was 600 W m^{-2} and 1000 W m^{-2} to simulate partial and full sun conditions, respectively, wind speed was 2.0 m s^{-1}, relative humidity was 65%, leaf angle was 20° from horizontal, absorptance to SWR was 0.50, emissivity was 0.96, and leaf length in the direction of wind was 100 mm. Incident photosynthetically active radiation

(PAR) for each SWR level at a wavelength of 550 nm (average wavelength for the 400-700 nm PAR range): ~1380 and ~2300 µmol m^{-2} s^{-1}, respectively. PAR is assumed ~50% of SWR (Britton & Dodd, 1976).

Statistical analysis

A three-way factorial linear mixed-effects model was developed with leaf age, treatment, and day as main fixed effects. Nested random effects in the model were plant and leaf within plant. Response variables were: photosynthesis, stomatal conductance, i*WUE*, F_V/F_M, total NSC, starch, sucrose, and glucose + fructose. To choose a correlation structure that would account for the repeated measurements of leaves within plants through time, four models that allowed for different residual correlation structures were fit and selected based on the minimum Bayesian Information Criterion (BIC) value. Assumptions of constant variance and normality were checked using residual and quantile-quantile plots. Log transformations were necessary to meet assumptions for starch and glucose + fructose. For ease of interpretation, we present back-transformed data in results and figures. All interactive and main effects of factors on the response were tested using marginal F-tests (also known as Type III tests) that account for unbalanced sample sizes. Posthoc comparisons were made using a 95% confidence interval and $P<0.05$. Due to sufficient degrees of freedom, we did not make multiple comparisons corrections. If no significant differences between leaf age classes existed, NSC components of expanding and mature leaves were combined by averaging over leaf age to simplify data visualization.

The slope of F_V/F_M recovery was determined for each plant by fitting a line of best fit (linear regression) from the F_V/F_M value two days after treatment (i.e. the minimum F_V/F_M value or maximum damage after treatment) through the day at which F_V/F_M recovered to day 0 values. The slope of recovery was log-transformed and its relationship with the F_V/F_M two days after treatment was described by a logarithmic nonlinear regression equation (f=y0 + a*ln(abs(x)). A two-way factorial linear mixed effects model was developed with leaf age and treatment as main fixed effects for slope of recovery and minimum F_V/F_M as response variables. Procedures to select a correlation structure and check assumptions were the same as stated above.

Pearson product-moment correlation was used to quantify the strength of the relationship between photosynthesis and each NSC component (total NSC, starch, sucrose, glucose + fructose) within each treatment group (control (0 min), 45 min 90 min) for all days sampled. Statistical analyses were conducted in SigmaPlot 13.0 (Systat Software, San Jose, CA, USA) and R version 3.2.3 (2015-12-10, The R Foundation for Statistical Computing).

3.4 Results

Both the 45 min and 90 min treatments induced significant shifts in gas exchange, F_V/F_M, and NSC content and dynamics. It was also observed that after the experiment, the controls (0 min) produced flowers and fruits whereas the 45 min and 90 min treatment groups did not.

Gas exchange and F_V/F_M

Interactions among the main effects (age, treatment, day) on photosynthesis and F_V/F_M are summarized in Table 3.1. Photosynthesis significantly declined two days after treatment in both the 45 min and 90 min groups for both expanding and mature leaves but slower recovery to control values in the 90 min group compared to the 45 min group (Figure 3.1A,C). Photosynthesis of mature leaves in the 45 min group recovered to control values by day 15 while that of the 90 min group recovered by day 25. In contrast, expanding leaves took longer to recover to control values than mature leaves regardless of treatment with photosynthesis of the 45 min group recovering by day 25 and that of the 90 min group recovering by day 50. Within-day and -treatment differences between leaf age classes were variable. Like photosynthesis, F_V/F_M also declined two days after treatment, yet the amount of the reduction in F_V/F_M two days after treatment was significantly greater in the 90 min group than the 45 min group in both leaf age classes (Figure 3.1B,D). Regardless of leaf age class, F_V/F_M of the 45 min group recovered to control values by day 15 while the 90 min group did not fully recover by day 50, similar to the slower recovery of the 90 min group compared to the 45 min group as measured with photosynthesis.

The log-transformed slope of recovery (ln(slope of recovery) back to control values significantly decreased with increasing damage assessed with F_V/F_M two days after treatment ($P=0.0007$, $R^2=0.57$, Figure 3.2). Mean ln(slope of recovery) did not differ among leaf age classes ($P= 0.86$) but significantly differed between treatments where the 90 min treatment exhibited a significantly lower ln(slope of recovery) than the 45 min treatment ($P=0.002$). Similarly, the mean damage assessed with F_V/F_M two days

after treatment was significantly greater in the 90 min group compared to the 45 min group (P=0.006).

Although mean post-treatment stomatal conductance (g_s) of expanding leaves exhbited a decline similar to that of photosynthesis (*A*, Figure 3.1) , mean post-treatment g_s of mature leaves did not significantly differ among treatments (P>0.05, Figure 3.3A,C). This influenced mean post-treatment intrinsic water-use efficiency (A/g_s) where expanding leaves of the 90 min group had a significantly lower mean A/g_s than the control and 45 min groups, and mature leaves of the 90 min group had significantly lower mean A/g_s than the controls (Figure 3.3B,D).

The leaf energy balance model results showed that T_{leaf}-T_{air} increased with decreasing g_s in both partial (600 W m^{-2}) and full (1000 W m^{-2}) sun conditions (Figure 3.4A,B). T_{leaf} was consistently greater in full sun (Figure 3.4B) than partial sun (Figure 3.4A). Even at higher values of g_s (e.g. 0.15 mol m^{-2} s^{-1}), T_{leaf} in full sun at T_{air} of 35°C-45°C (Figure 3.4B) was 42.0°C-51.2°C. Mean post-treatment g_s of expanding leaves of control plants was 0.0796 mol m^{-2} s^{-1} and treated plants was 0.0451 mol m^{-2} s^{-1} (Figure 3.3B). The model estimated that this observed heat stress-induced reduction in g_s (denoted by vertical lines in Figure 3.4A,B) would yield: at T_{air} of 35°C, T_{leaf} of 41.6°C in partial sun and T_{leaf} of 44.5°C in full sun; at T_{air} of 40°C, T_{leaf} of 46.6°C in partial sun and T_{leaf} of 49.5°C in full sun; and at T_{air} of 45°C, T_{leaf} of 51.7°C in partial sun and T_{leaf} of 54.5°C in full sun (Figure 3.4A,B).

Non-structural carbohydrates (NSCs)

NSC dynamics differed significantly across all three treatment groups (controls (0 min), 45 min, 90 min; Figure 3.5, 6). Interactions among the main effects (age, treatment, day) on total NSC, starch, sucrose, and glucose + fructose are summarized in Table 3.2. Due to lack of significant leaf age-related differences within day and treatment, total NSC, starch, and sucrose of expanding and mature leaves were combined by averaging over leaf age to simplify data visualization (Figure 3.5). Total NSC and starch in the controls steadily declined with time and were significantly less than day 0 values by day 50 (Figure 3.5A,B). In the 45 min group, total NSC and starch significantly declined two days after treatment and were significantly less than that of any other day. At days 15 and 25, total NSC and starch of the 45 min group significantly increased and became significantly greater than that of the control and 90 min groups (Figure 3.5A,B). In contrast to the control and 45 min groups, total NSC and starch of the 90 min group did not significantly change with day (Figure 3.5A,B).

Sucrose of the control and 45 min groups did not significantly change with day (Figure 3.5C). In contrast, sucrose of the 90 min group was significantly greater than that of controls two days after treatment before significantly declining and becoming significantly less than day 0 values at day 50 (Figure 3.5C). Although sucrose of the 45 min group did not significantly change with day, it was significantly greater than that of controls and the 90 min group at days 15 and 25, and that of the 90 min group at day 50.

In contrast to total NSC, starch, and sucrose, glucose + fructose were significantly affected by leaf age ($F=52.792$, $P<0.0001$, Table 3.2) but did not significantly differ among treatments nor with day in either age class (Figure 3.6A,B), Glucose + fructose of

controls was greater in expanding leaves than mature leaves at days 0, 15, 25, and in the 45 min group at day 2. There were no age differences in the 90 min group.

Pearson product-moment correlation indicated significant positive associations between photosynthesis and total NSC (r=0.409, P=0.00145, Table 3.3), and between photosynthesis and starch in the controls (r=0.362, P=0.00530, Table 3.3), and between photosynthesis and starch in the 45 min group (r=0.332, P=0.0445, Table 3.3). In contrast, photosynthesis was not significantly related to any NSC component in the 90 min group (P>0.05, Table 3.3).

3.5 Discussion

Implications for combined heat and drought scenarios

The sudden heat stress disrupted coordination between A and g_s, leading to declining i*WUE* (A/g_s) with increasing heat stress duration in both expanding and mature leaves (Figure 3.3). Under a combined heat and drought scenario expected throughout the 21st century (IPCC, 2014), sudden heat-induced reductions in the ratio of carbon gain to water loss could accelerate the point at which drought, even in the absence of heat, would further restrict carbon gain (Chaves *et al.*, 2002). Persistent reductions in g_s and therefore evaporative cooling (Monteith, 1981; Ball *et al.*, 1988; Schymanski *et al.*, 2013) of expanding leaves on heat-stressed plants undergoing drought would place them at additional risk of further heat damage in closely spaced heat waves. The leaf energy balance model indicated that the extent to which T_{leaf} would increase in response to reduced g_s would be greatest at higher T_{air} (e.g. 45°C) compared to lower T_{air} (e.g. 35°C) and in full compared to partial sun (Figure 3.4A,B). T_{leaf} was especially sensitive to

changes in g_s at relatively low g_s, which would be expected during drought. For example, at T_{air} of 45°C and g_s of ~0.04 mol m^{-2} s^{-1} as observed in expanding leaves of the treatment groups (Figure 3.3A), T_{leaf} would be ~51.7°C in partial sun (Figure 3.A) and ~54.5°C in full sun (Figure 3.4B). These temperatures would cause significant damage, if not death, because the temperature causing a 90% reduction in initial F_V/F_M estimated from chlorophyll fluorescence thermotolerance curves was 50.1°C in expanding leaves and 54.1°C in mature leaves (data not shown, see Marias *et al.*, 2016). A factor not considered in the leaf energy balance model was stomatal sensitivity to VPD. Photosynthesis and g_s in *C. arabica* decline with increasing VPD (Oren *et al.*, 1999) that typically ranges from 1.0-3.5 kPa throughout the day (Ronquim *et al.*, 2006). This VPD-related decline in g_s would further increase T_{leaf} and therefore the risk of damaging heat stress. In contrast to expanding leaves, mature leaves maintained relatively high g_s and relatively high intercellular [CO_2] across all treatments, which may have contributed to the faster recovery of *A* than F_V/F_M in mature leaves (Figure 3.1). However, plants experiencing drought would not be able to maintain relatively high g_s without risking hydraulic failure and death (Adams *et al.*, 2009). Therefore, recovery from heat stress would likely be inhibited during drought.

Greater sensitivity to heat stress in expanding leaves

Consistent with our first hypothesis, mature leaves showed faster recovery of photosynthesis than expanding leaves (Figure 3.1). However, the extent of damage as measured with photosynthesis at day 2 did not differ between leaf age classes nor treatment, suggesting that leaf age may influence the capacity to recover more than the

extent of damage incurred, although both characteristics influence the ability to withstand heat stress (Escandón *et al.*, 2016). Consistent with our second hypothesis, the 90 min duration of heat stress resulted in both greater physiological damage and slower recovery than the 45 min group as measured with F_V/F_M, and slower recovery as measured with photosynthesis (Figure 3.1). This was due to the apparent slower rate of F_V/F_M recovery and greater damage at day 2 induced by the 90 min treatment than the 45 min treatment (Figure 3.1, 2). Taken together, these results showed that leaf age affected the recovery rate of photosynthesis but not that of F_V/F_M, suggesting that PSII photochemistry may be conserved across different leaf ages in low light (Ishida *et al.*, 1999), and that longer lived foliage may be protected by the greater capacity of older leaves to photosynthetically recover (Yamada *et al.*, 1996). The declines in F_V/F_M indicate that F_O increased and/or F_V decreased, both of which indicate stress-induced changes to photochemistry including PSII inactivation, photodamage, heat dissipation, photoinhibition or damage to the oxygen evolving complex and water splitting system that disrupts electron donation to PSII reaction centers (Yamashita & Butler, 1968; Schreiber & Berry, 1977; Demmig *et al.*, 1987; Weis & Berry, 1987; Havaux, 1993; Yamada *et al.*, 1996; Maxwell & Johnson, 2000).

In addition to their slower recovery, g_s of expanding leaves declined in the 45 min and 90 min treatments while that of mature leaves did not change with treatment. Besides reducing water loss, this response may reflect the impact of damaged membrane integrity on the ability to maintain g_s (Bita & Gerats, 2013). As discussed above, reduced g_s would exacerbate the effects of heat stress on expanding leaves by further increasing their temperature and putting them at greater risk of additional heat-induced damage.

Interestingly, total NSC, starch, and sucrose content were not significantly different between leaf age classes (Figure 3.5) suggesting that these components were highly regulated. In contrast, glucose + fructose content was significantly greater in expanding leaves than mature leaves (Figure 3.6), which may occur because free sugars are needed as building blocks for structural carbohydrates (e.g. cellulose, lignin) in cell walls of expanding leaves, whereas sugars in mature leaves have already been allocated to structural carbohydrates required for structural support (Cavatte *et al.*, 2012).

Impact of heat-induced inhibition of flowering on NSC dynamics

In contrast to controls, none of the heat-treated plants produced flowers or fruits. This is not surprising because coffee reproduction is highly sensitive to heat (Camargo, 1985, 2010; Bita & Gerats, 2013). Our results showed that even a short, sudden heat stress event can inhibit reproduction and have negative consequences for *C. arabica* productivity (Davis *et al.*, 2012; Bunn *et al.*, 2014). The treatment temperature of 49°C for 45 min and 90 min durations may occur in the field because leaf temperatures can exceed air temperature by 15-20ºC in sun grown *C. arabica* (Butler, 1977; Alvim & Kozlowski, 2013). This was supported by the leaf energy balance model (Figure 3.4). It is possible that *C. arabica* may acclimate and respond differently to gradual increases in average air temperature as opposed to a sudden heat stress event simulated in this study (Stone & Nicolas, 1995; Zou, 2009; Bauweraerts *et al.*, 2013, 2014). However, dramatic aseasonal fluctuations in temperature are expected to become more frequent in the future (Filewod & Thomas, 2014). Further, elevated ambient [CO_2] may partially mitigate the impacts of high temperature stress on *C. arabica* (Martins *et al.*, 2016; Rodrigues *et al.*,

2016) and *C. arabica* may be able to maintain adequate mineral balance under combined high temperature and elevated [CO2] situations (Martins *et al.*, 2014).F

Because NSCs are utilized for reproduction (e.g. flowers, fruits) in *C. arabica* (Cannell, 1976), the decline in total NSC and starch of controls (Figure 3.5A,B) was likely due to the subsequent formation of flowers and fruits (Chaves *et al.*, 2012). Costa *et al.* (2006) also observed reduced starch in high fruit-bearing plants and no decrease in soluble sugars, consistent with the patterns of starch, sucrose, and glucose + fructose in the flower-bearing control plants in this study.

Since fruit production is the strongest carbohydrate sink in *C. arabica* (Cannell, 1976) and competes with vegetative growth (Amaral *et al.*, 2001; Vaast *et al.*, 2005; DaMatta *et al.*, 2007, 2008), the lack of fruiting in the heat treatments should theoretically result in more NSC available for growth, storage, metabolic maintenance, and repair (Chapin *et al.*, 1990; Kozlowski, 1992; Dietze *et al.*, 2014). This helps elucidate the patterns in total NSC and starch of the 45 min group (Figure 3.5A,B). The sharp but transient reduction in total NSC and starch at day 2 coincided with the treatment-induced reductions in photosynthesis and F_V/F_M, indicating significant heat stress-induced damage and reductions in carbohydrate production (Wahid *et al.*, 2007). The decline in starch with no significant shifts in sucrose and glucose + fructose at day 2 may indicate the allocation of NSC to metabolic maintenance and repair in response to the 45 min treatment (Bita & Gerats, 2013). This may also be due to increased respiration (Way & Yamori, 2014), as well as the remobilization of starch from source leaves to roots (Blessing *et al.*, 2015), although we did not measure NSC in roots. By days 15 and 25, total NSC, starch, and sucrose of the 45 min group had significantly accumulated

compared to controls, coinciding with the full recovery of photosynthesis and F_V/F_M. Due to the lack of demand for reproduction and repair by day 15 and later, carbon supply was greater than carbon demand (Génard *et al.*, 2008) so starch was stored resulting in an increase in total NSC. By day 50, starch and total NSC levels of the 45 min group declined to day 0 values suggesting that the stored NSC may have been utilized for renewed vegetative growth and metabolic maintenance.

Despite the greater damage induced by the 90 min heat treatment compared to the 45 min treatment (Figure 3.1, 2), total NSC, starch, and glucose + fructose of the 90 min group unexpectedly did not change significantly throughout the 50 days of the experiment (Figure 3.5, 6). This may reflect a balance between NSC supply and sink demand in the 90 min treatment. The supply of NSC was likely low due to the ongoing inhibition of photosynthesis and incomplete recovery of photochemistry (F_V/F_M) by day 50 (Figure 3.1). The sink demand in this treatment was also low due to the inhibition of reproduction. In contrast to the other NSC constituents that did not change with time in the 90 min treatment, the transient increase in sucrose content at day 2 may reflect an initial repair or defense response to the substantial damage caused by the 90 min treatment because sucrose has been linked to defense against ROS (Bita & Gerats, 2013), antioxidant production (Couée *et al.*, 2006), osmotic adjustment (Cavatte *et al.*, 2012), and stress response signaling (Sugio *et al.*, 2009; Secchi & Zwieniecki, 2011, 2016; El Sayed *et al.*, 2014; Wang & Ruan, 2016). Also, soluble sugars such as sucrose are among the primary metabolites and osmolytes known to accumulate in response to heat stress (Wahid *et al.*, 2007) and are necessary for protection from elevated temperature and maintaining water balance and membrane stability (Farooq *et al.*, 2008; Bita & Gerats,

2013). Sucrose is translocated from source leaves to sink organs through the phloem and its transient increase in plants subjected to 90 min of heat stress may also be associated with a disruption or inhibition of phloem transport (Sala *et al.*, 2012; Woodruff, 2014; Blessing *et al.*, 2015). The subsequent decline in sucrose after day 2 suggests that the demand for sucrose for repair, renewed growth, and ongoing metabolism was greater than the supply from photosynthesis, which was still inhibited on day 50.

Heat stress duration impacts on NSC dynamics

The observed effect of heat stress duration on PSII photochemistry and photosynthesis was associated with significant impacts on NSC dynamics. Although starch dynamics were presumably linked to reproduction in the control group, and a repair and storage response in the 45 min group, the 90 min group only exhibited shifts in sucrose content in response to treatment. This suggests that the greater duration of heat stress may have made starch inaccessible or overly energy-intensive to utilize (Chapin *et al.*, 1990; Kozlowski, 1992; Dietze *et al.*, 2014) thereby resulting in the use of sucrose to allocate to repair. Escandón *et al.* (2016) also found that soluble sugars seemed more closely associated with plant responses to increasing number of days exposed to heat stress, although they did not measure starch. Interestingly, glucose + fructose was not significantly affected by day or treatment in the 45 min and 90 min groups (Figure 3.6), consistent with Lafta & Lorenzen (1995) that found no effect of temperature on sugar levels in potato and attributed this to coordinated control of sugar metabolism in response to high temperature stress.

Downregulation of photosynthesis has been associated with NSC accumulation in *C. arabica* (e.g. starch in DaMatta *et al.* (1997), sucrose in Franck *et al.* 2006), while other studies have found no link between NSC and photosynthetic downregulation (Silva *et al.*, 2004; Batista *et al.*, 2011; DaMatta *et al.*, 2016). In contrast, we found a positive relationship between starch and photosynthesis in controls and the 45 min group (Table 3.3). These different results may be a consequence of previous studies of NSC and photosynthesis in *C. arabica* having examined NSC as a cause of photosynthetic regulation, whereas in this study we examined changes in NSC dynamics as a consequence of heat stress-induced inhibition of photosynthesis and other physiological processes. The lack of a significant relationship between photosynthesis and starch in the 90 min group suggests a decoupling of starch dynamics and photosynthesis under greater heat stress duration, complicating predictions of plant carbon allocation under increasing temperature stress.

Currently it is not well understood how photosynthate is partitioned under high temperature stress (Wahid *et al.*, 2007). In this study, the differences in NSC dynamics among treatments emphasize that plant carbon utilization is influenced by heat stress duration and may be related to the capacity to recover (Filewod & Thomas, 2014; Teskey *et al.*, 2015). The 45 min treatment that induced less damage and faster recovery exhibited an NSC pattern of repair and storage as indicated by starch dynamics while the 90 min treatment that induced more damage and slower recovery exhibited an NSC pattern of repair and/or phloem transport inhibition as indicated by sucrose dynamics. Expanding leaves were more sensitive to heat stress, exhibited by slower photosynthetic recovery and lower stomatal conductance with increasing heat stress duration, a response

likely to exacerbate heat stress effects during combined heat and drought scenarios. Reproduction and NSC dynamics are tightly linked in *C. arabica* and the heat-induced inhibition of flowering significantly impacted NSC allocation dynamics, making the timing of heat stress at key developmental stages such as reproduction critical for interpreting and predicting responses to heat stress. The investigation of the impacts of heat stress duration and leaf age on NSC dynamics and recovery are essential for understanding plant carbohydrate metabolism and how *C. arabica* may respond to future climate change scenarios.

3.6 Acknowledgements

This work was supported by the NSF Graduate Research Fellowship Program and NSF grant IOS 11-46746. We are grateful to the OSU Greenhouse Operations staff for their assistance with the maintenance of plant material.

3.7 References

Adams HD, Guardiola-Claramonte M, Barron-Gafford GA *et al.* (2009) Temperature sensitivity of drought-induced tree mortality portends increased regional die-off under global-change-type drought. *Proceedings of the National Academy of Sciences of the United States of America*, **106**, 7063–7066.

Alvim P de T, Kozlowski TT (2013) *Ecophysiology of Tropical Crops*. Elsevier, 517 pp.

Amaral J a. T, Matta D, M F, Rena AB (2001) Effects of fruiting on the growth of Arabica coffee trees as related to carbohydrate and nitrogen status and to nitrate reductase activity. *Revista Brasileira de Fisiologia Vegetal*, **13**, 66–74.

Ball M, Cowan I, Farquhar G (1988) Maintenance of Leaf Temperature and the Optimisation of Carbon Gain in Relation to Water Loss in a Tropical Mangrove Forest. *Australian Journal of Plant Physiology*, **15**, 263.

Barnabás B, Jäger K, Fehér A (2008) The effect of drought and heat stress on reproductive processes in cereals. *Plant, cell & environment*, **31**, 11–38.

Batista KD, Araújo WL, Antunes WC, Cavatte PC, Moraes GABK, Martins SCV, DaMatta FM (2011) Photosynthetic limitations in coffee plants are chiefly governed by diffusive factors. *Trees*, **26**, 459–468.

Battisti DS, Naylor RL (2009) Historical Warnings of Future Food Insecurity with Unprecedented Seasonal Heat. *Science*, **323**, 240–244.

Bauweraerts I, Wertin TM, Ameye M, McGuire MA, Teskey RO, Steppe K (2013) The effect of heat waves, elevated [CO2] and low soil water availability on northern red oak (Quercus rubra L.) seedlings. *Global Change Biology*, **19**, 517–528.

Bauweraerts I, Ameye M, Wertin TM, McGuire MA, Teskey RO, Steppe K (2014) Water availability is the decisive factor for the growth of two tree species in the occurrence of consecutive heat waves. *Agricultural and Forest Meteorology*, **189**–**190**, 19–29.

Bita CE, Gerats T (2013) Plant tolerance to high temperature in a changing environment: scientific fundamentals and production of heat stress-tolerant crops. *Frontiers in Plant Science*, **4**.

Blessing CH, Werner RA, Siegwolf R, Buchmann N (2015) Allocation dynamics of recently fixed carbon in beech saplings in response to increased temperatures and drought. *Tree Physiology*, **35**, 585–598.

Bolhar-Nordenkampf H, Long S, Baker N, Oquist G, Schreiber U, Lechner E (1989) Chlorophyll fluorescence as a probe of the photosynthetic competence of leaves in the field: a review of current instrumentation. *Functional Ecology*, 497–514.

Britton CM, Dodd JD (1976) Relationships of photosynthetically active radiation and shortwave irradiance. *Agricultural Meteorology*, **17**, 1–7.

Buchner O, Karadar M, Bauer I, Neuner G (2013) A novel system for in situ determination of heat tolerance of plants: first results on alpine dwarf shrubs. *Plant Methods*, **9**, 7.

Bunn C, Läderach P, Rivera OO, Kirschke D (2014) A bitter cup: climate change profile of global production of Arabica and Robusta coffee. *Climatic Change*, **129**, 89–101.

Butler DR (1977) Coffee Leaf Temperatures in a Tropical Environment. *Acta Botanica Neerlandica*, **26**, 129–140.

Camargo AP (1985) Florescimento e frutificação de café arábica nas diferentes regiões cafeeiras do Brasil. *Pesquisa Agropecuária Brasileira*, **20**, 831–839.

Camargo MBP de (2010) The impact of climatic variability and climate change on arabic coffee crop in Brazil. *Bragantia*, **69**, 239–247.

Cannell M (1976) Crop physiological aspects of coffee bean yield: a review. *Kenya coffee*.

Cavatte PC, Rodríguez-López NF, Martins SCV, Mattos MS, Sanglard LMVP, DaMatta FM (2012) Functional analysis of the relative growth rate, chemical composition, construction and maintenance costs, and the payback time of Coffea arabica L. leaves in response to light and water availability. *Journal of Experimental Botany*, ers027.

Chapin FS, Schulze E, Mooney HA (1990) The Ecology and Economics of Storage in Plants. *Annual Review of Ecology and Systematics*, **21**, 423–447.

Chaves MM, Pereira JS, Maroco J *et al.* (2002) How Plants Cope with Water Stress in the Field? Photosynthesis and Growth. *Annals of Botany*, **89**, 907–916.

Chaves ARM, Martins SCV, Batista KD, Celin EF, DaMatta FM (2012) Varying leaf-to-fruit ratios affect branch growth and dieback, with little to no effect on photosynthesis, carbohydrate or mineral pools, in different canopy positions of field-grown coffee trees. *Environmental and Experimental Botany*, **77**, 207–218.

Colombo S, Timmer V (1992) Limits of Tolerance to High-Temperatures Causing Direct and Indirect Damage to Black Spruce. *Tree Physiology*, **11**, 95–104.

Corlett RT (2011) Impacts of warming on tropical lowland rainforests. *Trends in Ecology & Evolution*, **26**, 606–613.

Costa MJ, Zambolim L, Rodrigues FA (2006) Efeito de níveis de desbaste de frutos do cafeeiro na incidência da ferrugem, no teor de nutrientes, carboidratos e açúcares redutores. *Fitopatologia Brasileira*, **31**, 564–571.

Couée I, Sulmon C, Gouesbet G, Amrani AE (2006) Involvement of soluble sugars in reactive oxygen species balance and responses to oxidative stress in plants. *Journal of Experimental Botany*, **57**, 449–459.

Cramer W, Bondeau A, Woodward FI *et al.* (2001) Global response of terrestrial ecosystem structure and function to CO2 and climate change: results from six dynamic global vegetation models. *Global Change Biology*, **7**, 357–373.

Craparo ACW, Van Asten PJA, Läderach P, Jassogne LTP, Grab SW (2015) Coffea arabica yields decline in Tanzania due to climate change: Global implications. *Agricultural and Forest Meteorology*, **207**, 1–10.

Cunningham SC, Read J (2006) Foliar temperature tolerance of temperate and tropical evergreen rain forest trees of Australia. *Tree Physiology*, **26**, 1435–1443.

DaMatta FM, Ramalho JDC (2006) Impacts of drought and temperature stress on coffee physiology and production: a review. *Brazilian Journal of Plant Physiology*, **18**, 55–81.

DaMatta FM, Maestri M, Mosquim PR, Barros RS (1997) Photosynthesis in coffee (Coffea arabica and C. canephora) as affected by winter and summer conditions. *Plant Science*, **128**, 43–50.

DaMatta FM, Ronchi CP, Maestri M, Barros RS (2007) Ecophysiology of coffee growth and production. *Brazilian Journal of Plant Physiology*, **19**, 485–510.

DaMatta FM, Cunha RL, Antunes WC, Martins SCV, Araujo WL, Fernie AR, Moraes GABK (2008) In field-grown coffee trees source–sink manipulation alters photosynthetic rates, independently of carbon metabolism, via alterations in stomatal function. *New Phytologist*, **178**, 348–357.

DaMatta FM, Godoy AG, Menezes-Silva PE *et al.* (2016) Sustained enhancement of photosynthesis in coffee trees grown under free-air CO2 enrichment conditions: disentangling the contributions of stomatal, mesophyll, and biochemical limitations. *Journal of Experimental Botany*, **67**, 341–352.

Davis AP, Gole TW, Baena S, Moat J (2012) The impact of climate change on indigenous arabica coffee (Coffea arabica): predicting future trends and identifying priorities. *PLoS One*, **7**, e47981.

Della-Marta PM, Haylock MR, Luterbacher J, Wanner H (2007) Doubled length of western European summer heat waves since 1880. *Journal of Geophysical Research: Atmospheres*, **112**, D15103.

Demmig B, Winter K, Krüger A, Czygan FC (1987) Photoinhibition and zeaxanthin formation in intact leaves : a possible role of the xanthophyll cycle in the dissipation of excess light energy. *Plant Physiology*, **84**, 218–224.

Dietze MC, Sala A, Carbone MS, Czimczik CI, Mantooth JA, Richardson AD, Vargas R (2014) Nonstructural carbon in woody plants. *Annual Review of Plant Biology*, **65**, 667–687.

Diffenbaugh NS, Scherer M (2011) Observational and model evidence of global emergence of permanent, unprecedented heat in the 20th and 21st centuries. *Climatic Change*, **107**, 615–624.

Duan H, Amthor JS, Duursma RA, O'Grady AP, Choat B, Tissue DT (2013) Carbon dynamics of eucalypt seedlings exposed to progressive drought in elevated [CO2] and elevated temperature. *Tree Physiology*, tpt061.

El Sayed AI, Rafudeen MS, Golldack D (2014) Physiological aspects of raffinose family oligosaccharides in plants: protection against abiotic stress. *Plant Biology*, **16**, 1–8.

Escandón M, Cañal MJ, Pascual J, Pinto G, Correia B, Amaral J, Meijón M (2016) Integrated physiological and hormonal profile of heat-induced thermotolerance in Pinus radiata. *Tree Physiology*, **36**, 63–77.

Farooq M, Basra SMA, Wahid A, Cheema ZA, Cheema MA, Khaliq A (2008) Physiological Role of Exogenously Applied Glycinebetaine to Improve Drought Tolerance in Fine Grain Aromatic Rice (Oryza sativa L.). *Journal of Agronomy and Crop Science*, **194**, 325–333.

Filewod B, Thomas SC (2014) Impacts of a spring heat wave on canopy processes in a northern hardwood forest. *Global change biology*, **20**, 360–371.

Franck N, Vaast P, Génard M, Dauzat J (2006) Soluble sugars mediate sink feedback down-regulation of leaf photosynthesis in field-grown Coffea arabica. *Tree Physiology*, **26**, 517–525.

Génard M, Dauzat J, Franck N, Lescourret F, Moitrier N, Vaast P, Vercambre G (2008) Carbon allocation in fruit trees: from theory to modelling. *Trees*, **22**, 269–282.

Genty B, Briantais J-M, Baker NR (1989) The relationship between the quantum yield of photosynthetic electron transport and quenching of chlorophyll fluorescence. *Biochimica et Biophysica Acta (BBA)-General Subjects*, **990**, 87–92.

Hao Z, AghaKouchak A, Phillips TJ (2013) Changes in concurrent monthly precipitation and temperature extremes. *Environmental Research Letters*, **8**, 34014.

Havaux M (1993) Characterization of thermal damage to the photosynthetic electron transport system in potato leaves. *Plant Science*, **94**, 19–33.

Intergovernmental Panel on Climate Change (2014) IPCC Fifth Assessment Synthesis Report. *IPCC 5th Assessment Synthesis Report*.

International Coffee Organization (2016) The Current State of the Global Coffee Trade | #CoffeeTradeStats.

Ishida A, Uemura A, Koike N, Matsumoto Y, Hoe AL (1999) Interactive effects of leaf age and self-shading on leaf structure, photosynthetic capacity and chlorophyll fluorescence in the rain forest tree, Dryobalanops aromatica. *Tree Physiology*, **19**, 741–747.

Jones HG (2009) What is water use efficiency? In: Bacon M (ed) Water use efficiency in plant biology. Blackwell Publishing, Oxford, UK, pp. 27-41.

Jones HG (2013) *Plants and microclimate: a quantitative approach to environmental plant physiology*. Cambridge university press.

Knoerr KR, Gay LW (1965) Tree Leaf Energy Balance. *Ecology*, **46**, 17–24.

Kozlowski T (1992) Carbohydrate sources and sinks in woody plants. *The Botanical Review*, **58**, 107–222.

Krause GH (1988) Photoinhibition of photosynthesis. An evaluation of damaging and protective mechanisms. *Physiologia Plantarum*, **74**.

Lafta AM, Lorenzen JH (1995) Effect of High Temperature on Plant Growth and Carbohydrate Metabolism in Potato. *Plant Physiology*, **109**, 637–643.

Liu X, Huang B (2000) Heat Stress Injury in Relation to Membrane Lipid Peroxidation in Creeping Bentgrass. *Crop Science*, **40**, 503.

Ludlow M (1987) Light stress at high temperature. *Photoinhibition. Elsevier, Amsterdam*, 89–110.

Marias DE, Meinzer FC, Still C (2016) Leaf age and methodology impact assessments of thermotolerance of Coffea arabica. *Trees*.

Martins LD, Tomaz MA, Lidon FC, DaMatta FM, Ramalho JC (2014) Combined effects of elevated [CO2] and high temperature on leaf mineral balance in Coffea spp. plants. *Climatic Change*, **126**, 365–379.

Martins MQ, Rodrigues WP, Fortunato AS *et al.* (2016) Protective Response Mechanisms to Heat Stress in Interaction with High [CO2] Conditions in Coffea spp. *Plant Physiology*, 947.

Maxwell K, Johnson GN (2000) Chlorophyll fluorescence—a practical guide. *Journal of experimental botany*, **51**, 659–668.

Monteith JL (1981) Evaporation and surface temperature. *Quarterly Journal of the Royal Meteorological Society*, **107**, 1–27.

Monteith J, Unsworth M (2007) *Principles of environmental physics*. Academic Press.

Niinemets Ü (2010) Responses of forest trees to single and multiple environmental stresses from seedlings to mature plants: Past stress history, stress interactions, tolerance and acclimation. *Forest Ecology and Management*, **260**, 1623–1639.

Oren R, Sperry JS, Katul G, Pataki DE, Ewers B, Phillips N, Schäfer K (1999) Survey and synthesis of intra-and interspecific variation in stomatal sensitivity to vapour pressure deficit. *Plant, Cell & Environment*, **22**, 1515–1526.

Ramalho JC, Rodrigues AP, Semedo JN *et al.* (2013) Sustained Photosynthetic Performance of Coffea spp. under Long-Term Enhanced [CO 2]. *PLOS ONE*, **8**, e82712.

Rodrigues WP, Martins MQ, Fortunato AS *et al.* (2016) Long-term elevated air [CO2] strengthens photosynthetic functioning and mitigates the impact of supra-optimal temperatures in tropical Coffea arabica and C. canephora species. *Global change biology*, **22**, 415–431.

Roitsch T, González M-C (2004) Function and regulation of plant invertases: sweet sensations. *Trends in plant science*, **9**, 606–613.

Ronchi CP, DaMatta FM, Batista KD, Moraes GABK, Loureiro ME, Ducatti C (2006) Growth and photosynthetic down-regulation in Coffea arabica in response to restricted root volume. *Functional Plant Biology*, **33**, 1013–1023.

Ronquim J, Prado C, Novaes P, Fahl J, Ronquim C (2006) Carbon gain in Coffea arabica during clear and cloudy days in the wet season. *Experimental agriculture*, **42**, 147–164.

Ruan Y-L, Jin Y, Yang Y-J, Li G-J, Boyer JS (2010) Sugar input, metabolism, and signaling mediated by invertase: roles in development, yield potential, and response to drought and heat. *Molecular Plant*, **3**, 942–955.

Sala A, Woodruff DR, Meinzer FC (2012) Carbon dynamics in trees: feast or famine? *Tree Physiology*, tpr143.

Schreiber U, Berry JA (1977) Heat-induced changes of chlorophyll fluorescence in intact leaves correlated with damage of the photosynthetic apparatus. *Planta*, **136**, 233–238.

Schymanski SJ, Or D, Zwieniecki M (2013) Stomatal Control and Leaf Thermal and Hydraulic Capacitances under Rapid Environmental Fluctuations. *PLOS ONE*, **8**, e54231.

Secchi F, Zwieniecki MA (2011) Sensing embolism in xylem vessels: the role of sucrose as a trigger for refilling. *Plant, Cell & Environment*, **34**, 514–524.

Secchi F, Zwieniecki MA (2016) Accumulation of sugars in the xylem apoplast observed under water stress conditions is controlled by xylem pH. *Plant, Cell & Environment*.

Sevanto S, Dickman LT (2015) Where does the carbon go?—Plant carbon allocation under climate change. *Tree physiology*, **35**, 581–584.

Silva EA, DaMatta FM, Ducatti C, Regazzi AJ, Barros RS (2004) Seasonal changes in vegetative growth and photosynthesis of Arabica coffee trees. *Field Crops Research*, **89**, 349–357.

Sridhar V, Elliott RL (2002) On the development of a simple downwelling longwave radiation scheme. *Agricultural and Forest Meteorology*, **112**, 237–243.

Stone P, Nicolas M (1995) Comparison of Sudden Heat Stress With Gradual Exposure to High Temperature During Grain Filling in Two Wheat Varieties Differing in Heat Tolerance. I. Grain Growth. *Australian Journal of Plant Physiology*, **22**, 935.

Sugio A, Dreos R, Aparicio F, Maule AJ (2009) The cytosolic protein response as a subcomponent of the wider heat shock response in Arabidopsis. *The Plant Cell*, **21**, 642–654.

Teketay D (1999) History, botany and ecological requirements of coffee. *Walia*, **20**, 28–50.

Teskey R, Wertin T, Bauweraerts I, Ameye M, Mcguire MA, Steppe K (2015) Responses of tree species to heat waves and extreme heat events. *Plant, Cell & Environment*, **38**, 1699–1712.

Vaast P, Angrand J, Franck N, Dauzat J, Génard M (2005) Fruit load and branch ring-barking affect carbon allocation and photosynthesis of leaf and fruit of Coffea arabica in the field. *Tree Physiology*, **25**, 753–760.

Wahid A, Gelani S, Ashraf M, Foolad MR (2007) Heat tolerance in plants: an overview. *Environmental and experimental botany*, **61**, 199–223.

Wang L, Ruan Y-L (2016) Shoot–root carbon allocation, sugar signalling and their coupling with nitrogen uptake and assimilation. *Functional Plant Biology*, **43**, 105–113.

Way DA, Yamori W (2014) Thermal acclimation of photosynthesis: on the importance of adjusting our definitions and accounting for thermal acclimation of respiration. *Photosynthesis Research*, **119**, 89–100.

Weis E, Berry JA (1987) Quantum efficiency of photosystem II in relation to "energy"-dependent quenching of chlorophyll fluorescence. *Biochimica et Biophysica Acta (BBA)-Bioenergetics*, **894**, 198–208.

Woodruff DR (2014) The impacts of water stress on phloem transport in Douglas-fir trees. *Tree Physiology*, **34**, 5–14.

Woodruff DR, Meinzer FC (2011) Water stress, shoot growth and storage of non-structural carbohydrates along a tree height gradient in a tall conifer. *Plant, cell & environment*, **34**, 1920–1930.

Wright IJ, Leishman MR, Read C, Westoby M (2006) Gradients of light availability and leaf traits with leaf age and canopy position in 28 Australian shrubs and trees. *Functional Plant Biology*, **33**, 407–419.

Yamada M, Hidaka T, Fukamachi H (1996) Heat tolerance in leaves of tropical fruit crops as measured by chlorophyll fluorescence. *Scientia Horticulturae*, **67**, 39–48.

Yamashita T, Butler WL (1968) Photoreduction and Photophosphorylation with Tris-Washed Chloroplasts. *Plant Physiology*, **43**, 1978–1986.

Zhang J-L, Poorter L, Hao G-Y, Cao K-F (2012) Photosynthetic thermotolerance of woody savanna species in China is correlated with leaf life span. *Annals of Botany*, **110**, 1027–1033.

Zhao J, Hartmann H, Trumbore S, Ziegler W, Zhang Y (2013) High temperature causes negative whole-plant carbon balance under mild drought. *New Phytologist*, **200**, 330–339.

Zheng D, Hunt Jr ER, Running SW (1993) A daily soil temperature model based on air temperature and precipitation for continental applications. *Climate Research*, **2**, 183–191.

Zou L (2009) Effects of gradual and sudden heat stress on seed quality of Andean lupin, Lupinus mutabilis.

3.8 Figures & Tables

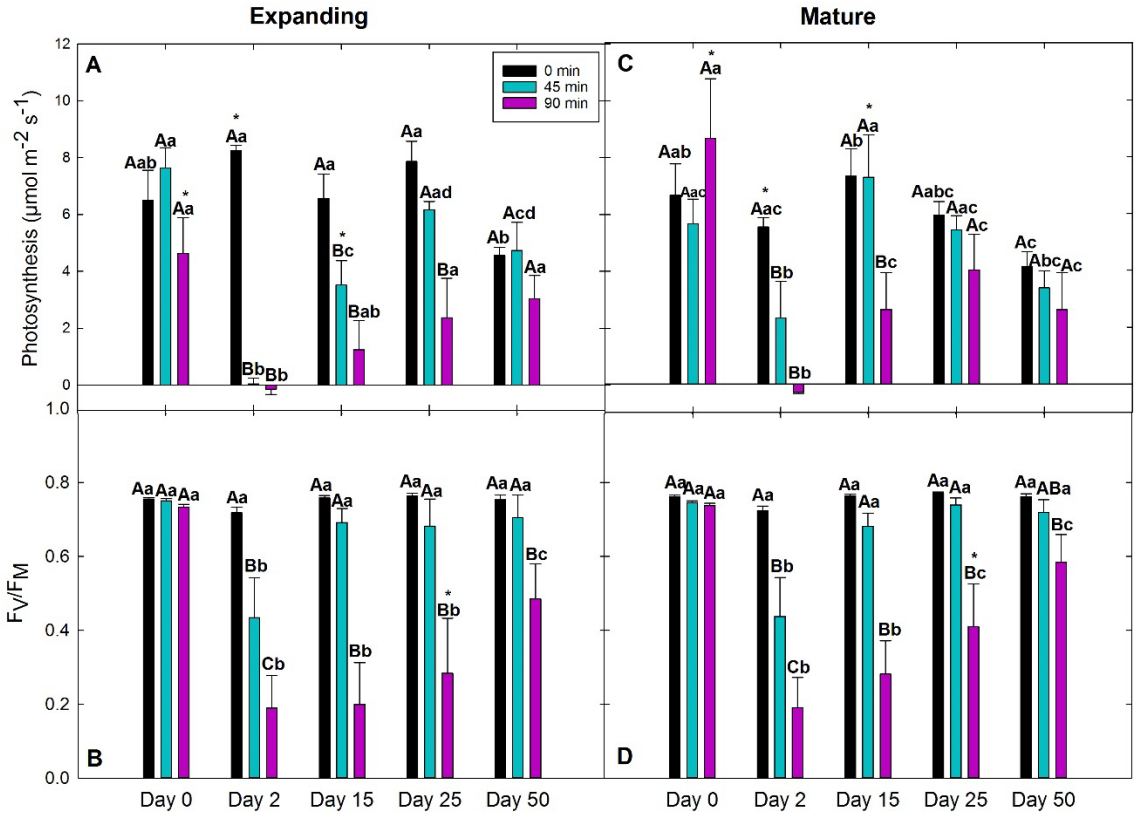

Figure 3.1 Time courses of photosynthesis and F_V/F_M of expanding (A, B) and mature (C, D) leaves from the same plants (N=4) of the 0 min (controls), 45 min, and 90 min groups at 0, 2, 15, 25, and 50 days after treatment. Different uppercase letters represent significant significant differences among treatments within each day and leaf age. Different lowercase letters represent significant differences among days within treatment and leaf age. Asterisks represent significant differences between leaf age within treatment and day. Error bars represent ± SE.

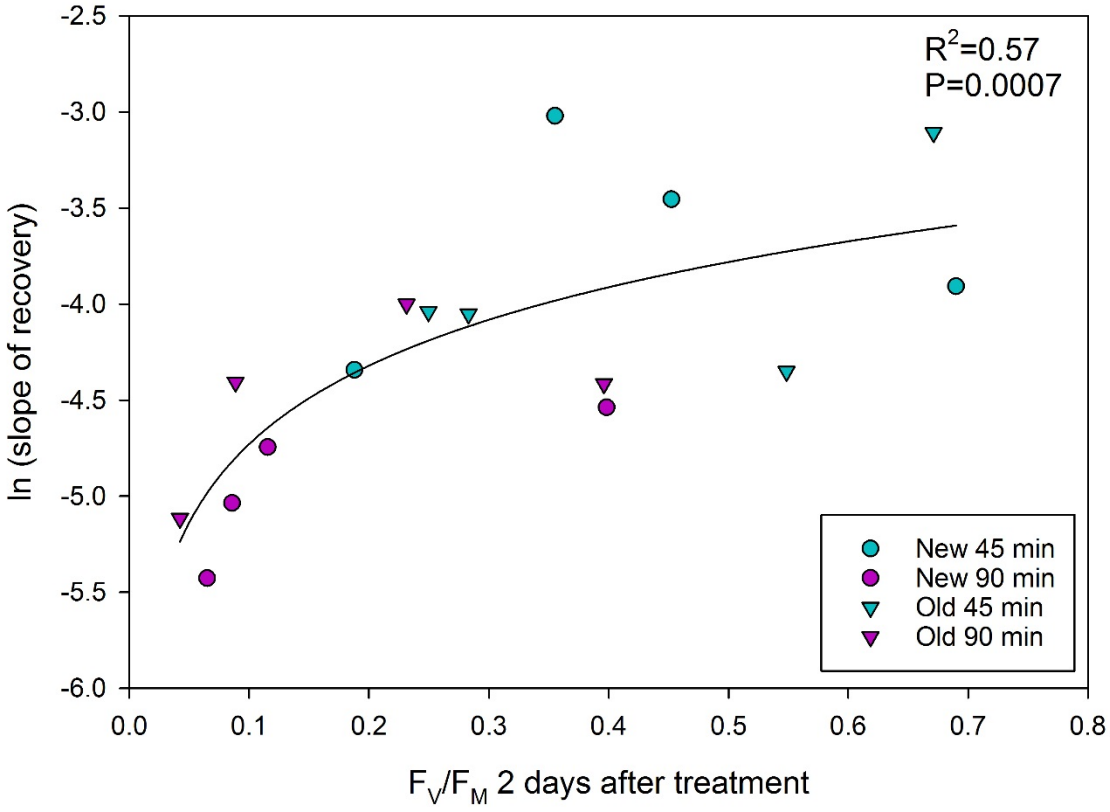

Figure 3.2 F_V/F_M values reached two days after treatment (i.e. maximum damage after treatment) significantly related to the log-transformed slope of F_V/F_M recovery across leaf age class and treatment (R^2=0.57, P=0.0007). Nonlinear regression equation: f = y0+a*ln(abs(x). Each data point represents an individual plant. N=4.

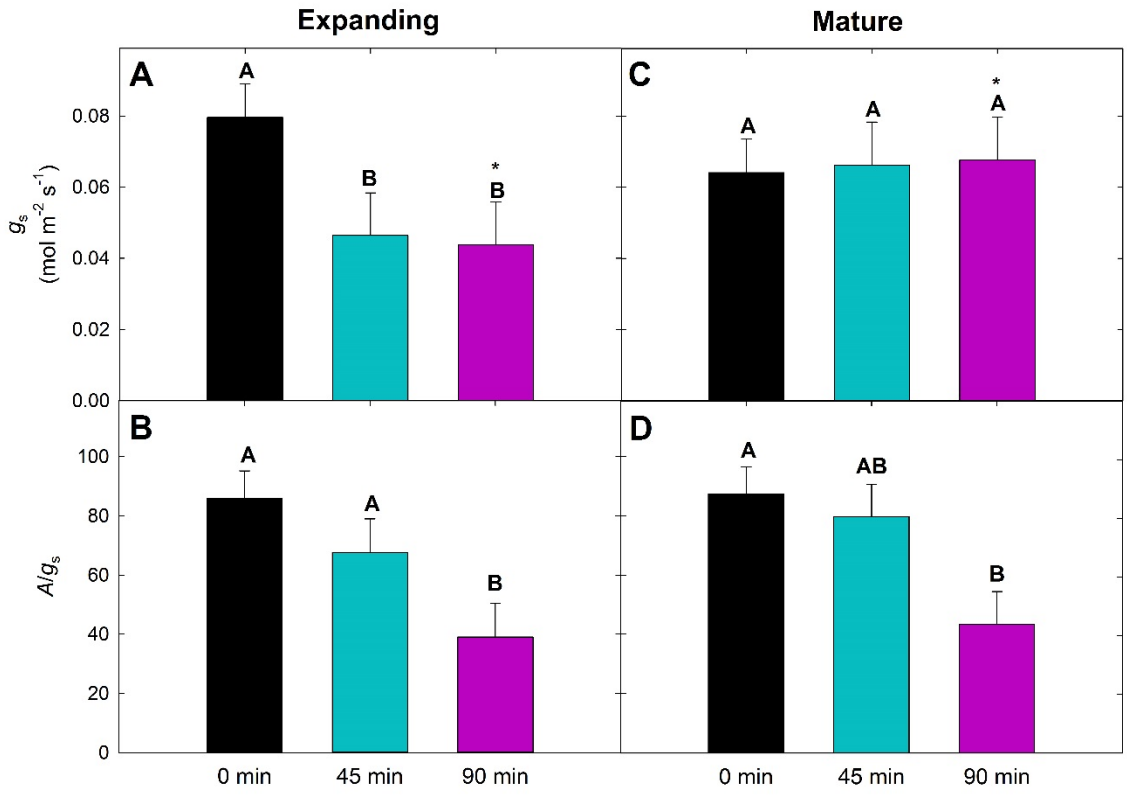

Figure 3.3 Mean post-treatment stomatal conductance (g_s) and intrinsic water use efficiency (A/g_s) for 0 min (controls), 45 min, and 90 min groups. Different uppercase letters represent significant differences among treatments within leaf age class. Error bars represent ± SE.

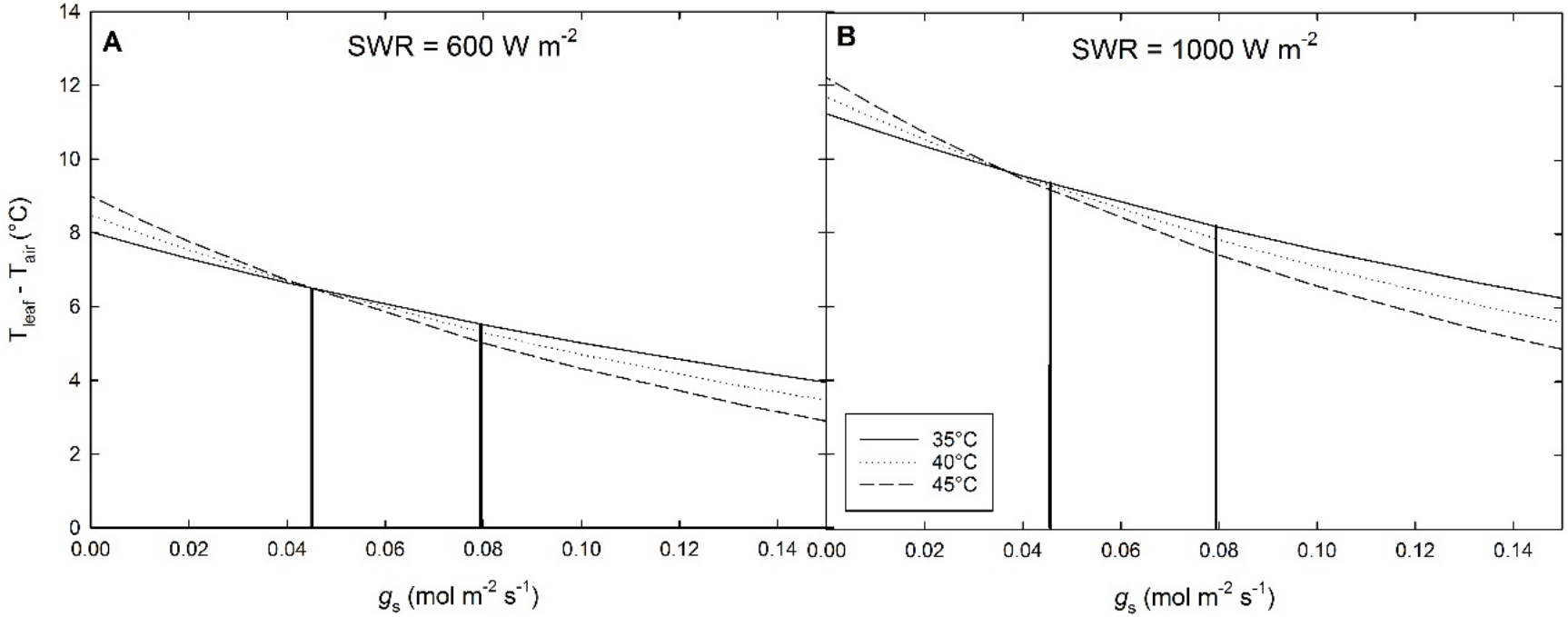

Figure 3.4 Modeled relationships between stomatal conductance (g_s) and leaf temperature (T_{leaf}) – air temperature (T_{air}) at T_{air} = 35°C, 40°C, and 45°C at short wave radiation (SWR) of 600 W m^{-2} (A) and 1000 W m^{-2} (B) to represent partial and full sun conditions, respectively. Vertical lines indicate mean post-treatment g_s values of controls (0.0796 mol m^{-2} s^{-1}) and of the 45 min and 90 min groups (0.0451 mol m^{-2} s^{-1} for expanding leaves). Incident photosynthetically active radiation (PAR) for each SWR level at a wavelength of 550 nm (average wavelength for the 400-700 nm PAR range): ~1380 and ~2300 µmol m^{-2} s^{-1}, respectively. PAR is assumed ~50% of SWR (Britton & Dodd, 1976).

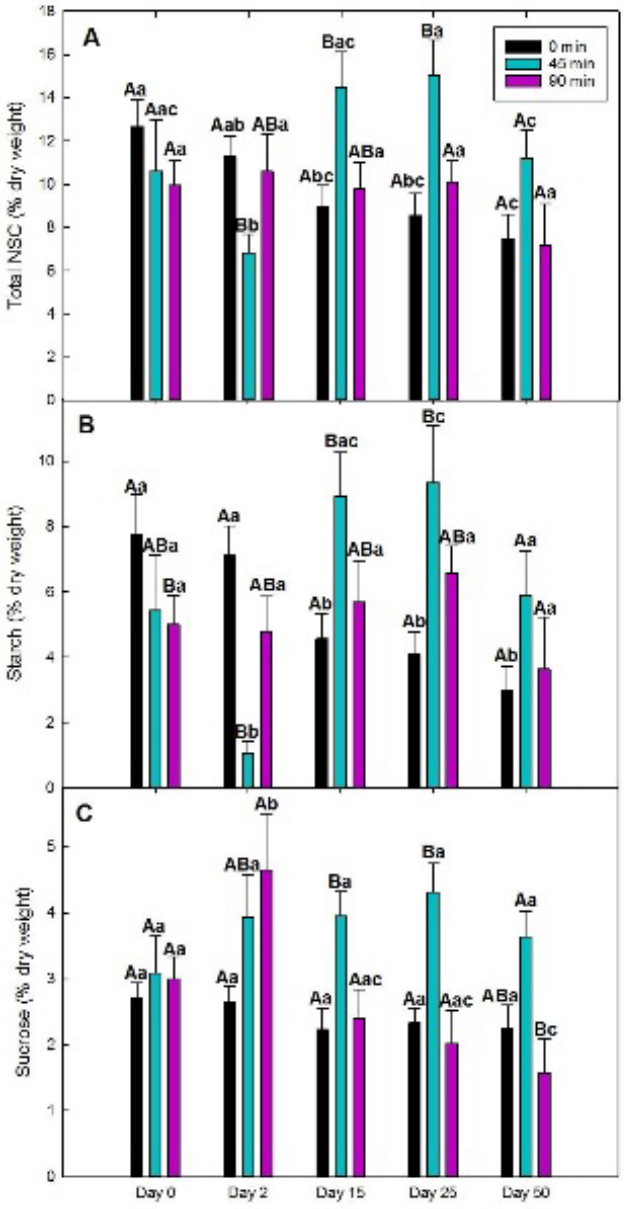

Figure 3.5 Time courses of mean total non-structural carbohydrates (total NSC), starch, and sucrose of expanding and mature leaves from the same plants (N=4) of the 0 min (controls), 45 min, and 90 min groups at 0, 2, 15, 25, and 50 days after treatment. Different uppercase letters represent significant differences between treatments within each day. Different lowercase letters represent significant differences between days within each treatment. Error bars represent ± SE.

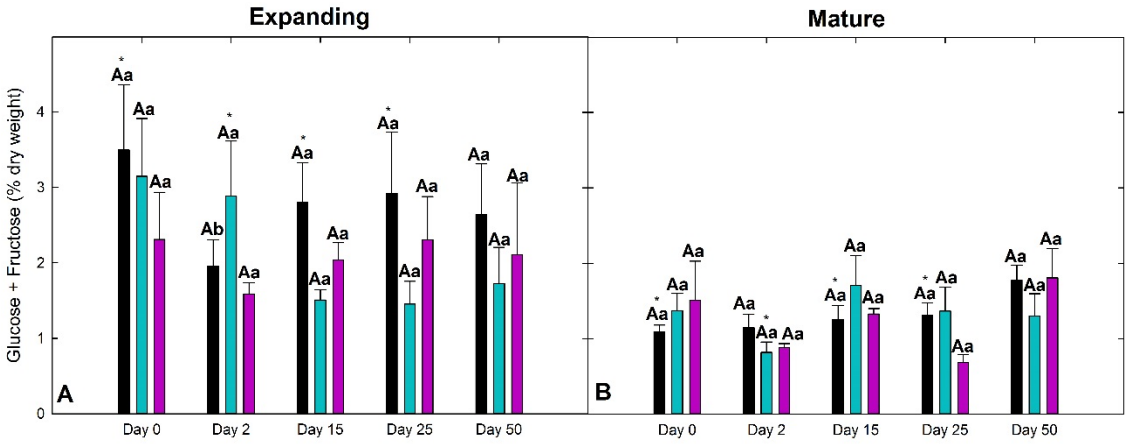

Figure 3.6 Time courses of glucose + fructose of expanding (A) and mature (B) leaves from the same plants (N=4) of the 0 min (controls), 45 min, and 90 min groups at 0, 2, 15, 25, and 50 days after treatment. Different uppercase letters represent significant differences among treatments within each day. Different lowercase letters represent significant differences among days within each treatment. Asterisks represent significant differences between leaf age classes. Error bars represent ± SE.

Table 3.1 Marginal F-tests for photosynthesis and F_V/F_M.

	Photosynthesis (μmol m^{-2} s^{-1})				**F_V/F_M**			
	numDF	denDF	F-value	P-value	numDF	denDF	F-value	P-value
Intercept	1	93	366.41	**<.0001**	1	104	883.02	**<.0001**
Age	1	13	1.6028	0.2277	1	13	6.846	**0.0213**
Treatment	2	13	21.357	**0.0001**	2	13	26.312	**<.0001**
Day	4	93	20.077	**<.0001**	4	104	94.940	**<.0001**
Age x Treatment	2	13	3.4666	0.0621	2	13	2.8695	0.0929
Age x Day	4	93	3.8058	**0.0065**	4	104	1.2742	0.2849
Treatment x Day	8	93	8.2791	**<.0001**	8	104	38.442	**<.0001**
Age x Treatment x Day	8	93	3.5207	**0.0013**	8	104	0.6461	0.7373

N=4. Bolded P-values indicate P<0.05. NumDF and denDF are the degrees of freedom in the numerator and denominator, respectively.

Table 3.2 Marginal F-tests for total NSC, starch, sucrose, and glucose+fructose.

	Total NSC				**Starch**				**Sucrose**				**Glucose + Fructose**			
	num DF	den DF	F-value	P-value	num DF	den DF	F-value	P-value	num DF	den DF	F-value	P-value	num DF	den DF	F-value	P-value
Intercept	1	79	850.78	**<.0001**	1	79	271.56	**<.0001**	1	79	620.69	**<.0001**	1	79	144.68	**<.0001**
Age	1	13	3.202	0.0969	1	13	0.5649	0.4657	1	13	4.833	**0.0466**	1	13	52.792	**<.0001**
Treatment	2	13	4.280	**0.0373**	2	13	0.123	0.8856	2	13	11.66	**0.0013**	2	13	1.974	0.1784
Day	4	79	3.420	**0.0124**	4	79	8.526	**<.0001**	4	79	4.385	**0.0030**	4	79	2.481	0.0505
Age x Treatment	2	13	0.442	0.6523	2	13	1.015	0.3899	2	13	0.66	0.5333	2	13	0.511	0.6113
Age x Day	4	79	1.846	0.1282	4	79	1.276	0.2867	4	79	1.010	0.4072	4	79	2.497	**0.0493**
Treatment x Day	8	79	5.682	**<.0001**	8	79	11.670	**<.0001**	8	79	3.222	**0.0032**	8	79	0.702	0.6893
Age x Treatment x Day	8	79	0.956	0.4767	8	79	1.457	0.1865	8	79	0.509	0.8466	8	79	2.146	**0.0408**

N=4. Bolded P-values indicate P<0.05. NumDF and denDF are the degrees of freedom in the numerator and denominator, respectively.

Table 3.3 Pearson correlation coefficients (R) and P-values describing the relationship between mean expanding and mature leaf photosynthesis and NSC component (total NSC, starch, sucrose, glucose + fructose) within the 0 min (controls), 45 min, and 90 min groups.

			Total NSC	Starch	Sucrose	Glucose + Fructose
Photosynthesis	0 min	R	**0.409**	**0.362**	0.210	0.141
		P-value	**0.00145**	**0.00530**	0.113	0.291
	45 min	R	0.318	**0.332**	0.0100	0.161
		P-value	0.0551	**0.0445**	0.953	0.342
	90 min	R	-0.0427	-0.0177	-0.0920	0.0606
		P-value	0.805	0.919	0.594	0.726

Bold values are significant $P<0.05$.

3.9 Appendices

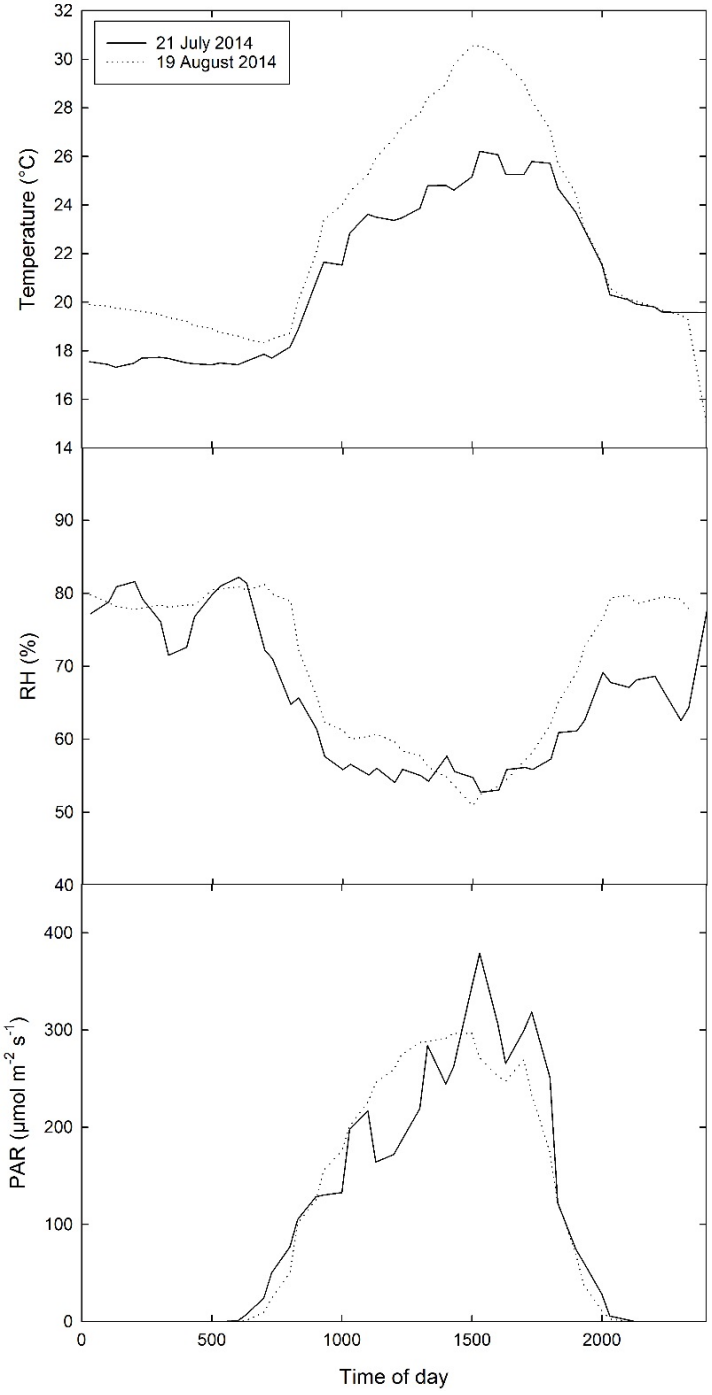

Appendix Figure 3.1 Air temperature, relative humidity (RH), and maximum photosynthetically active radiation (PAR) of the greenhouse during the two experimental rounds in the summer of 2014.

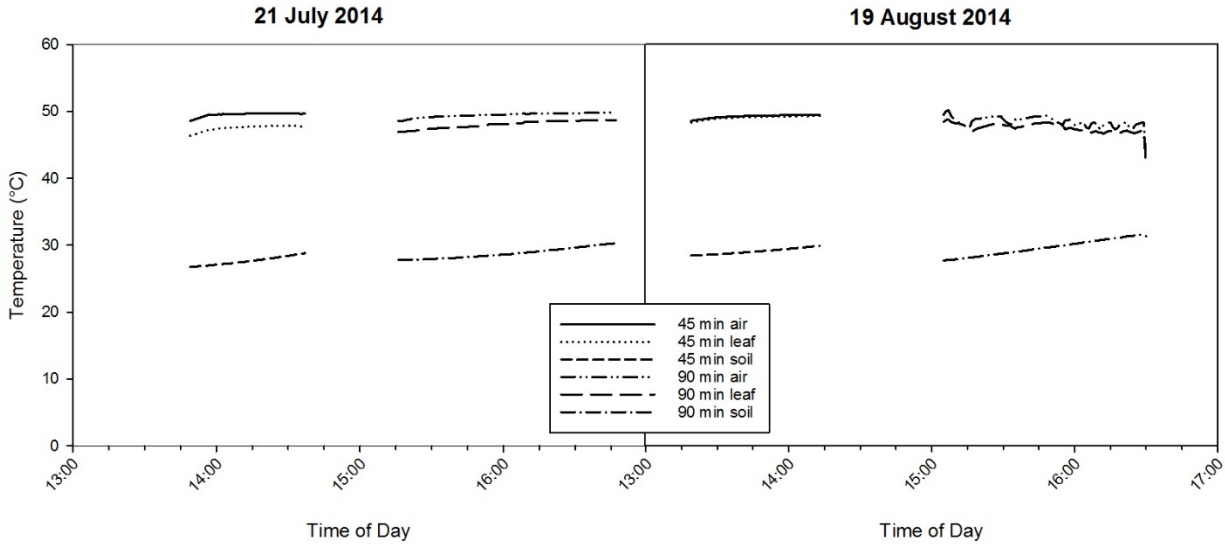

Appendix Figure 3.2 Air, leaf, and soil temperatures of plants during treatment exposure to 49°C for 45 min and 90 min in the growth chamber on 21 July 2014 and 19 August 2014.

Appendix Table 3.1 Average daily daytime and nighttime air temperature, relative humidity, and maximum photosynthetically active radiation (PAR) of the greenhouse during the two experimental rounds in the summer of 2014.

	21 July 2014	**19 August 2014**
Average daily daytime temperature (°C)	24.2	22.3
Average daily nighttime temperature (°C)	18.3	18.0
Average daily daytime relative humidity (%)	64.1	63.5
Average daily nighttime relative humidity (%)	80.2	77.5
Daily maximum PAR ($\mu mol\ m^{-2}\ s^{-1}$)	319.9	332.8

Appendix Table 3.2 Symbols, definitions, units, and equations of parameters used in the leaf energy balance model.

Symbol	Definition	Units	Equation	Definition of symbols in equation
T_{leaf}	leaf temperature	°C		
T_{air}	air temperature	°C		
γ_m	modified psychometric constant	kPa K^{-1}	$\gamma_m = \gamma(\frac{r_{st}}{r_{bl}})$	r_{st} = stomatal resistance (s m^{-1}), r_{bl} = boundary layer resistance (s m^{-1})
R_n	net radiation	W m^{-2}	$R_n = SWR_{abs} + LWR_{in} - LWR_{out}$	SWR_{abs} = absorbed short wave radiation (W m^{-2}), LWR_{in} = incoming long-wave radiation (W m^{-2}), LWR_{out} = outgoing long-wave radiation
r_{bl}	leaf boundary layer resistance	s m^{-1}	$r_{bl} = \frac{1}{g\,(u\,\frac{j}{d(1-j)}}$	j = 0.5 for a flat leaf, g = 0.00662 for a flat leaf, u = wind speed, d = leaf length in the direction of wind
VPD	water vapor pressure deficit of the air	kPa	$VPD = e_{sat} - e_a$	e_{sat} = saturation vapor pressure = $a\,e^{\frac{b\,T_{air}}{T_{air}+z}}$, where a = 0.61121 kPa, b = 17.502, z = 240.97°C ea = water vapor pressure of the air = $e_{sat}\frac{RH}{100}$, where RH = relative humidity (%)
ρ	density of dry air	kg m^{-3}	ρ = 1.292 kg m^{-3}	
C_p	heat capacity of dry air	J kg^{-1} K^{-1}	C_p = 1010 J kg^{-1} K^{-1}	
s	slope of the e_{sat}/temperature curve	kPa	$s = \frac{e_{sat}\,b\,z}{(T_{air}+z)^2}$	e_{sat} = saturation vapor pressure, b = 17.502, z = 240.97°C

The modified leaf energy balance equation from Sridhar & Elliott (2002), Monteith & Unsworth (2007), and Jones (2013) to solve for $T_{leaf} - T_{air}$ was:

$$T_{leaf} - T_{air} = \frac{\frac{\gamma_m R_n r_{bl}}{\rho C_p} - VPD}{s + \gamma_m}$$

Symbols and definitions are in Appendix Table 3.2. The equation is based on the principle that for a leaf at steady state or equilibrium, the amount of energy entering the leaf via solar radiation and ambient heat is equal to the amount of energy that exits the leaf via heat loss, reflected light, and transpiration (e.g. Knoerr & Gay, 1965).

4. THERMOTOLERANCE AND HEAT STRESS RESPONSES OF DOUGLAS-FIR AND PONDEROSA PINE SEEDLING POPULATIONS FROM CONTRASTING CLIMATES

Danielle E. Marias, Frederick C. Meinzer, David R. Woodruff, Katherine A. McCulloh

4.1 Abstract

Temperature and the frequency and intensity of heat waves are predicted to increase throughout the 21st century. Germinant seedlings are expected to be particularly vulnerable to heat stress because they are in the boundary layer close to the soil surface where intense heating occurs in open habitats. We quantified leaf thermotolerance and whole-plant physiological responses to heat stress in first-year germinant seedlings in two populations each of *Pinus ponderosa* P. and C. Lawson (PIPO) and *Pseudotsuga menziesii* (Mirb.) Franco (PSME) from climates with contrasting precipitation and temperature regimes. Thermotolerance of detached needles was evaluated using chlorophyll fluorescence (F_V/F_M, F_O) and electrolyte leakage. PSME was more heat tolerant than PIPO according to both independent assessments of thermotolerance. Following exposure of whole seedlings to a simulated heat wave at 45°C for 1 h in a growth chamber, we monitored F_V/F_M, photosynthesis, stomatal conductance, non-structural carbohydrates (NSCs), and carbon isotope ratios ($\delta^{13}C$) for 14 days. Heat treatment induced significant reductions in F_V/F_M in both species and a transient reduction in photosynthetic gas exchange only in PIPO one day after treatment. Heat treatment induced an increase in glucose + fructose concurrent with a decrease in starch in both species, whereas total NSC and sucrose were not affected by heat treatment. The negative relationship between glucose + fructose and starch observed in treated plants may be due to the conversion of starch to glucose + fructose to aid recovery from heat-induced damage. Populations from drier sites displayed greater $\delta^{13}C$ values than those from wetter sites, consistent with higher intrinsic water use efficiency and drought

resistance of populations from drier climates. Thermotolerance and heat stress responses appeared to be phenotypically plastic and representative of the environment in which plants were grown, whereas intrinsic water use efficiency appeared to reflect ecotypic differentiation and the climate of origin.

4.2 Introduction

High temperature stress and heat waves are expected to increase in frequency and intensity throughout the 21st century (Intergovernmental Panel on Climate Change, 2014). Although temperature is a strong driver of plant species' distributions, the impacts of high temperature and heat stress on plant physiological performance are not fully understood. While heat and drought are closely related, future increases in temperature and heat waves are predicted to occur with and without drought (Hao *et al.*, 2013), emphasizing the need for research that isolates the effect of high temperature stress on physiological processes. Seedlings represent the most vulnerable plant developmental stage because of their high susceptibility to abiotic and biotic stressors. High temperature stress at the soil surface is a major threat to seedling establishment. (Kolb & Robberecht, 1996) measured air temperatures exceeding 75°C at 5 mm above the soil surface, and 45°C at seedling height or 50 mm above the soil surface during two growing seasons where maximum ambient air temperatures were ~30°C. Given that soil surface temperatures are expected to increase along with projected increases in ambient air temperature and the frequency of heat waves, characterizing seedling physiological responses to heat stress is crucial.

Heat stress impacts plant function from the cellular to whole plant scale. High temperatures damage photosystem II (PSII) photochemistry, electron transport, thylakoid and cell membrane fluidity, RUBISCO function, and induce reactive oxygen species (ROS) production (Wahid *et al.*, 2007; Bita & Gerats, 2013; Teskey *et al.*, 2015). Heat stress also increases respiration, reduces photosynthesis, stomatal conductance, growth, and reproduction, and leads to leaf abscission, visible foliar damage, and mortality (Wahid *et al.*, 2007; Bita & Gerats, 2013; Teskey *et al.*, 2015). Plants employ mechanisms that influence the ability to withstand and/or avoid heat stress. This includes producing heat shock proteins that desaturate membrane lipids to maintain cell membrane integrity (Horváth *et al.*, 2012), using assimilated carbon to repair heat-induced damage (Sevanto & Dickman, 2015), and regulating evaporative cooling to avoid high leaf temperatures (Tomlinson *et al.*, 2013). Quantifying these physiological responses from the cellular to whole plant scale informs our understanding of heat (high temperature) tolerance or thermotolerance and mechanisms to cope with heat stress.

Although increased allocation of assimilated carbon (i.e. photosynthate) to repair processes may facilitate recovery from heat stress-induced damage (Bita & Gerats, 2013), shifts in plant carbon allocation in response to heat stress are poorly understood due to contradictory results (Génard *et al.*, 2008; Sala *et al.*, 2012; Hartmann & Trumbore, 2016). Non-structural carbohydrates (NSCs) include starch and free soluble sugars (sucrose, glucose, and fructose) and have multiple fates including growth, storage, reproduction, metabolism, root exudation, and repair after stress-induced damage (Kozlowski, 1992; Dietze *et al.*, 2014). High levels of leaf NSCs have been associated

with heat stress tolerance (Liu & Huang, 2000; Niinemets, 2010) and are used for damage prevention, osmoregulation, and sugar signaling (Roitsch & González, 2004; Couée *et al.*, 2006; Sugio *et al.*, 2009). NSCs may be allocated to above-ground tissues for repair from heat stress and leaf NSC levels may increase (Sevanto & Dickman, 2015). In contrast, leaf NSCs may decrease in response to heat stress because photosynthesis and stomatal conductance are inhibited, reducing carbon gain and assimilation (i.e. decreased supply). This may occur concurrently with heat-induced increases in respiration that utilizes carbon (i.e. increased demand) and depletes NSC reserves (Duan *et al.*, 2013; Zhao *et al.*, 2013; Escandón *et al.*, 2016). Heat stress may also induce shifts between NSC pools (e.g. starch, sugars), as well as turnover of NSC that may be reflected in shifts in the carbon isotope ratios of leaves (Gutierrez & Meinzer, 1994). Investigating the impacts of heat stress on NSC dynamics will provide insights into the nature of physiological responses to high temperature stress.

Plant responses to heat stress may vary depending on the climate of origin. Species originating from warmer climates are more heat tolerant and are better adapted to withstand heat stress than species originating from cooler climates (Salvucci & Crafts-Brandner, 2004; Cunningham & Read, 2006). Similar patterns have been observed within a species whose geographic range spans contrasting climate regimes. Populations within a species can acclimate to varying environmental conditions through phenotypic plasticity where the physiological characteristics reflect the climate in which they are grown (Knight & Ackerly, 2002; Ghouil *et al.*, 2003; Gimeno *et al.*, 2009). A species can also survive contrasting climate regimes through ecotypic variation that results from

genetically distinct populations within a species that have traits representing different ecotypes and climates of origin (Lindgren & Hällgren, 1993; Aranda *et al.*, 2009; Ramírez-Valiente *et al.*, 2010; Du *et al.*, 2014; Matías *et al.*, 2016). Kerr *et al.* (2015) showed strong evidence for the existence of ponderosa pine ecotypes because a seedling population from a dry climate displayed physiological traits associated with greater drought resistance than a population from a mesic climate despite being grown in a common garden. Phenotypic plasticity and ecotypic variation both enable species to survive diverse climates and buffer against predicted changes in temperature. Thus, species adapted to a wide range of climates may have an advantage over narrowly adapted species (Gimeno *et al.*, 2009) in response to the predicted increases in heat stress. Populations and species originating from contrasting climates are expected to exhibit different heat tolerances and associated physiological responses to heat stress.

Pinus ponderosa P. and C. Lawson (PIPO) and *Pseudotsuga menziesii* (Mirb.) Franco (PSME) are ecologically, economically, and socially important native species in the northwestern USA. PIPO and PSME have overlapping geographic ranges with both species ranging from British Columbia, Canada to Mexico and from the Pacific coast to the Rocky Mountains (Burns and Hankala 1990). PIPO is found at elevations from sea level to 3050 m (Oliver *et al.* 1990) and PSME is found at elevations from sea level to 2700 m (Hermann and Lavender 1990). Generally, PIPO is more tolerant of drought, frost, sun, and fire than PSME (Hermann and Lavender 1990, Oliver *et al.* 1990). Populations of both PIPO and PSME originating from contrasting climates have exhibited ecotypic adaptations that reflect the climate of origin (Sorensen, 1983; Perić *et*

al., 2009; Du *et al.*, 2014; Kerr *et al.*, 2015). Because drought results in stomatal closure and increased leaf temperatures (Kolb & Robberecht, 1996), populations from drier climates are expected to also have greater heat tolerances.

In this study, we evaluated physiological responses to heat stress in greenhouse-grown first-year germinant seedlings in two populations each of PIPO and PSME originating from climates with contrasting precipitation and temperature regimes. We first quantified heat tolerance of detached needles using two independent methods: chlorophyll fluorescence and electrolyte leakage. We then evaluated whole-plant responses to heat stress *in situ* by exposing seedlings to a simulated heat wave in a growth chamber and monitoring chlorophyll fluorescence, photosynthesis, stomatal conductance, carbon isotope ratios, and NSC dynamics for 14 days after heat exposure. We hypothesized that 1) populations originating from drier climates would display greater homeostasis of physiological properties (chlorophyll fluorescence, photosynthesis, stomatal conductance, intrinsic water use efficiency as estimated from carbon isotope ratios, and NSC content and composition) indicating greater heat tolerance than those from wetter climates, and 2) based on stability of the preceding physiological properties, PIPO would display greater heat tolerance than PSME.

4.3 Materials & Methods

Plant material

Pinus ponderosa P. and C. Lawson (PIPO) and Pseudotsuga menziesii (Mirb.) Franco (PSME) seeds were obtained from the Oregon Department of Forestry and the

USFS Pacific Northwest Research Station, respectively. Two populations of each species originated from a drier and a wetter climate (PIPOdry, PIPOwet, PSMEdry, PSMEwet) based on mean annual precipitation (MAP) and temperature for each population within each species (Table 4.1, PRISM). PIPOdry originated near Spray, OR (44.8343°N, 119.7944°W) on the east side of the Cascade mountains ~325 km from the coast and has a MAP of 337 mm. PIPOwet originated from the Willamette Valley, OR with climate similar to Corvallis, OR (44.5646N, 123.2620W) on the west side of the Cascade mountains ~84 km from the coast and has a MAP of 1043 mm. PSMEdry originated from near Tiller, OR (42.895N, 123.0W) and has a MAP of 1056 mm. PSMEwet originated from the Coast Range (44.851N, 123.818W) and has a MAP of 3054 mm. For clarity, populations were named 'dry' and 'wet' based on relative differences in MAP between each population within each species. Climate information of each population is summarized in Table 4.1. Seeds were stratified in February of 2014 and planted in 3 L pots with a peat-perlite-pumice growing mix (Sunshine LA4P) in a temperature-controlled greenhouse in Corvallis, Oregon in March of 2014. During the sampling campaigns in October and November 2014, seedlings were ~10 cm tall, average daytime temperature in the greenhouse was 22ºC, average nighttime temperature 19ºC, average daytime relative humidity 67%, and average daily maximum photosynthetic photon flux density (PPFD) was 285 µmol m-2 s-1 (see Appendix Table 4.1). Average daily maximum PPFD was 391 µmol m-2 s-1 for the growing season from April-September. Seedlings were watered three times per week and fertilized once every two weeks (12%N, 4%P2O5, 8%K2O).

Thermotolerance curves derived from chlorophyll fluorescence

During October of 2014, two mature needles were collected from each of five seedlings per population prior to dawn to ensure needles were dark-acclimated. Needles were placed in closed plastic bags and immersed in a preheated water bath (General Purpose Aquabath Model 2343, Thermo Fisher Scientific, Marietta, OH, USA) for 15 min at nine temperatures ranging from 25-59°C for PIPO and 12 temperatures ranging from 25-61°C for PSME. Different sets of needles were exposed to each temperature. A fine-wire thermocouple in each plastic bag recorded that needles reached each desired temperature within 1 min. Chlorophyll fluorescence was measured at room temperature with a portable pulse-amplitude modulated chlorophyll fluorometer (Mini-PAM, Heinz Walz GmbH, Germany) 24 h after exposure to each temperature. Controls were not exposed to a water bath treatment. During the 24 h after temperature exposure, needles were stored in the dark on moist filter paper in Petri dishes.

Chlorophyll fluorescence was measured as the ratio of variable to maximum fluorescence (F_V/F_M) and the minimal level of fluorescence (F_O) in the convention of Maxwell & Johnson (2000). F_V/F_M is a proxy for the maximum quantum efficiency of PSII photochemistry (Genty *et al.*, 1989) and is calculated as:

$$\frac{F_V}{F_M} = \frac{F_M - F_O}{F_M} = 1 - \frac{F_O}{F_M} \quad (1)$$

F_O was induced by turning on a measuring light (red light-emitting diode, 650 nm, 0.15 µmol m^{-2} s^{-1} PPFD) with a pulse-width of 3 µs at a pulse modulation frequency of 0.6 kHz. F_V/F_M was then determined by applying a 0.8 s saturating pulse of white light,

which transiently closed all PSII reaction centers, minimized heat dissipation, and induced maximum fluorescence, allowing the determination of variable fluorescence. Reductions in F_V/F_M indicate stress-induced changes in photochemistry such as inhibition of PSII reaction centers and increased non-radiative (heat) dissipation. Optimal F_V/F_M values are ~0.83 (Björkman & Demmig, 1987). An increase in F_O indicates PSII inactivation, damage to the oxygen evolving complex and water splitting system and disruptions in electron donation to PSII reaction centers (Yamashita & Butler, 1968; Weis & Berry, 1987; Havaux, 1996). We did not measure F_O during continuous heating (Schreiber & Berry, 1977) to avoid the confounding effects of previous temperature exposure (e.g. Cunningham and Read 2006; Krause *et al*. 2010).

Thermotolerance curves derived from electrolyte leakage

During December of 2014, six needles were collected before dawn from each of five seedlings per population and placed in 6 mL of deionized H_2O in 15 mL polycarbonate tubes. Samples were infiltrated under vacuum for 15 min. Tubes were heated for 20 min in a preheated water bath at each of the eight desired temperatures ranging from 30-65°C. Different sets of needles were exposed to each temperature. Tubes were shaken for 1.5 h and the conductivity of the water in each tube was measured with a conductivity meter (Product catalog number 89094-958, VWR International, Radnor, PA, USA). Tubes were then heated for 20 min in a 100˚C water bath and shaken again for 1.5 h. The final conductivity of the solution represented the electrolyte leakage

of completely killed leaf tissue. Percent electrolyte leakage or percent damage was calculated as:

$$\%\ electrolyte\ leakage = \frac{Conductivity\ after\ exposure\ to\ temperature\ (°C)}{Conductivity\ after\ exposure\ to\ 100°C}\ x\ 100 \quad (2)$$

Growth chamber heat treatment

Seedlings (N=7 per PSME population, N=10 per PIPO population) were exposed to 45ºC for 1 h in a growth chamber (Model I-35LVL, Percival, Boone, IA) with cool white lighting (PPFD=25 µmol m^{-2} s^{-1}). The treatment temperature of 45°C was selected based on the chlorophyll fluorescence thermotolerance curves and preliminary experiments at other temperatures that showed that 45°C induced enough heat stress to be damaging without completely killing needles. This enabled us to evaluate time courses of physiological responses to heat treatment. The treatment temperature is also well-above the temperature optimum for photosynthesis between 20-30°C across boreal, temperate, and tropical species (Teskey *et al.*, 2015), but realistic for soil surface temperatures experienced during conifer seedling establishment (Kolb & Robberecht, 1996). PSME seedlings were heat treated on 16 October 2014 and PIPO seedlings were heat treated on 17 November 2014 (see Appendix Table 4.1). Plants were watered to drainage directly before treatment to avoid drought effects and to buffer changes in soil temperature during treatment. Fine-wire thermocouples measured air, leaf, and soil (~10 cm depth) temperatures during treatment exposure (see Appendix Table 4.2). Pots were completely wrapped with reflective bubble wrap to isolate the soil and roots from heat exposure. This prevented soil temperatures from exceeding 23ºC (see Appendix Table 4.2), which is

realistic for soil temperatures in summer (Zheng *et al.*, 1993; Kolb & Robberecht, 1996). Control plants were not exposed to a treatment in the growth chamber. F_V/F_M, photosynthesis, stomatal conductance, foliar carbon isotope ratios, and foliar NSC content were monitored in control and treated plants prior to treatment (day 0) and 1, 2, 7, and 14 days after treatment in 5 randomly selected plants per treatment group in each population.

Chlorophyll fluorescence, photosynthesis, and stomatal conductance

F_V/F_M was measured on five seedlings per treatment group and population at ambient greenhouse temperature with a portable pulse-amplitude modulated chlorophyll fluorometer (Mini-PAM, Heinz Walz Gmbh, Germany) at predawn to ensure leaves were dark-acclimated. Photosynthesis and stomatal conductance were measured between 1000-1300 h on five randomly selected seedlings per group and population using a portable photosynthesis system (LI-6400, Li-Cor, Lincoln, NE, USA). In the cuvette, photosynthetic photon flux density (PPFD) was set to 1000 µmol m^{-2} s^{-1}, leaf temperature 25°C, reference [CO_2] 400 µmol mol^{-1}, and flow rate 500 µmol s^{-1}. Gas exchange was measured on flattened juvenile needles not in fascicles. Needles were allowed to acclimate to cuvette conditions as long as was required for photosynthesis and conductance levels to stabilize. Needles in the gas exchange chamber were collected and their area was computed using ImageJ software. Measured projected leaf area was used to normalize gas exchange values. Pretreatment (day 0) photosynthesis values were estimated from photosynthesis-intercellular CO_2 (C_i) curves. To compare intrinsic

photosynthesis at the ambient atmospheric CO_2 concentration of 400 µmol mol^{-1}, photosynthesis was estimated at the average C_i value of the control (0 min) group for all sampling days.

Carbon isotope ratios

Five needles from each of five individuals were collected early morning (directly after F_V/F_M measurements were made) on each sampling date, immediately put on ice in a cooler, and transported to the nearby laboratory where samples were microwaved for 90 s to stop all enzymatic activity because NSC assays were subsequently conducted on aliquots of the same samples. The samples were then oven-dried at 75ºC and stored in a freezer before being ground to a fine powder. Approximately 0.8 mg of dried needle powder was packed in tin capsules for C combustion for subsequent analysis by an isotope ratio mass spectrometer (IRMS). The C isotopic ratio ($\delta^{13}C$) was recorded as deviations per mil (‰) from the Vienna Peedee Belemnite international standard. Samples were analyzed for $\delta^{13}C$ at Oregon State University's College of Earth, Oceanic, Atmospheric Sciences stable isotope laboratory. Samples were flash combusted using a Carlo Erba elemental analyzer (NA 1500, Thermo Scientific, Waltham, MA, USA), and the resulting CO_2 was analyzed by a Delta Plus XL continuous-flow mass spectrometer (Finnigan MAT, now Thermo Scientific, Waltham, MA, USA). Runs were calibrated daily using the international standards USGS40 (glutamic acid) and ANU sucrose. The typical error was ±0.1‰ or less as determined by repeated measures of internal quality control standards (IAEA-600) and from sample replicates.

The $\delta^{13}C$ of leaf tissue ($\delta^{13}C_{leaf}$) reflects the $\delta^{13}C$ of CO_2 in the atmosphere ($\delta^{13}C_{air}$), the fractionation against the heavier C isotope (^{13}C) due to physiological processes, and the ratio of the concentration of CO_2 inside the leaf (C_i) to that in the ambient air (C_a):

$$\delta^{13}C_{leaf} = \delta^{13}C_{air} - a - (b - a)\frac{C_i}{C_a}, \quad (3)$$

where *a* is the fractionation effect of diffusion of CO_2 through stomata (4.4‰), and *b* is the fractionation effect (27‰) associated with discrimination against ^{13}C by the enzyme RUBISCO (ribulose bisphosphate carboxylase-oxygenase) during C fixation (Farquhar *et al.*, 1982; Farquhar & Richards, 1984). $\delta^{13}C_{leaf}$ is also an integrated measure of intrinsic water use efficiency (iWUE) at the time the tissue was formed where greater $\delta^{13}C_{leaf}$ (i.e. less negative) indicates greater iWUE (Farquhar *et al.*, 1989) and drought resistance (Hubick *et al.*, 1986; Jones, 2009). Therefore, carbon isotope ratios can indicate ecotypic differences in drought resistance across populations of a species when grown in a common garden situation (Hubick *et al.*, 1986; Zhang *et al.*, 1993; Kerr *et al.*, 2015). Changes in carbon isotope ratios of mature leaves over time can also reflect turnover of NSCs as regulation of photosynthetic gas exchange varies seasonally or following imposition of stress (Gutierrez & Meinzer, 1994; Damesin *et al.*, 1998; Scartazza *et al.*, 2013).

Non-structural carbohydrates (NSCs)

The ground needle samples used for $\delta^{13}C$ analyses (described above) were also analyzed for content of total NSC, starch, sucrose, and glucose + fructose as described by

Woodruff & Meinzer (2011). Water was added to the powdered samples and NSC was extracted from the solutions by heating them in steam for 1.5 h. The concentration of free glucose + fructose was determined photometrically on a 96-well microplate photometer (Multiskan FC, Thermo Scientific, Waltham, MA, USA) after enzymatic conversion of glucose + fructose to gluconate-6-phosphate. Samples were hydrolyzed by enzymatic treatment: invertase for sucrose and amyloglucosidase for total NSC. Photometric analysis was based on absorbance of samples at 340 nm in solution with reference to the absorbance of a glucose reference solution. Total NSC was calculated as the sum of starch, sucrose, and glucose + fructose. NSC values are presented as % dry weight.

Statistics

F_V/F_M values were converted to a percent scale so that the F_V/F_M value of the untreated (control) group was considered 100% (no damage). For ease of comparison with the F_V/F_M thermotolerance curves, the percent electrolyte leakage axis (y-axis) was inverted in figures. Thermotolerance curves assessed with F_V/F_M and electrolyte leakage were determined from third order sigmoidal functions fitted to the data:

$$f = a/(1 + exp(-(x - x_0)/b) \quad (4)$$

where f is percent of untreated (control) F_V/F_M or percent electrolyte leakage, x is the treatment temperature, and a, x_0, and b are fitting parameters. From this equation, thermotolerance parameters were determined: T_{50} of F_V/F_M is the temperature that caused a 50% reduction in untreated (control) F_V/Fm. T_{50} of electrolyte leakage is the temperature that caused a 50% increase in percent electrolyte leakage or percent damage.

The temperature at which F_O begins to rise in response to increasing temperature (T_{crit}) was determined from the intersection of two regression lines extrapolated from the slow- and fast-rising portions of the F_O-temperature curve (Schreiber and Berry 1977). A two sample t-test was used to compare the T_{50}s assessed from the F_V/F_M and electrolyte leakage methods, and to compare T_{50} and T_{crit} between populations and species.

A three-way factorial linear mixed-effects model was developed with treatment (control, heat), type ($species_{population}$, i.e. $PSME_{dry}$, $PSME_{wet}$, $PIPO_{dry}$, $PIPO_{wet}$), and day (0, 1, 2, 7, 14) as fixed main effects. The nested random effect in the model was plant. Response variables were: F_V/F_M, photosynthesis, stomatal conductance, $\delta^{13}C$, total NSC, starch, sucrose, and glucose + fructose. To choose a correlation structure that would account for the repeated measurements of plants through time, four models that allowed for different residual correlation structures were fit and selected based on the minimum Bayesian Information Criterion (BIC) value. Assumptions of constant variance and normality were checked using residual and quantile-quantile plots. Log transformations were necessary to meet assumptions for stomatal conductance, total NSC, starch, sucrose, and glucose + fructose. For ease of interpretation, we present back-transformed data in results and figures. All interactive and main effects of factors on the response were tested using marginal F-tests (also known as Type III tests) that account for unbalanced sample sizes. Post-hoc comparisons were made using a 95% confidence interval and $P<0.05$. Due to sufficient degrees of freedom, we did not make multiple comparisons corrections. If no significant differences existed among populations, treatments, and/or days, the response variable was pooled by averaging over population, treatment, and/or day to

simplify data visualization. Statistical analyses were conducted in SigmaPlot 13.0 (Systat Software, San Jose, CA, USA) and R version 3.2.3 (2015-12-10, The R Foundation for Statistical Computing).

4.4 Results

Needle thermotolerance curves

Mean F_V/F_M of untreated, detached needles was 0.72±0.003 for $PIPO_{dry}$, 0.73±0.004 for $PIPO_{wet}$, 0.75±0.006 for $PSME_{dry}$, and 0.74±0.004 for $PSME_{wet}$ and did not significantly differ between populations or species (P>0.05). Thermotolerance curves based on F_V/F_M, electrolyte leakage, and Fo showed that PSME was less heat-sensitive to temperatures >50°C than PIPO regardless of population (Figure 4.1). T_{50} and T_{crit} did not show significant differences between populations but did show significant differences between species where T_{50} (F_V/F_M), T_{50} (electrolyte leakage), and T_{crit} were significantly greater in PSME than PIPO (P<0.05, Table 4.2).

Whole-plant responses to heat stress

Interactions among the main effects (treatment, type (i.e., $species_{population}$: $PIPO_{dry}$, $PIPO_{wet}$, $PSME_{dry}$, $PSME_{wet}$), and day) on F_V/F_M, photosynthesis, stomatal conductance, and $\delta^{13}C$ are summarized in Table 4.3. F_V/F_M was significantly affected by treatment and day, and the interaction between treatment and day was significant (P<0.0001, Table 4.3) but the effect of type was not significant (P=0.9552, Table 4.3). Because there were no significant differences in F_V/F_M, photosynthesis, and stomatal conductance between

populations within species, populations were pooled (Figure 4.2). Heat treatment significantly and similarly reduced F_V/F_M 1 and 2 days after treatment in both species (Figure 4.2A,B). Both species did not recover to pretreatment (day 0) F_V/F_M values until day 7. F_V/F_M values of controls did not differ between species.

Photosynthesis was significantly affected by treatment, species, and day, and all interactions among main effects were significant ($P<0.05$, Table 4.3). Photosynthesis was significantly greater in PIPO than PSME on days 0, 2, and 7 in controls and on days 0 and 2 in the heated group (Figure 4.2C,D). One day after heat treatment, photosynthesis of treated PIPO significantly declined by 81% relative to day 0 values and became significantly lower than that of treated PSME. Photosynthesis of treated PIPO recovered to control values on day 14, although photosynthesis on day 14 was not significantly different from that on days 2 and 7. In contrast, photosynthesis of the PSME treatment group did not significantly change with day nor differ from the PSME control group.

Stomatal conductance was significantly affected by species and day ($P<0.0001$, Table 4.3), but not treatment ($P=0.2411$, Table 4.3). Stomatal conductance of PIPO was significantly greater than PSME on all days in the controls (Figure 4.2E). This pattern held in the heated group with the only exception on day 1 after treatment when stomatal conductance of treated PIPO significantly declined from day 0 by 42% and did not differ from that of treated PSME (Figure 4.2F). In contrast, treated PSME stomatal conductance did not significantly change between days 0 and 1. Treated PIPO and PSME stomatal conductance changed with day but not in a consistent pattern.

$\delta^{13}C$ was significantly affected by type ($species_{population}$, P=0.0157) and day (P<0.0001), but not treatment (P=0.2123, Table 4.3). Because $\delta^{13}C$ was not significantly affected by treatment (P=0.2123) and the interaction between day and type was also not significant (P=0.3381), control and treatment $\delta^{13}C$ were pooled for all sampled days in Figure 4.3. In contrast to all other response variables, $\delta^{13}C$ significantly differed between populations (P=0.015 for PIPO, P=0.032 for PSME) but not between species when populations were pooled (P=0.48, Figure 4.3). $PSME_{wet}$ and $PIPO_{wet}$ $\delta^{13}C$ values were significantly more negative (i.e. lower) than those of $PSME_{dry}$ and $PIPO_{dry}$ (Figure 4.3).

Interactions among the main effects (treatment, type, and day) on total NSC, starch, sucrose, and glucose + fructose are summarized in Table 4.4. NSC constituents of populations within species did not significantly differ so populations were pooled within species. Total NSC was significantly affected by day (P=0.0009) and marginally by treatment (P=0.0465, Table 4.4). Total NSC did not differ between species in the control group and only differed between species in the treatment group on days 7 and 14 and not in a consistent pattern (Figure 4.4A,B). Starch was significantly affected by day (P=0.0001) and the interaction between treatment and day was significant (P=0.0001). Starch of treated PIPO significantly declined at day 2 relative to day 0 before increasing back to pretreatment values at days 7 and 14 (Figure 4.4C,D). In contrast, starch of treated PSME steadily declined from day 0 to day 14 and was significantly lower than pretreatment values by day 14. Starch of control PIPO and PSME did not significantly change with day. Sucrose was significantly affected by treatment (P=0.0203), type (P=0.0051), day (P=0.002), and the interaction between treatment and type was

significant (P=0.0008). However, sucrose of both PIPO and PSME treatment groups did not significantly differ from that of controls on any day. Sucrose of the heated group only differed between species at days 1 and 14 and not consistently, while sucrose did not significantly differ between species in the controls (Figure 4.4E,F). Glucose + fructose was significantly affected by day (P<0.0001) and the interaction between type and day was significant (P=0.0033). Glucose + fructose of both heat treated PIPO and PSME spiked on day 2 before declining back to pretreatment values by day 14 (Figure 4.4G,H). Control glucose + fructose increased with day in PSME but did not change with day in PIPO. Starch and glucose + fructose of both species were negatively related in the treatment group (P=0.049, R^2=0.40) but not in the controls (Figure 4.5).

4.5 Discussion

Thermotolerance assessments

Contrary to our hypothesis, PSME had a greater T_{50} assessed with both F_V/F_M and electrolyte leakage and T_{crit} assessed from F_O than PIPO, suggesting that PSME was more heat tolerant than PIPO. This is surprising given the habit of PIPO to establish on sunny, dry sites that experience higher temperatures than the cooler, moister sites on which the relatively more shade-tolerant PSME establishes (Hermann and Lavender 1990, Oliver *et al.* 1990). This result however is consistent with a study on co-occurring field-grown *Pinus halepensis* and *Quercus ilex* where (Méthy *et al.*, 1997) also hypothesized that *P. halepensis*, that naturally occurs under warmer and drier conditions and has become more dominant than *Q. ilex* in southern France, would be more heat tolerant than *Q. ilex*.

However, the authors found that *P. halepensis* was less heat tolerant than *Q. ilex,* underscoring that leaf heat tolerance is not always directly indicative of a species' distribution pattern and that other life history strategies related to reproductive age, germination rate, and dormancy may also impact species' distributions (Méthy *et al.*, 1997). In our study, life history strategies related to seasonal shifts in heat tolerance and rooting may help to elucidate our unexpected results. Heat tolerance of PSME seedlings remains the same year round whereas that of PIPO has been observed to fluctuate seasonally where heat tolerance declines during dormancy when it becomes fully cold-hardy (Burr *et al.*, 1993). The thermotolerance curves in this study were constructed in October when dormancy of field-grown plants begins, which may be why PIPO appeared to be less heat tolerant than PSME.

Another explanation for the lower heat tolerance in PIPO than PSME may be related to rooting strategies. Unlike PSME, which has a relatively shallow root system, PIPO has a deep root system that enables it to access deep soil water and maintain stomatal conductance and evaporative cooling during drought (Kolb & Robberecht, 1996; Kerr *et al.*, 2015). This is consistent with the observed greater stomatal conductance in PIPO than PSME (Figure 4.2). Thus, if grown in the same environment, PSME may experience higher leaf temperatures than does PIPO, which would require a greater heat tolerance in PSME (Cunningham & Read, 2006). PIPO seedlings that survived a summer drought in the field used transpiration to maintain leaf and stem temperatures 15°C and 30°C, respectively, below surrounding air temperature than those that died (Kolb & Robberecht, 1996). Consistent with these findings, PIPO seedlings were less susceptible

to drought-induced mortality than PSME seedlings in a common garden experiment (D. Marias, unpublished observations; (Rother *et al.*, 2015).

Regardless of population or species, T_{50} measured with electrolyte leakage was significantly greater than T_{50} assessed using F_V/F_M (Table 4.2, Figure 4.1), indicating that PSII was more sensitive to heat than cell membranes (Cunningham & Read, 2006). This highlights that different plant processes and tissues have different heat tolerances and that overall heat tolerance is difficult to evaluate with one metric (Bilger *et al.*, 1987; Larcher, 1995; Schreiber *et al.*, 1995; Teskey *et al.*, 2015).

The mean untreated F_V/F_M range of 0.72-0.75 for both populations and species is lower than optimal values of 0.83 (Björkman & Demmig, 1987), which could be related to the low PPFD conditions in the greenhouse. However, the F_V/F_M range is similar to previously reported values for PIPO and PSME in fall and winter, similar to the timing of this experiment (Marshall *et al.*, 2001; Adams III *et al.*, 2002). Regardless of population and species, F_V/F_M thermotolerance curves began to significantly decline above ~40°C (Figure 4.1A), also observed in tropical species (Krause *et al.*, 2010) and consistent with the finding that optimal leaf temperatures are relatively conserved from subtropical to boreal biomes (Helliker & Richter, 2008). F_V/F_M declined to 0 at ~55-58°C in both species, which is less than 63°C, the stem temperature of PIPO seedlings that resulted in mortality (Kolb & Robberecht, 1996). This suggests that needle thermotolerance is lower than stem thermotolerance and is consistent with the conclusion that stem temperatures may be a better indicator of seedling mortality than leaf temperatures (Kolb & Robberecht, 1996).

Responses to simulated heat wave

Both species exhibited significant reductions in F_V/F_M on days 1 and 2 after heat treatment (Figure 4.2), indicating substantial heat-induced damage including impairment of PSII reaction centers and disruptions in electron transport (Maxwell & Johnson, 2000; Sharkey, 2005; Chen *et al.*, 2012; Zhang *et al.*, 2012). However, heat treatment induced more significant reductions in F_V/F_M than gas exchange in both species (Figure 4.2). This is consistent with evidence that PSII is the most heat-sensitive component (Havaux, 1996) and that reductions in F_V/F_M can occur without corresponding shifts in photosynthesis (Baker, 1991; Murchie & Niyogi, 2011). Only PIPO displayed a transient reduction in photosynthesis and stomatal conductance one day after treatment that recovered to stable photosynthesis values by day 2. The transient decline in gas exchange only in PIPO is consistent with the lower T_{50}s, T_{crit}, and apparent heat tolerance of PIPO compared to PSME (Table 4.2, Figure 4.1) because chlorophyll fluorescence is a proxy for overall photosynthetic performance (Maxwell & Johnson, 2000). The greater relative decline in PIPO photosynthesis (81%) than stomatal conductance (42%) indicates that the ratio of photosynthesis to stomatal conductance or iWUE (Farquhar *et al.*, 1989) declined after treatment while that of PSME did not change. Although photosynthesis and stomatal conductance are often correlated, the smaller decline in stomatal conductance than photosynthesis in PIPO allowed evaporative cooling to occur when water supply was adequate. This was also observed in loblolly pine (*Pinus taeda*) seedlings in response to a 12°C heat wave under well-watered conditions (Ameye *et al.*, 2012).

Consistent with previous work, NSC dynamics after heat stress were variable (Sala *et al.*, 2012; Bita & Gerats, 2013; Escandón *et al.*, 2016). Although heat treatment did not affect total NSC or sucrose, heat treatment did induce a significant negative relationship between starch and glucose + fructose that was not observed in controls (Figure 4.5). In PSME from days 0 to 2, starch declined while glucose + fructose increased, and in PIPO on day 2, starch was lowest when glucose + fructose was highest (Figures 4.4, 4.5). This may indicate new production of glucose + fructose with concurrent consumption of starch and/or the conversion of starch to glucose + fructose (Geigenberger, 2011) in response to heat treatment. (Matías *et al.*, 2016) also observed an increase in total soluble sugars in response to elevated temperature in eastern and western provenances of silver fir (*Abies alba* Mill.) seedlings, and (Lafta & Lorenzen, 1995) found that starch declined in potato leaves in response to heat stress. The lack of treatment effect on sucrose, the end product of photosynthesis, suggests that this pattern was due to the conversion of starch to sugars rather than new production of photosynthate. Consistent with this, leaf $\delta^{13}C$, which can indicate turnover of NSC if $\delta^{13}C$ shifts (Gutierrez & Meinzer, 1994; Damesin *et al.*, 1998; Scartazza *et al.*, 2013), was also not affected by treatment. The accumulation of glucose + fructose in response to heat treatment may indicate the allocation of NSC to repairing the heat-induced damage (as indicated by F_V/F_M, Figure 4.2). Glucose + fructose are necessary for osmoregulation, maintaining cell water balance, and membrane stability (Bita & Gerats, 2013), and higher glucose levels have been associated with higher heat stress tolerance (Liu & Huang, 2000; Xiong *et al.*, 2015). Although heat treated PSME demonstrated no shifts in gas

exchange, starch of heat-treated PSME steadily declined with day unlike controls (Figure 4.4c,d). This suggests that heat stress can influence NSC dynamics without changes in gas exchange in PSME. These findings support that the shifts in starch and glucose + fructose (Figure 4.5) were related to NSC demand (i.e. repair, metabolism) rather than supply (i.e. gas exchange). Although this study was conducted under well-watered conditions, it is likely that high temperature stress will substantially impact carbon metabolism during drought (Adams *et al.*, 2013).

Population differences

We found no significant differences in thermotolerance parameters (e.g. T_{50}, T_{crit}), gas exchange, or NSC between populations from different climates of origin (Table 4.2), consistent with other studies (Maherali *et al.*, 2002; Daas *et al.*, 2008; Gimeno *et al.*, 2009). This may be because our seedlings were grown in and were acclimated to the same environmental growing conditions in the greenhouse. This was also the case in a common garden experiment where coastal and desert species expected to have heat tolerances reflecting the contrasting climates of origin did not display population differences in heat tolerance based on chlorophyll fluorescence (Knight & Ackerly, 2002). Similarly, (Gimeno *et al.*, 2009) found that the heat tolerance based on chlorophyll fluorescence of *Quercus ilex* seedlings increased with increasing exposure to drought and (Ghouil *et al.*, 2003) found that T_{crit} increased with greater acclimation temperature independent of climate of origin. Together, these suggest that phenotypic plasticity to the environmental growing conditions may override ecotypic adaptations to the climate of

origin (Gimeno *et al.*, 2009) in terms of heat stress responses. However, population differences may become more apparent under greater heat stress (Matías *et al.*, 2016) than that applied in this study.

In contrast to the thermotolerance parameters and heat stress responses, $\delta^{13}C$ significantly differed between populations and reflected each population's climate of origin and associated drought resistance. The $\delta^{13}C$ values were lower than previously reported due to the relatively higher [CO_2] in the greenhouse, common in greenhouse studies (Matías *et al.*, 2016). $PIPO_{dry}$ and $PSME_{dry}$ from climates with lower MAP had greater mean $\delta^{13}C$ than the $PIPO_{wet}$ and $PSME_{wet}$ populations from climates with higher MAP (Table 4.1, Figure 4.3). As $\delta^{13}C$ is a proxy for iWUE (Farquhar *et al.*, 1989) and drought resistance (Jones, 2009), these data provide support for ecotypic variation in iWUE between populations where populations from drier climates have greater iWUE and drought resistance than those from wetter climates (Schulze *et al.*, 1998; Diefendorf *et al.*, 2010; Kerr *et al.*, 2015). Greater iWUE potentially increases the ratio of carbon gained to water lost through stomata, which becomes increasingly important during drought when plants balance the competing risks of hydraulic failure and impaired carbon assimilation. Thus, populations with greater iWUE are better adapted to cope with drought stress. Although populations differed, $\delta^{13}C$ did not significantly differ between species when populations were pooled. This study was conducted under well-watered conditions but species differences may emerge under drought stress (Matías *et al.*, 2016), given the different drought tolerances and rooting strategies between species. Our results suggest that thermotolerance and heat stress responses may be governed by phenotypic

plasticity while drought resistance appeared to be determined by ecotypes and the climate of origin. This may be because the difference in MAP between wet and dry populations was greater than temperature (Table 4.1).

Conclusions

Due to the projected increases in the frequency of heat waves and drought, the high vulnerability of the seedling developmental stage to heat stress at the soil surface, and the major impacts of temperature and seedling survival on species' distributions, characterizing seedling physiological responses to heat stress is crucial. This study emphasizes that leaf thermotolerance is only one metric describing how seedlings manage heat stress and that mitigating heat stress involves whole plant traits and strategies likely including stem thermotolerance, seasonal shifts in thermotolerance, and rooting strategies. Heat stress influenced seedling NSC dynamics, providing more evidence that heat stress will impact carbon metabolism during drought. The results also suggest that population differences in drought resistance were driven by climate of origin while heat stress responses were governed more by phenotypic plasticity and acclimation to environmental growing conditions. This is important to consider when predicting responses to future climatic change and identifying physiological mechanisms underpinning shifts in species' distributions.

4.6 Acknowledgements

This work was supported by the NSF Graduate Research Fellowship Program and NSF grant IOS 11-46746. We are grateful to Kelly Kerr and Alicia Magedman for

assistance with sowing seeds and the OSU Greenhouse Operations staff for their assistance with the maintenance of plant material.

4.7 References

Adams HD, Germino MJ, Breshears DD, Barron-Gafford GA, Guardiola-Claramonte M, Zou CB, Huxman TE (2013) Nonstructural leaf carbohydrate dynamics of Pinus edulis during drought-induced tree mortality reveal role for carbon metabolism in mortality mechanism. *New Phytologist*, **197**, 1142–1151.

Adams III WW, Demmig-Adams B, Rosenstiel TN, Brightwell AK, Ebbert V (2002) Photosynthesis and Photoprotection in Overwintering Plants. *Plant Biology*, **4**, 545–557.

Ameye M, Wertin TM, Bauweraerts I, McGuire MA, Teskey RO, Steppe K (2012) The effect of induced heat waves on Pinus taeda and Quercus rubra seedlings in ambient and elevated CO2 atmospheres. *New Phytologist*, **196**, 448–461.

Aranda I, Alía R, Ortega U, Dantas ÂK, Majada J (2009) Intra-specific variability in biomass partitioning and carbon isotopic discrimination under moderate drought stress in seedlings from four Pinus pinaster populations. *Tree Genetics & Genomes*, **6**, 169–178.

Baker NR (1991) A possible role for photosystem II in environmental perturbations of photosynthesis. *Physiologia Plantarum*, **81**, 563–570.

Bilger W, Schreiber U, Lange OL (1987) Chlorophyll fluorescence as an indicator of heat induced limitation of photosynthesis in Arbutus unedo L. In: *Plant Response to Stress* (eds Tenhunen JD, Catarino FM, Lange OL, Oechel WC), pp. 391–399. Springer Berlin Heidelberg.

Bita CE, Gerats T (2013) Plant tolerance to high temperature in a changing environment: scientific fundamentals and production of heat stress-tolerant crops. *Frontiers in Plant Science*, **4**.

Björkman O, Demmig B (1987) Photon yield of O2 evolution and chlorophyll fluorescence characteristics at 77 K among vascular plants of diverse origins. *Planta*, **170**, 489–504.

Burr KE, Wallner SJ, Tinus RW (1993) Heat Tolerance, Cold Hardiness, and Bud Dormancy Relationships in Seedlings of Selected Conifers. *Journal of the American Society for Horticultural Science*, **118**, 840–844.

Chen WR, Zheng JS, Li YQ, Guo WD (2012) Effects of high temperature on photosynthesis, chlorophyll fluorescence, chloroplast ultrastructure, and antioxidant activities in fingered citron. *Russian Journal of Plant Physiology*, **59**, 732–740.

Couée I, Sulmon C, Gouesbet G, Amrani AE (2006) Involvement of soluble sugars in reactive oxygen species balance and responses to oxidative stress in plants. *Journal of Experimental Botany*, **57**, 449–459.

Cunningham SC, Read J (2006) Foliar temperature tolerance of temperate and tropical evergreen rain forest trees of Australia. *Tree Physiology*, **26**, 1435–1443.

Daas C, Montpied P, Hanchi B, Dreyer E (2008) Responses of photosynthesis to high temperatures in oak saplings assessed by chlorophyll-a fluorescence: inter-specific diversity and temperature-induced plasticity. *Annals of Forest Science*, **65**, 1.

Damesin C, Rambal S, Joffre R (1998) Seasonal and annual changes in leaf δ13C in two co-occurring Mediterranean oaks: relations to leaf growth and drought progression. *Functional Ecology*, **12**, 778–785.

Diefendorf AF, Mueller KE, Wing SL, Koch PL, Freeman KH (2010) Global patterns in leaf 13C discrimination and implications for studies of past and future climate. *Proceedings of the National Academy of Sciences*, **107**, 5738–5743.

Dietze MC, Sala A, Carbone MS, Czimczik CI, Mantooth JA, Richardson AD, Vargas R (2014) Nonstructural carbon in woody plants. *Annual Review of Plant Biology*, **65**, 667–687.

Du B, Jansen K, Junker LV *et al.* (2014) Elevated temperature differently affects foliar nitrogen partitioning in seedlings of diverse Douglas fir provenances. *Tree Physiology*, tpu074.

Duan H, Amthor JS, Duursma RA, O'Grady AP, Choat B, Tissue DT (2013) Carbon dynamics of eucalypt seedlings exposed to progressive drought in elevated [CO2] and elevated temperature. *Tree Physiology*, tpt061.

Escandón M, Cañal MJ, Pascual J, Pinto G, Correia B, Amaral J, Meijón M (2016) Integrated physiological and hormonal profile of heat-induced thermotolerance in Pinus radiata. *Tree Physiology*, **36**, 63–77.

Farquhar G, Richards R (1984) Isotopic composition of plant carbon correlates with water-use efficiency of wheat genotypes. *Functional Plant Biology*, **11**, 539–552.

Farquhar G, O'Leary M, Berry J (1982) On the Relationship Between Carbon Isotope Discrimination and the Intercellular Carbon Dioxide Concentration in Leaves. *Functional Plant Biology*, **9**, 121–137.

Farquhar GD, Hubick KT, Condon AG, Richards RA (1989) Carbon Isotope Fractionation and Plant Water-Use Efficiency. In: *Stable Isotopes in Ecological Research* (eds Rundel PW, Ehleringer JR, Nagy KA), pp. 21–40. Springer New York.

Geigenberger P (2011) Regulation of Starch Biosynthesis in Response to a Fluctuating Environment. *Plant Physiology*, **155**, 1566–1577.

Génard M, Dauzat J, Franck N, Lescourret F, Moitrier N, Vaast P, Vercambre G (2008) Carbon allocation in fruit trees: from theory to modelling. *Trees*, **22**, 269–282.

Genty B, Briantais J-M, Baker NR (1989) The relationship between the quantum yield of photosynthetic electron transport and quenching of chlorophyll fluorescence. *Biochimica et Biophysica Acta (BBA)-General Subjects*, **990**, 87–92.

Ghouil H, Montpied P, Epron D, Ksontini M, Hanchi B, Dreyer E (2003) Thermal optima of photosynthetic functions and thermostability of photochemistry in cork oak seedlings. *Tree Physiology*, **23**, 1031–1039.

Gimeno TE, Pías B, Lemos-Filho JP, Valladares F (2009) Plasticity and stress tolerance override local adaptation in the responses of Mediterranean holm oak seedlings to drought and cold. *Tree Physiology*, **29**, 87–98.

Gutierrez M, Meinzer F (1994) Carbon Isotope Discrimination and Photosynthetic Gas Exchange in Coffee Hedgerows During Canopy Development. *Functional Plant Biology*, **21**, 207–219.

Hao Z, AghaKouchak A, Phillips TJ (2013) Changes in concurrent monthly precipitation and temperature extremes. *Environmental Research Letters*, **8**, 34014.

Hartmann H, Trumbore S (2016) Understanding the roles of nonstructural carbohydrates in forest trees – from what we can measure to what we want to know. *New Phytologist*, **211**, 386–403.

Havaux M (1996) Short-term responses of Photosystem I to heat stress : Induction of a PS II-independent electron transport through PS I fed by stromal components. *Photosynthesis Research*, **47**, 85–97.

Helliker BR, Richter SL (2008) Subtropical to boreal convergence of tree-leaf temperatures. *Nature*, **454**, 511–514.

Horváth I, Glatz A, Nakamoto H *et al.* (2012) Heat shock response in photosynthetic organisms: Membrane and lipid connections. *Progress in Lipid Research*, **51**, 208–220.

Hubick K, Farquhar G, Shorter R (1986) Correlation Between Water-Use Efficiency and Carbon Isotope Discrimination in Diverse Peanut (*Arachis*) Germplasm. *Australian Journal of Plant Physiology*, **13**, 803.

Intergovernmental Panel on Climate Change (2014) IPCC Fifth Assessment Synthesis Report. *IPCC 5th Assessment Synthesis Report*.

Jones HG (2009) What is water use efficiency? In: Bacon M (ed) Water use efficiency in plant biology. Blackwell Publishing, Oxford, UK, pp. 27-41.

Kerr KL, Meinzer FC, McCulloh KA, Woodruff DR, Marias DE (2015) Expression of functional traits during seedling establishment in two populations of Pinus ponderosa from contrasting climates. *Tree Physiology*, **35**, 535–548.

Knight CA, Ackerly DD (2002) An ecological and evolutionary analysis of photosynthetic thermotolerance using the temperature-dependent increase in fluorescence. *Oecologia*, **130**, 505–514.

Kolb PF, Robberecht R (1996) High temperature and drought stress effects on survival of Pinus ponderosa seedlings. *Tree Physiology*, **16**, 665–672.

Kozlowski T (1992) Carbohydrate sources and sinks in woody plants. *The Botanical Review*, **58**, 107–222.

Krause GH, Winter K, Krause B, Jahns P, García M, Aranda J, Virgo A (2010) High-temperature tolerance of a tropical tree, Ficus insipida: methodological reassessment and climate change considerations. *Functional Plant Biology*, **37**, 890–900.

Lafta AM, Lorenzen JH (1995) Effect of High Temperature on Plant Growth and Carbohydrate Metabolism in Potato. *Plant Physiology*, **109**, 637–643.

Larcher W (1995) Photosynthesis as a Tool for Indicating Temperature Stress Events. In: *Ecophysiology of Photosynthesis* (eds Schulze PDE-D, Caldwell PDMM), pp. 261–277. Springer Berlin Heidelberg.

Lindgren K, Hällgren J-E (1993) Cold acclimation of Pinus contorta and Pinus sylvestris assessed by chlorophyll fluorescence. *Tree Physiology*, **13**, 97–106.

Liu X, Huang B (2000) Carbohydrate Accumulation in Relation to Heat Stress Tolerance in Two Creeping Bentgrass Cultivars. *Journal of the American Society for Horticultural Science*, **125**, 442–447.

Maherali H, Williams BL, Paige KN, Delucia EH (2002) Hydraulic differentiation of Ponderosa pine populations along a climate gradient is not associated with ecotypic divergence. *Functional Ecology*, **16**, 510–521.

Marshall JD, Rehfeldt GE, Monserud RA (2001) Family differences in height growth and photosynthetic traits in three conifers. *Tree Physiology*, **21**, 727–734.

Matías L, Gonzalez-Díaz P, Quero JL, Camarero JJ, Lloret F, Jump AS (2016) Role of geographical provenance in the response of silver fir seedlings to experimental warming and drought. *Tree Physiology*, tpw049.

Maxwell K, Johnson GN (2000) Chlorophyll fluorescence—a practical guide. *Journal of experimental botany*, **51**, 659–668.

Méthy M, Gillon D, Houssard C (1997) Temperature-induced changes of photosystem II activity in Quercus ilex and Pinus halepensis. *Canadian Journal of Forest Research*, **27**, 31–38.

Murchie EH, Niyogi KK (2011) Manipulation of Photoprotection to Improve Plant Photosynthesis. *Plant Physiology*, **155**, 86–92.

Niinemets Ü (2010) Responses of forest trees to single and multiple environmental stresses from seedlings to mature plants: Past stress history, stress interactions, tolerance and acclimation. *Forest Ecology and Management*, **260**, 1623–1639.

Perić S, JAZBEC A, Tijardović M, Margaletić J, Ivanković M, Pilaš I, Medak J (2009) Provenance studies of Douglas fir in the locality of» Kontija «(Istria). *Periodicum biologorum*, **111**, 487–493.

Ramírez-Valiente JA, Sánchez-Gómez D, Aranda I, Valladares F (2010) Phenotypic plasticity and local adaptation in leaf ecophysiological traits of 13 contrasting cork oak populations under different water availabilities. *Tree Physiology*, **30**, 618–627.

Roitsch T, González M-C (2004) Function and regulation of plant invertases: sweet sensations. *Trends in plant science*, **9**, 606–613.

Rother MT, Veblen TT, Furman LG (2015) A field experiment informs expected patterns of conifer regeneration after disturbance under changing climate conditions. *Canadian Journal of Forest Research*, **45**, 1607–1616.

Sala A, Woodruff DR, Meinzer FC (2012) Carbon dynamics in trees: feast or famine? *Tree Physiology*, tpr143.

Salvucci ME, Crafts-Brandner SJ (2004) Relationship between the heat tolerance of photosynthesis and the thermal stability of rubisco activase in plants from contrasting thermal environments. *Plant Physiology*, **134**, 1460–1470.

Scartazza A, Moscatello S, Matteucci G, Battistelli A, Brugnoli E (2013) Seasonal and inter-annual dynamics of growth, non-structural carbohydrates and C stable isotopes in a Mediterranean beech forest. *Tree physiology*, **33**, 730–742.

Schreiber U, Berry JA (1977) Heat-induced changes of chlorophyll fluorescence in intact leaves correlated with damage of the photosynthetic apparatus. *Planta*, **136**, 233–238.

Schreiber U, Bilger W, Neubauer C (1995) Chlorophyll Fluorescence as a Nonintrusive Indicator for Rapid Assessment of In Vivo Photosynthesis. In: *Ecophysiology of Photosynthesis* (eds Schulze PDE-D, Caldwell PDMM), pp. 49–70. Springer Berlin Heidelberg.

Schulze E-D, Williams RJ, Farquhar GD, Schulze W, Langridge J, Miller JM, Walker BH (1998) Carbon and nitrogen isotope discrimination and nitrogen nutrition of trees along a rainfall gradient in northern Australia. *Functional Plant Biology*, **25**, 413–425.

Sevanto S, Dickman LT (2015) Where does the carbon go?—Plant carbon allocation under climate change. *Tree physiology*, **35**, 581–584.

Sharkey TD (2005) Effects of moderate heat stress on photosynthesis: importance of thylakoid reactions, rubisco deactivation, reactive oxygen species, and thermotolerance provided by isoprene. *Plant, Cell & Environment*, **28**, 269–277.

Sorensen FC (1983) Geographic Variation in Seedling Douglas-Fir (Pseudotsuga Menziesii) from the Western Siskiyou Mountains of Oregon. *Ecology*, **64**, 696–702.

Sugio A, Dreos R, Aparicio F, Maule AJ (2009) The cytosolic protein response as a subcomponent of the wider heat shock response in Arabidopsis. *The Plant Cell*, **21**, 642–654.

Teskey R, Wertin T, Bauweraerts I, Ameye M, McGuire MA, Steppe K (2015) Responses of tree species to heat waves and extreme heat events. *Plant, cell & environment*, **38**, 1699–1712.

Tomlinson KW, Poorter L, Sterck FJ, Borghetti F, Ward D, de Bie S, van Langevelde F (2013) Leaf adaptations of evergreen and deciduous trees of semi-arid and humid savannas on three continents. *Journal of Ecology*, **101**, 430–440.

Wahid A, Gelani S, Ashraf M, Foolad MR (2007) Heat tolerance in plants: an overview. *Environmental and experimental botany*, **61**, 199–223.

Weis E, Berry JA (1987) Quantum efficiency of photosystem II in relation to "energy"-dependent quenching of chlorophyll fluorescence. *Biochimica et Biophysica Acta (BBA)-Bioenergetics*, **894**, 198–208.

Woodruff DR, Meinzer FC (2011) Water stress, shoot growth and storage of non-structural carbohydrates along a tree height gradient in a tall conifer. *Plant, cell & environment*, **34**, 1920–1930.

Xiong D, Yu T, Ling X, Fahad S, Peng S, Li Y, Huang J (2015) Sufficient leaf transpiration and nonstructural carbohydrates are beneficial for high-temperature

tolerance in three rice (Oryza sativa) cultivars and two nitrogen treatments. *Functional Plant Biology*, **42**, 347–356.

Yamashita T, Butler WL (1968) Photoreduction and Photophosphorylation with Tris-Washed Chloroplasts. *Plant Physiology*, **43**, 1978–1986.

Zhang J, Marshall JD, Jaquish BC (1993) Genetic differentiation in carbon isotope discrimination and gas exchange in Pseudotsuga menziesii. *Oecologia*, **93**, 80–87.

Zhang J-L, Poorter L, Hao G-Y, Cao K-F (2012) Photosynthetic thermotolerance of woody savanna species in China is correlated with leaf life span. *Annals of Botany*, **110**, 1027–1033.

Zhao J, Hartmann H, Trumbore S, Ziegler W, Zhang Y (2013) High temperature causes negative whole-plant carbon balance under mild drought. *New Phytologist*, **200**, 330–339.

Zheng D, Hunt Jr ER, Running SW (1993) A daily soil temperature model based on air temperature and precipitation for continental applications. *Climate Research*, **2**, 183–191.

4.8 Figures & Tables

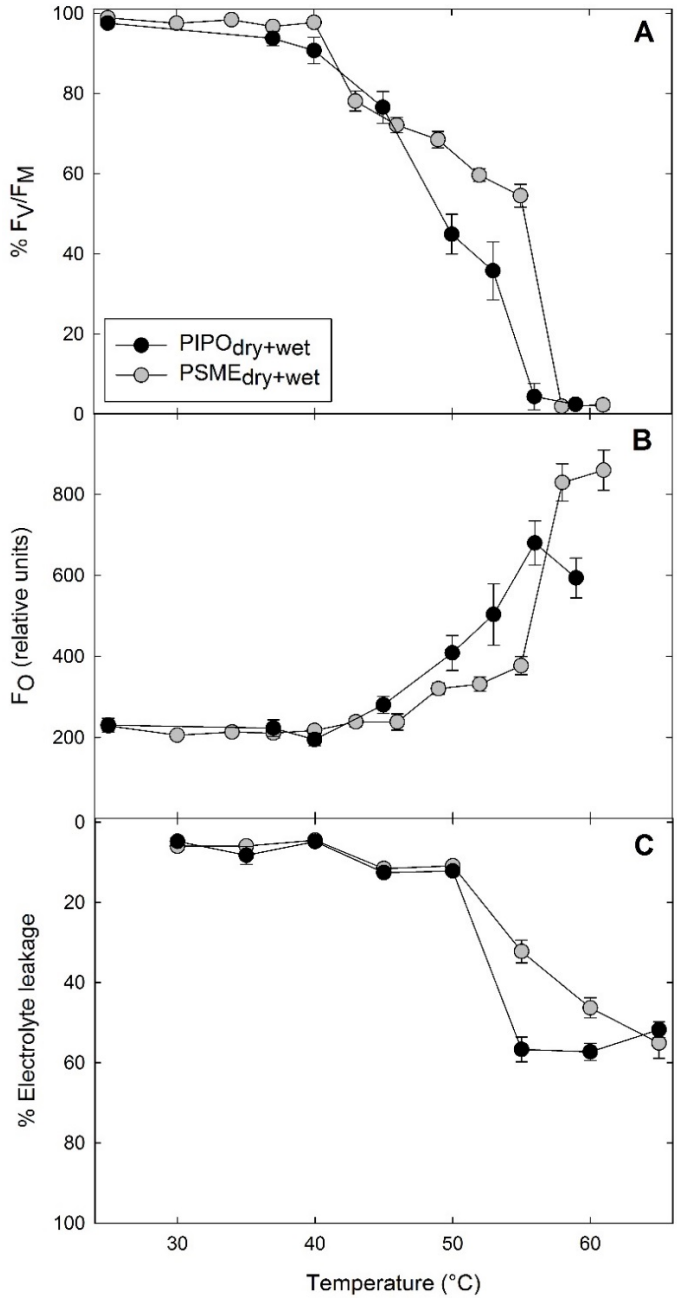

Figure 4.1 Thermotolerance curves measured with F_V/F_M (A), Fo (B), and electrolyte leakage (C) as a function of temperature for dry, wet, and dry+wet populations of PIPO and PSME used to derive thermotolerance parameters: T_{50} (F_V/F_M), T_{50} (electrolyte leakage), and T_{crit} (F_O), respectively. N=5. Error bars represent SE.

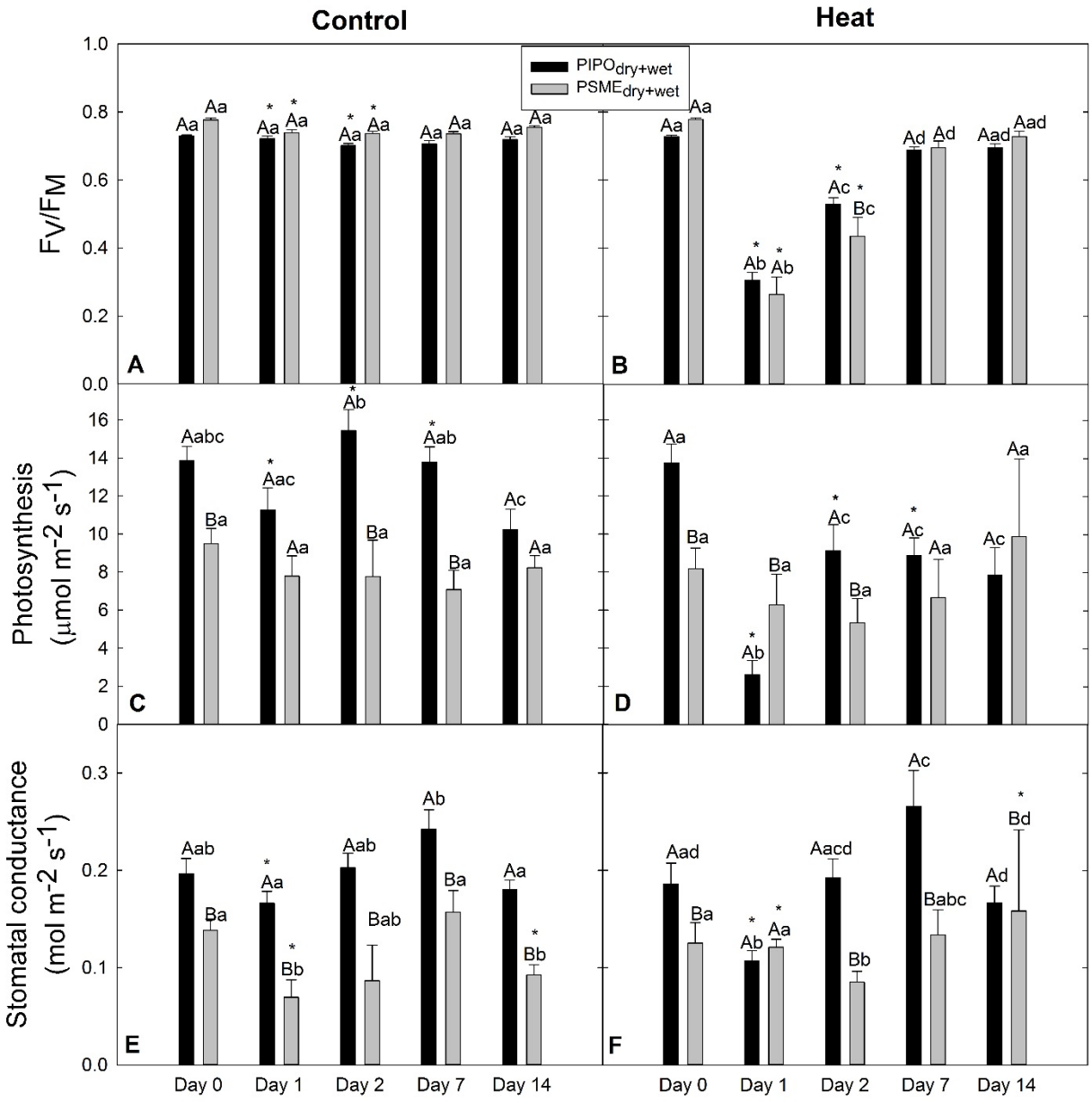

Figure 4.2 Time courses of mean F_V/F_M (A,B), photosynthesis (C,D), and stomatal conductance (E,F) of PIPO and PSME in control (A,C,E) and heat treatment (B,D,F) groups. Uppercase letters indicate significant differences between species within each day and group. Lowercase letters indicate significant differences among days within species and group. Asterisks indicate significant differences between control and heat treatment groups within species and day. N=10. Error bars represent ± SE.

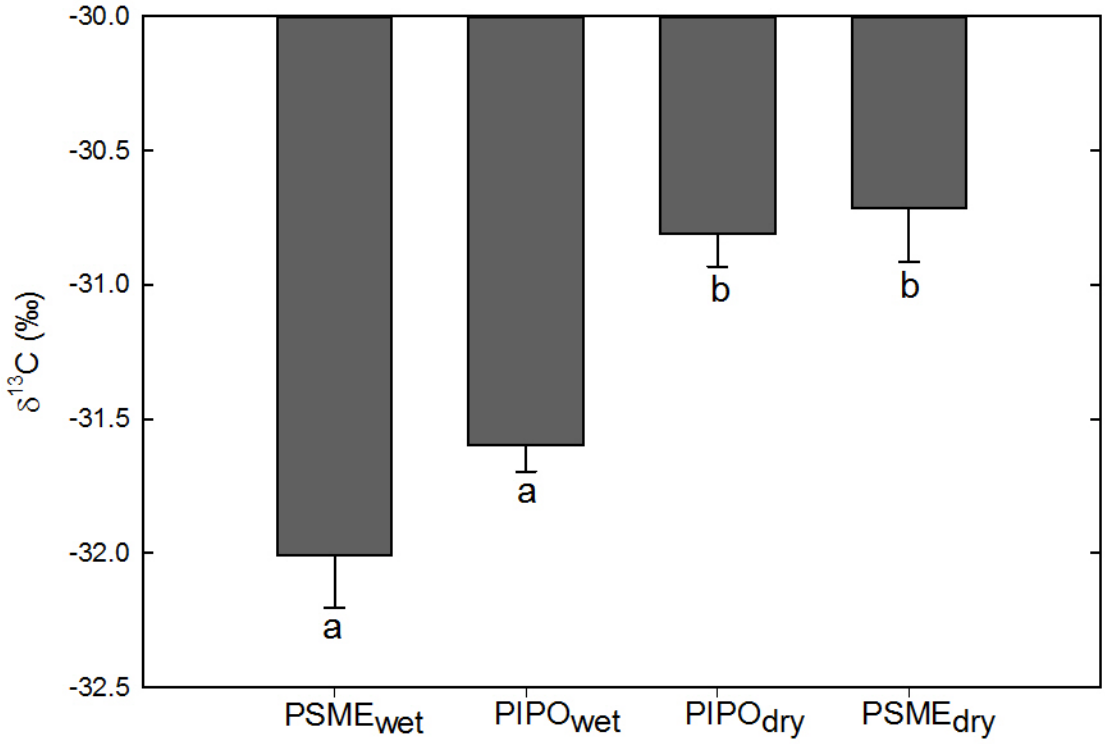

Figure 4.3 Mean leaf $\delta^{13}C$ of $PIPO_{dry}$, $PIPO_{wet}$, $PSME_{dry}$, and $PSME_{wet}$ pooled for all sampling days and both treatment groups. Letters indicate significant differences among type (i.e. $species_{population}$). Error bars represent ± SE.

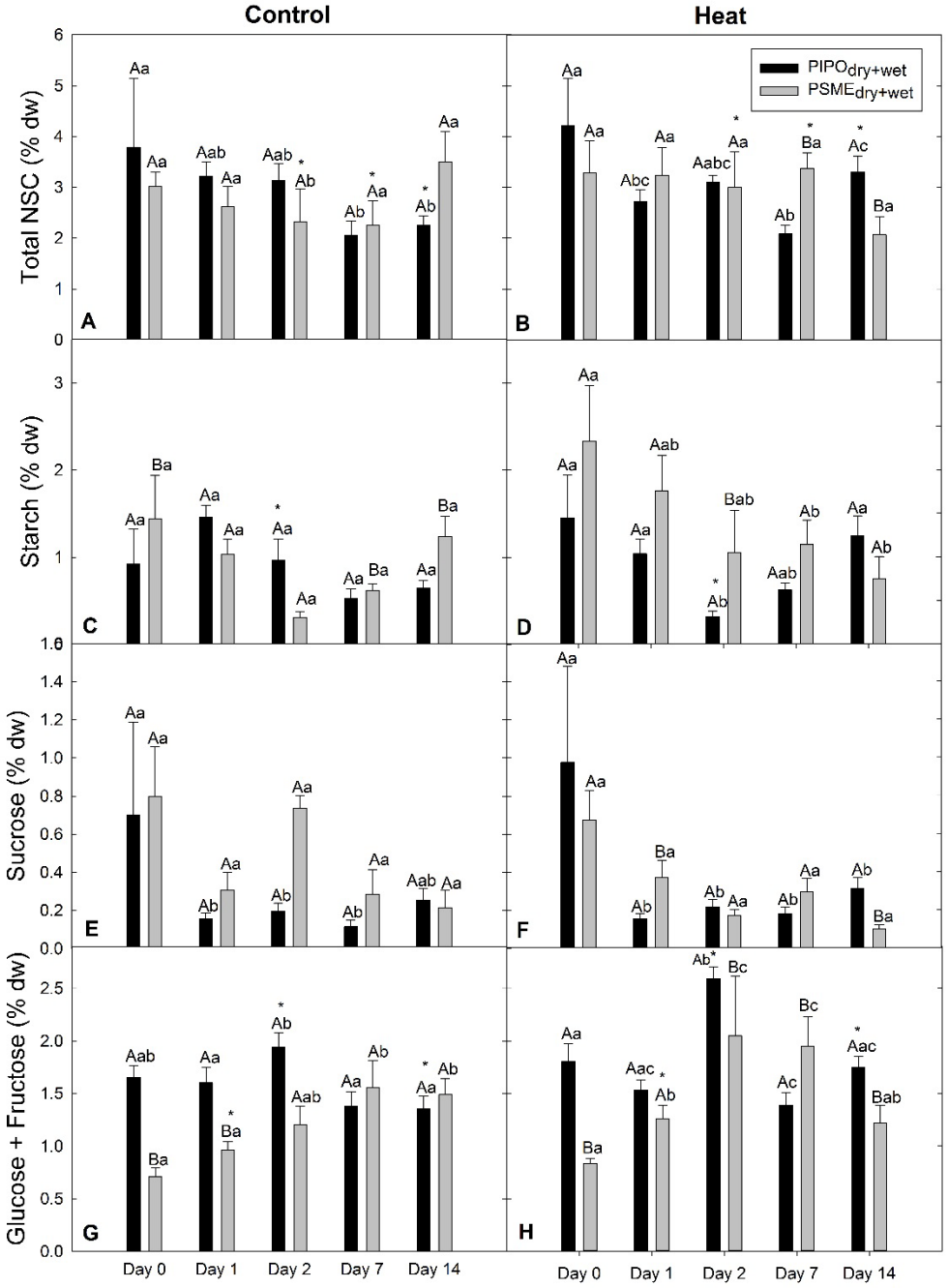

Figure 4.4 Time courses of mean leaf total NSC (A,B), starch (C,D), sucrose (E,F), and glucose + fructose (G,H) of PIPO and PSME in control (A,C,E,G) and heat treatment (B,D,F,H) groups. Uppercase letters indicate significant differences between species within each day and group. Lowercase letters indicate significant differences among days within species and group. Asterisks indicate significant differences between control and heat treatment groups within species and day. N=10. Error bars represent ± SE.

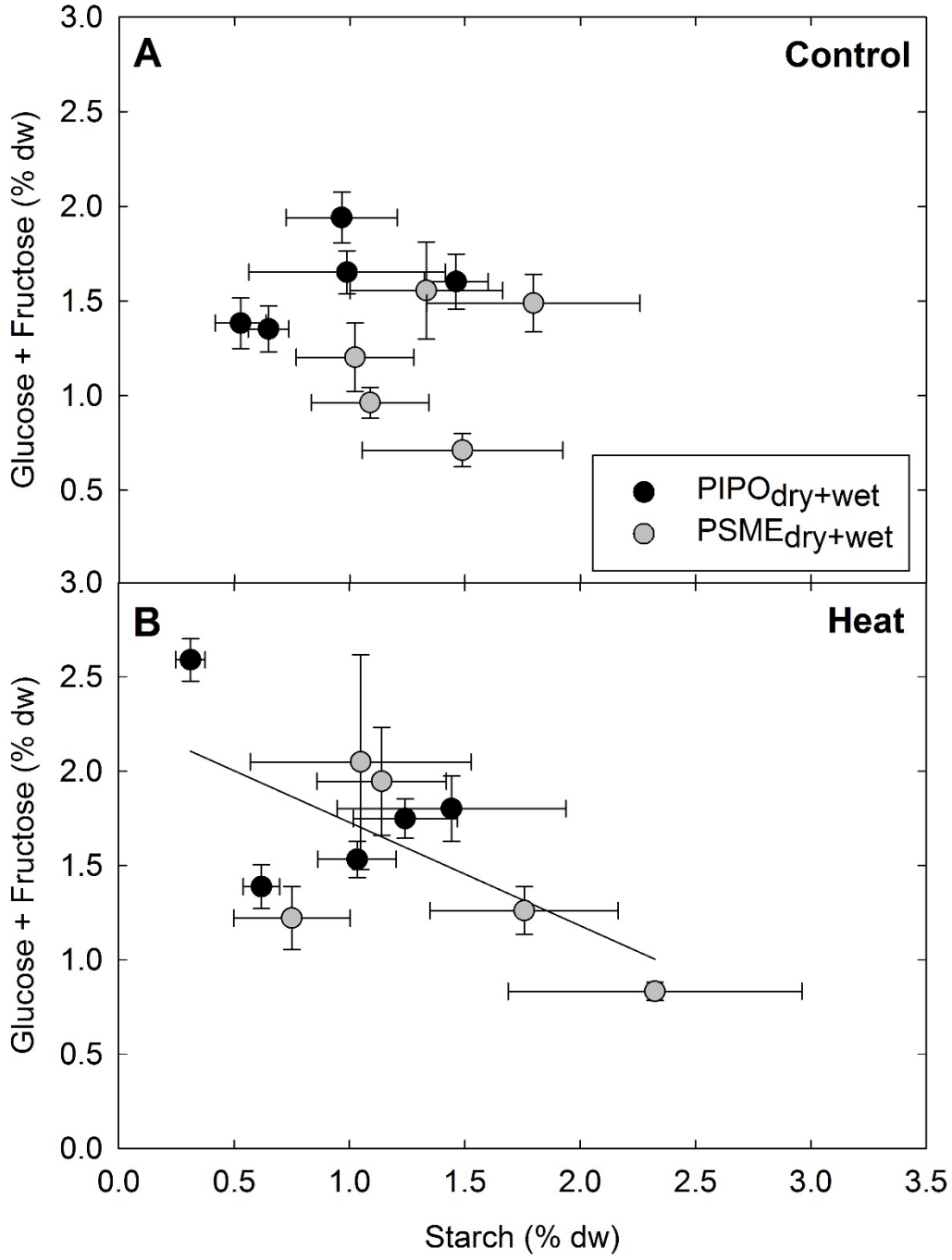

Figure 4.5 Mean leaf starch plotted against mean glucose + fructose for each sampling day in PIPO and PSME control (A) and heat (B) treatment groups (R^2=0.40, P=0.049). Error bars represent ± SE.

Table 4.1 Mean annual precipitation (MAP) and mean minimum and maximum temperatures in winter (December-February) and summer (June-August) of each PIPO and PSME population.

		$PIPO_{dry}$	$PIPO_{wet}$	$PSME_{dry}$	$PSME_{wet}$
	Coordinates	44.8343°N, 119.7944°W	44.5646°N, 123.2620°W	42.895N, 123.0W	44.851N, 123.818W
	Elevation (m)	621	71	750	401
	MAP (mm)	337	1043	1056	3054
Winter (Dec-Feb)	**Minimum temperature (°C)**	-2.7	1.2	0.2	1.5
	Maximum temperature (°C)	8.4	8.6	9.1	8.3
Summer (Jun-Aug)	**Minimum temperature (°C)**	10.7	10.2	10.4	9.2
	Maximum temperature (°C)	32.4	25.8	26.9	21.1

Table 4.2 Thermotolerance parameters (°C) derived from curves of F_V/F_M, electrolyte leakage, and F_O as a function of treatment temperature for dry, wet, and dry+wet populations of PIPO and PSME. Uppercase letters indicate significant differences between species. There were no significant differences between populations. Asterisks indicate significant differences in T_{50} between F_V/F_M and electrolyte leakage methods.

	$PIPO_{dry}$	**$PIPO_{wet}$**	**$PIPO_{dry+wet}$**	**$PSME_{dry}$**	**$PSME_{wet}$**	**$PSME_{dry+wet}$**
T_{50} (F_V/F_M)	48.8 ± 1.4 *	50.5 ± 0.41 *	49.6 ± 0.76 B *	52.8 ± 1.2 *	52.0 ± 0.22 *	52.4 ± 0.29 A *
T_{50} (electrolyte leakage)	61.8 ± 1.8 *	61.6 ± 1.7 *	61.7 ± 1.6 B *	63.6 ± 1.5 *	66.0 ± 2.4 *	64.8 ± 2.3 A *
T_{crit} (F_O)	45.1 ± 0.33	42.3 ± 1.1	44.3 ± 1.0 B	48.1 ± 0.88	48.3 ± 0.30	48.2 ± 0.45 A

N=5. Significance level is $P<0.05$. Means ± SE.

Table 4.3 Marginal F-tests for F_V/F_M, photosynthesis, stomatal conductance, and $\delta^{13}C$.

	F_V/F_M				**Photosynthesis (μmol m^{-2} s^{-1})**				**Stomatal Conductance (mol m^{-2} s^{-1})**				**$\delta^{13}C$ (‰)**			
	numDF	denDF	F-value	P-value	numDF	denDF	F-value	P-value	numDF	denDF	F-value	P-value	numDF	denDF	F-value	P-value
Intercept	1	713	11530.7	**<0.0001**	1	59	1147.0	**<0.0001**	1	58	3219.2	**<0.0001**	1	48	94418.91	**<0.0001**
Treatment	1	62	126.8	**<0.0001**	1	58	29.2	**<0.0001**	1	58	1.4	0.2411	1	48	1.60	0.2123
Type ($species_{population}$)	1	62	0.003	0.9552	2	58	12.9	**<0.0001**	2	58	34.5	**<0.0001**	1	48	6.27	**0.0157**
Day	4	713	141.0	**<0.0001**	4	59	12.2	**<0.0001**	4	57	10.0	**<0.0001**	2	37	19.87	**<0.0001**
Treatment x Type	1	62	0.12	0.7322	2	58	4.8	**0.0123**	2	58	0.90	0.4141	1	48	0.25	0.6226
Treatment x Day	4	713	131.6	**<0.0001**	4	59	4.5	**0.0030**	4	57	0.19	0.9451	2	37	4.55	**0.0172**
Type x Day	4	713	0.99	0.4103	8	59	3.6	**0.0017**	8	57	1.5	0.1735	2	37	1.12	0.3381
Treatment x Type x Day	4	713	0.45	0.7692	8	59	2.1	**0.0456**	8	57	1.7	0.1218	2	37	1.85	0.1711

N=5. Bolded P-values indicate P<0.05. Type = $PIPO_{dry}$, $PIPO_{wet}$, $PSME_{dry}$, $PSME_{wet}$. NumDF and denDF are the degrees of freedom in the numerator and denominator, respectively.

Table 4.4 Marginal F-tests for total NSC, starch, sucrose, and glucose + fructose.

	Total NSC				**Starch**				**Sucrose**				**Glucose + Fructose**			
	numDF	denDF	F-value	P-value	numDF	denDF	F-value	P-value	numDF	denDF	F-value	P-value	numDF	denDF	F-value	P-value
Intercept	1	97	571.1	**<0.0001**	1	96	14.2	**0.0003**	1	80	472.7	**<0.0001**	1	97	132.7	**<0.0001**
Treatment	1	62	4.1	**0.0465**	1	62	0.11	0.7389	1	62	5.7	**0.0203**	1	62	3.4	0.0699
Type ($species_{population}$)	1	62	1.0	0.3101	1	62	2.1	0.1545	1	62	8.4	**0.0051**	1	62	2.0	0.1583
Day	4	97	5.1	**0.0009**	4	96	7.0	**0.0001**	4	80	6.1	**0.0002**	4	97	8.4	**<0.0001**
Treatment x Type	1	62	1.8	0.1845	1	62	1.7	0.1944	1	62	12.3	**0.0008**	1	62	0.35	0.5581
Treatment x Day	4	97	2.0	0.1041	4	96	6.4	**0.0001**	4	80	0.31	0.8678	4	97	1.1	0.3542
Type x Day	4	97	2.3	0.0688	4	96	1.6	0.1802	4	80	0.43	0.7845	4	97	4.2	**0.0033**
Treatment x Type x Day	4	97	2.7	**0.0374**	4	96	2.4	0.0548	4	80	1.2	0.3294	4	97	0.63	0.6379

N=5. Bolded P-values indicate P<0.05. Type = $PIPO_{dry}$, $PIPO_{wet}$, $PSME_{dry}$, $PSME_{wet}$. NumDF and denDF are the degrees of freedom in the numerator and denominator, respectively

4.9 Appendices

Appendix Table 4.1 Average daytime and nighttime air temperature, relative humidity, and maximum photosynthetic photon flux density (PPFD) in the greenhouse during the two growth chamber experimental rounds in the fall of 2014.

	16-30 October 2014 PSME	**17 November-1 December 2014 PIPO**
Average daytime temperature (°C)	22.2	20.9
Average nighttime temperature (°C)	19.1	18.2
Average daytime relative humidity (%)	67.6	66.6
Average nighttime relative humidity (%)	73.8	72.1
Daily maximum PPFD (µmol m^{-2} s^{-1})	357.3	213.2

Appendix Table 4.2 Average air, soil, and leaf temperatures during 1 h of temperature treatment in the growth chamber.

	16-30 October 2014 PSME	17 November-1 December 2014 PIPO
Air (°C)	45.7	45.5
Soil (°C)	22.1	22.6
Leaf (°C)	45.4	43.9

5. INVESTIGATING OLD-GROWTH PONDEROSA PINE PHYSIOLOGY USING TREE-RINGS $\Delta^{13}C$, $\Delta^{18}O$, AND A PROCESS-BASED MODEL

Danielle E. Marias, Christopher Still, J. Renée Brooks, Youngil Kim, Frederick C. Meinzer

5.1 Abstract

The carbon and oxygen isotope ratios of tree-ring cellulose ($\delta^{13}C_{cell}$, $\delta^{18}O_{cell}$) are useful for reconstructing physiological responses to environmental conditions underlying tree growth and productivity. The Physiological Principles in Predicting Growth (3-PG) model utilizes physiological principles to predict forest stand responses to changing environmental conditions. We incorporated a $\delta^{18}O$ submodel into 3-PG to complement the recently added $\delta^{13}C$ submodel. We parameterized the model using long-term trajectories of tree-ring growth, $\delta^{13}C_{cell}$, and $\delta^{18}O_{cell}$ collected from the Metolius AmeriFlux site (Me-2) in central Oregon (~1 km from the Metolius river: 'upland'). We then applied the parameterized model to a nearby set of trees closer to the Metolius river (~0.015 km: 'riparian') to investigate the physiological drivers underpinning the differences in observed basal area increment (BAI) and $\delta^{13}C_{cell}$ trajectories between upland and riparian trees. The model showed that greater available soil water and maximum canopy conductance (g_c) likely explain the greater BAI and lower $\delta^{13}C_{cell}$ of riparian trees. Unexpectedly the observed and simulated $\delta^{18}O_{cell}$ trajectories did not differ between the upland and riparian trees, likely due to similar source water as indicated by measured $\delta^{18}O$ values of river water, stem water, and atmospheric water vapor. The $\delta^{18}O_{cell}$ with the Peclet effect simulated observed values more accurately than without the Peclet effect. Because the 3-PG-simulated transpiration (E) is used in the $\delta^{18}O$ submodel, this suggested that leaf-level physiology such as the effective path length could be predicted using the stand-level 3-PG estimates of E. The $\delta^{18}O$ submodel may improve 3-

PG predictions because parameterization based on g_c and E must account for both $\delta^{18}O_{cell}$ and $\delta^{13}C_{cell}$, providing a useful and novel way to constrain 3-PG.

5.2 Introduction

The Physiological Principles in Predicting Growth (3-PG) model is a process-based model developed by Landsberg and Waring (1997) to estimate forest growth and productivity using radiation use efficiency, carbon balance, and biomass partitioning. Its development was motivated by the need for more accurate growth and yield models used by foresters to address silvicultural and management needs. Empirical growth and yield models were inaccurate under changing environmental conditions, could only be applied to the stand on which original measurements were made, and were limited to relatively short timescales (Landsberg, 2003a). Thus, 3-PG addressed these deficiencies by incorporating physiological principles to accurately estimate growth and productivity in changing environmental conditions, on diverse forested stands, and across longer timescales. 3-PG utilizes simple light-use efficiency and allometric equations that estimate the amount of energy absorbed by the canopy and converted to below- and aboveground biomass. 3-PG has been widely applied to and tested on diverse forest types using available information on environmental conditions, stand characteristics, and species-specific physiological measurements to parameterize the model (Coops *et al.*, 1998, 2007; Law *et al.*, 2000; Waring & Gao, 2016).

Because 3-PG uses physiological principles governing carbon productivity and allocation, tree-rings are often used in conjunction with the model, especially to predict

long-term growth (Waring & Gao, 2016). Tree-rings provide valuable information because their annual resolution allows researchers to reconstruct past environmental conditions, such as precipitation, drought, temperature, and relative humidity throughout the lifetime of the tree. However, tree-rings are limited in what they can tell us about more detailed aspects of tree physiological responses to environmental conditions. One way to address this limitation is by using tree-ring stable isotopes (McCarroll & Loader, 2004).

Environmental conditions such as drought or extreme temperatures influence how foliage obtains C from CO_2 in the atmosphere and O from H_2O in the soil for photosynthesis. The products of photosynthesis are converted to cellulose and laid down in the cell walls of the xylem. Thus, the isotopic ratios of C and O ($\delta^{13}C$, $\delta^{18}O$) of tree-ring cellulose ($\delta^{13}C_{cell}$, $\delta^{18}O_{cell}$) are used to reconstruct environmental growing conditions and the tree's leaf-level physiology (McCarroll & Loader, 2004; Gessler *et al.*, 2014). These proxies for past leaf-level gas exchange shed light on physiological responses to environmental conditions such as precipitation, temperature, relative humidity, fertilization, thinning, and pests (e.g. Williams *et al.*, 2010; Brooks & Mitchell, 2011; Marias *et al.*, 2014; Saffell *et al.*, 2014; Voelker *et al.*, 2014a, 2014b; Hartl-Meier *et al.*, 2015). Therefore, tree-ring growth and stable isotopes advance modeling efforts to examine physiological processes underlying growth and productivity including carbon allocation, water use, and gas exchange at the stand level.

Improving process-based models such as 3-PG informs our understanding of the physiological mechanisms underpinning forest responses to changing climatic conditions.

Submodels and additional routines have successfully been added to 3-PG such as structural stand variation across landscapes (Seidl *et al.*, 2012), mixed species interactions (Forrester & Tang, 2016), soil organic matter decomposition (Xenakis *et al.*, 2008), soil properties affecting soil water balance (Nolè *et al.*, 2013), and carbon accumulation (Nolè *et al.*, 2009). These often improve model predictions as the submodels account for study-specific conditions (Law *et al.*, 2000; Wei *et al.*, 2014a, 2014b). Wei *et al.*, (2014b) applied a submodel with tree-ring $\delta^{13}C$ to *Abies grandis* stands that constrained and improved 3-PG growth predictions because $\delta^{13}C$ was sensitive to key parameters controlling canopy conductance and carbon assimilation. Consistent with this, the tree-ring $\delta^{13}C$ signal is a proxy for both stomatal conductance (g_s) and photosynthesis (A) because $\delta^{13}C$ is influenced by the relative stomatal limitation of A, which determines the ratio of intercellular to ambient [CO_2], and consequently ^{13}C discrimination (Farquhar *et al.*, 1989). Thus, an increase in $\delta^{13}C$ can be interpreted as an increase in A/g_s.

$\delta^{18}O$ has been used to tease apart the contributions of A and g_s to the $\delta^{13}C$ signal because the $\delta^{18}O$ signal only reflects processes affecting g_s. This combination of both $\delta^{13}C$ and $\delta^{18}O$ is known as a 'dual isotope approach' and is a useful proxy for leaf-level gas exchange (Scheidegger *et al.* 2000, Barnard *et al.* 2012). Therefore, the addition of a tree-ring $\delta^{18}O_{cell}$ submodel along with the existing the $\delta^{13}C$ submodel could reveal more information about stand carbon dynamics and water use, improving 3-PG predictions and our understanding of physiological responses to environmental conditions.

However, interpretations of $\delta^{13}C_{cell}$ and $\delta^{18}O_{cell}$ are complex, and various models developed for the interpretation of $\delta^{18}O_{cell}$ vary in complexity with some containing variables that cannot be measured directly. The original $\delta^{18}O$ model is based on a model developed for bodies of water (Craig & Gordon, 1965) and accounts for isotopic evaporative enrichment of ^{18}O of source water at evaporative sites within the leaf, influencing $\delta^{18}O_{cell}$. However, this becomes complicated by the Peclet effect that describes the mixing of unenriched water arriving at the evaporative site via bulk flow driven by transpiration with the enriched water diffusing back from the evaporative site (Farquhar & Lloyd, 1993). For example, reduced g_s and thus transpiration reduces the amount of unenriched water moving from leaf veins to the evaporative site, while concurrently increasing the amount of back diffusion of enriched water. The Peclet effect can drive the $\delta^{18}O_{cell}$ signal more than effects of evaporative enrichment alone (Farquhar & Lloyd, 1993). Thus, the incorporation of the Peclet model has improved $\delta^{18}O_{cell}$ predictions in multiple systems (Barbour *et al.*, 2000; Holloway-Phillips *et al., 201*6). A component of the Peclet effect that impacts the water arriving via transpiration at the evaporative site is the effective path length (L). However, L is not possible to measure directly and its relationship with ^{18}O incorporated into photosynthate is still unclear (Song *et al.*, 2013; Loucos *et al.*, 2015). Due to these challenges, approaches for estimating L are needed to improve our understanding of oxygen isotope fractionation and $\delta^{18}O_{cell}$.

The goal of this study is to test the utility of the newly modified version of 3-PG that includes the $\delta^{13}C_{cell}$ and $\delta^{18}O_{cell}$ submodels to predict and understand physiological

drivers of stand characteristics using long-term tree-ring growth, $\delta^{13}C_{cell}$, and $\delta^{18}O_{cell}$ trajectories from old-growth *Pinus ponderosa* at the AmeriFlux Metolius site in the Oregon Cascades. The combination of measured tree-ring growth and stable isotopes, extensive historical meteorological and physiological measurements recorded at this site (Law *et al.*, 2000, 2001a; Warren *et al.*, 2005), and previous application of 3-PG to *P. ponderosa* (Law *et al.*, 2000; Coops *et al.*, 2005; Wei *et al.*, 2014a) makes this study well suited to evaluate the utility of the combination of tree-ring $\delta^{13}C_{cell}$ and $\delta^{18}O_{cell}$ into 3-PG. We parameterized the model using an 'upland' set of *P. ponderosa* trees ~1 km from the Metolius river. We then applied the parameterized model to a nearby 'riparian' set of trees closer (~0.015 km) to the Metolius river to examine the physiology driving the observed differences in BAI, $\delta^{13}C_{cell}$, and $\delta^{18}O_{cell}$ between sites. Our research questions were 1) How well can the 3-PG model be applied to the upland and riparian sets of trees? 2) Does incorporation of the Peclet effect improve 3-PG estimates of $\delta^{18}O_{cell}$? 3) How sensitive is $\delta^{18}O_{cell}$ to drivers of gas exchange? and 4) Can *L* be optimized by model calibration?

5.3 Materials & Methods

Study site

This study was conducted in a *P. ponderosa* forest on the eastern side of the Cascade Mountains in central Oregon within the Metolius Research Natural Area (RNA) (US Me-2, 44.4957, -121.6224) at an elevation of 915 m. The site consists of 27% old trees (~250 years), 25% younger trees (~45 years), and 48% mixed-age trees. Bitterbrush

(*Purshia tridentata*) and bracken fern (*Pteridium aquilinum*) comprise the sparse understory. Precipitation is greatest between October-June with dry summer months. Winters are wet and cool, snow cover in winter is intermittent, and freezing temperatures occur mostly at night and early morning. Soil is classified as sandy loam (73% sand, 21% silt, and 6% clay) and soil nutrients are low (Law *et al.*, 2000; Warren *et al.*, 2005).

Climate data

AmeriFlux CDIAC climate data for the intermediate ponderosa pine site (US-Me 2) was available for 2002-2012. To extrapolate back in time, minimum and maximum temperature obtained from PRISM (http://oldprism.nacse.org/) for 1895-2012 was compared with the site-level AmeriFlux data and that relationship ($y = 1.27T_{min\_AmeriFlux} + 2.46$, $R^2 = 0.92$; $y = 0.89T_{max\_AmeriFlux} -1.42$, $R^2 = 0.98$) was used to correct PRISM data because PRISM data are based on 4 km grid cells. Precipitation data were also obtained from PRISM. As PRISM climate data only went back to 1895, we focused on 1895-2002 in this study. Atmospheric [CO_2] and $\delta^{13}C$ of the atmosphere from Francey *et al.* (1999) were used.

Figure 5.1 describes annual average minimum air temperature (T_{min}), average air temperature (T_{av}), maximum air temperature (T_{max}), vapor pressure deficit (VPD), solar radiation, and precipitation from 1895-2002 although mean monthly climate data was used in the model. Mean monthly VPD was calculated as the difference between saturation vapor pressure at minimum and maximum temperature. Mean daily solar radiation was calculated from mean monthly T_{min} and T_{max} (Bristow & Campbell, 1984;

Thornton *et al.*, 1997; Coops *et al.*, 1998, 2000) in Landsberg *et al.* (2003). The number of frost days per month (F) was calculated based on mean monthly T_{min}:

$$F = T_{min} * (-2) + 11.6 \quad \text{Eqn 1}$$

If $T_{min} > 7$, then F was zero.

Tree-ring analyses

Tree cores were collected in early spring 2003 from two sets of trees: an upland set ~1 km from the Metolius River and a nearby riparian set within 0.015 km of the Metolius river. We sampled five upland and five riparian *P. ponderosa* of approximately the same stem diameter at 1.3 m height (upland: 87.8 ± 3.9 cm, riparian: 112.3 ± 8.2 cm) and age (mean age ≈ 260 years) (Table 5.1). In spring 2003 prior to diameter growth, three 12 mm cores from each tree were collected for isotopic analysis and a 5 mm core was collected as an archive. Cores were dried, and sanded, and the 5 mm core was mounted. All cores were age dated, and ring widths were measured using a sliding stage incremental micrometer (Velmex Inc., Bloomfield, NY, USA) with Measure J2X software (VoorTech Consulting, Holderness, NH, USA). Visual cross-dating was verified using the COFECHA program to identify false or missing rings (Holmes 1983) for all cores collected.

Sample preparation

The 12 mm cores were separated into annual increments spanning from 2002 to 1850 (152 years). The annual increments from three cores per tree were combined for a

single sample per tree per year. Each annual ring was ground with a ball mill to a fine powder. All samples were extracted for alpha-cellulose. Oils and resins were removed with toluene-ethanol and ethanol Soxhlet extractions (Leavitt & Danzer, 1993). Holocellulose was isolated by delignification in an acetic acid-acidified sodium chlorite solution and converted to alpha-cellulose in sodium hydroxide (Sternberg, 1989).

Approximately 0.8 mg of alpha-cellulose was loaded into tin capsules for C combustion and 0.4 mg into silver capsules for O pyrolysis for subsequent isotopic analysis by isotope ratio mass spectrometer (IRMS) at the Integrated Stable Isotope Research Facility at the Western Ecology Division of the U.S. EPA, Corvallis Oregon. Samples analyzed for ^{13}C were flash combusted using an elemental analyzer (ECS 4010, Costech, Valencia, CA), and the resulting CO_2 analyzed by continuous-flow IRMS (Delta Plus XP, Finnigan MAT, now Fisher Scientific). Each run was calibrated using three internal standards (NIST concentration standards of corn, bovine liver and tomato) spanning the range of expected values, with an independent QC standard (cellulose)to calculate accuracy. Internal standards were routinely calibrated to international standards USGS42 (Tibetan hair), NIST 8542 sucrose, NIST 8573 and 8574 glutamic acid, and NIST 8514 graphite. Typical precision and accuracy was ± 0.1‰ or better as determined by repeated measures of internal quality control standards and from sample replicates. Samples were analyzed for ^{18}O using a high temperature conversion elemental analyzer (TC/EA ThermoQuest Finnigan, now Fisher Scientific) interfaced to an IRMS (Thermo Electron Delta XL, now Fisher Scientific). Internal laboratory standards (NIST concentration standards of pine needles, sucrose, and corn) were used for calibration

standards with an independent QC standard (cellulose) for accuracy estimates. IAEA-601 and IAEA-602 benzoic acid were used to routinely calibrate the internal standards. Typical error was ± 0.2‰ or better as determined by repeated measures of internal quality control standards and from sample replicates. The C and O stable isotope ratios (R) of the heavier (i.e. ^{13}C, ^{18}O) to lighter isotope (i.e. ^{12}C, ^{16}O) were represented by delta (δ) notation in parts per thousand (‰) relative to the VPDB or VSMOW international standards (McCarroll and Loader 2004):

$$\delta^{13}C \text{ or } \delta^{18}O = \left(\frac{R_{sample}}{R_{standard}} - 1 \right) ‰ \quad \text{Eqn 2}$$

3-PG Isotope Model

3-PG is a process-based model that runs on a monthly timestep that incorporates physiological processes underlying net primary productivity (NPP), biomass allocation, water use, soil water balance, stem mortality (self-thinning), litterfall, and root turnover (Landsberg & Waring, 1997). The input/driving data include mean monthly values of T_{min}, T_{max}, T_{av}, precipitation, F, solar radiation, VPD, atmospheric [CO_2], $\delta^{13}C$ of the atmosphere, and $\delta^{18}O$ of source water. The outputs include biomass pools for roots, stems, and foliage, gross primary productivity (GPP), NPP, transpiration (E), growth and stand characteristics, and now $\delta^{13}C_{cell}$ and $\delta^{18}O_{cell}$.

3-PG is based on the light-use efficiency model that describes a positive linear relationship between aboveground growth/biomass/carbon and intercepted radiation. Thus, 3-PG calculates gross primary productivity (GPP) from absorbed photosynthetically active radiation ($\phi_{p.a}$, MJ m^{-2}) and canopy quantum efficiency (α_c, mol

C (mol photon)$^{-1}$) and is constrained by factors that influence stomatal closure including atmospheric VPD, soil moisture, temperature, frost, and site nutrient status:

$$GPP = \alpha_c \, \phi_{p.a} \approx \alpha_{cx} \, \phi_{p.a} \, f_T \, f_F \, f_N \, f_D \, f_\Theta \, f_{age} \, f_{phys} \quad \text{Eqn 3}$$

where f_T, f_F, f_N, f_D, f_Θ, f_{age}, and f_{phys} are the temperature, frost, nutrition, VPD, soil water, age, and physiology modifiers, respectively, and α_{cx} is the maximum canopy quantum efficiency.

The temperature modifier (f_T) incorporates the minimum, maximum, and optimum temperatures for growth. The frost modifier (f_F), calculated using F, assumes photosynthesis does not occur on days with temperatures below -2 (Waring, 2000). The nutrient modifier (f_N) is a function of site fertility rating (FR) ranging from 0-1 and is based on available nutrients. The VPD modifier (f_D) is a function of k_g, a species-specific coefficient describing the strength of the response of canopy conductance (g_c) to VPD (Law *et al.*, 2001a). The soil water modifier (f_Θ) is calculated using the moisture ratio of current:available water and a soil water constant (c_Θ) and power (r_Θ) that reflect different soil types (Landsberg *et al.*, 2003). For sandy loam at our study site, c_Θ is 0.4 and r_Θ is 7. The age and physiology modifiers (f_{age}, f_{phys}) account for reductions in hydraulic and stomatal conductance as stands age.

3-PG assumes the ratio of NPP to GPP is fixed at 0.47 (Waring *et al.*, 1998). NPP is allocated to foliage, woody tissue, and root biomass pools based on partitioning rates which depend on site and growth conditions, litterfall, and root turnover (Waring *et al.*, 1998). The model uses a simple relationship to determine root growth and turnover to estimate belowground biomass allocation. Allometric ratios are used to determine the

allocation of biomass to stems and foliage. Stem growth, stand density, and stem mortality are calculated according to the self-thinning rule based on the negative relationship between tree density and stem mass (Landsberg & Waring, 1997). Soil water balance is based on rainfall, irrigation, evapotranspiration, and runoff/drainage. Evapotranspiration is determined from the Penman-Monteith equation and canopy conductance (Penman, 1948; Monteith, 1965; Monteith & Unsworth, 2007).

We updated the calculation of canopy conductance by multiplying it by the frost modifier (f_F) to prevent any transpiration or conductance from occurring on days with frost. Canopy conductance (g_c) was calculated as:

$$g_c = (TK_2 + TK_3 T_{av})\, g_{cmax}\, f_F\, f_{age}\, f_{phys}\, (\mathrm{LAI} / \mathrm{LAI}_{gcx}) \qquad \text{Eqn 4}$$

where TK_2 and TK_3 are temperature modifiers (0.244, 0.0368, respectively, Wei *et al.* 2014a), g_{cmax} is maximum canopy conductance, LAI is leaf area index, and LAI_{gcx} is the LAI required for g_{cmax}.

Allometric equation to estimate stem biomass

Diameter at breast height (DBH) and biomass measured in Pinus species (Gholz *et al.*, 1979) were used to determine the stem constant (S_c) and stem power (S_p) used in 3-PG in Wei *et al.* (2014). Live branch mass, stem wood mass, and stem bark mass (Gholz *et al.*, 1979) were summed to calculate total stem biomass. Total stem biomass was then plotted against stem DBH. The relationship between DBH and total biomass (W) was described by an exponential function:

$$W = S_c DBH^{-S_p} \qquad \text{Eqn 5}$$

where 0.0273 is S_c and 2.6405 is S_p.

Basal area increment calculation

To compare with observed BAI (cm^2), simulated BAI (cm^2 $tree^{-1}$) was calculated from modeled outputs:

$$BAI = \frac{basal\ area\ (m^2\ ha^{-1})}{stand\ density\ (trees\ ha^{-1})} * 10000\ cm^2 \quad \text{Eqn 6}$$

$\delta^{13}C$ theory and submodel

The $\delta^{13}C$ of photosynthate ($\delta^{13}C_{plant}$) is described in Farquhar *et al.*, (1982) as:

$$\delta^{13}C_{plant} \approx \delta^{13}C_{air} - a - (b - a)\frac{c_i}{c_a} \quad \text{Eqn 7}$$

where a is the fractionation effect associated with diffusion of CO_2 through stomata (4.4‰) and b is the fractionation effect (27‰) associated with discrimination against ^{13}C by the enzyme RUBISCO (ribulose bisphosphate carboxylase-oxygenase) during C fixation, and c_i/c_a is the weighted mean ratio of the intercellular CO_2 concentration (c_i) to that in the ambient air (c_a) (Farquhar *et al.*, 1982, 1989). The c_i can be estimated from c_a, photosynthesis (A), and conductance (g) (Farquhar & Sharkey, 1982):

$$c_i = c_a - \frac{A}{0.66g} \quad \text{Eqn 8}$$

The value of 0.66 describes the ratio of diffusivities of CO_2 to water vapor in air. Therefore, tree-ring $\delta^{13}C_{plant}$ reflects factors that influence discrimination against ^{13}C during photosynthetic CO_2 fixation. These factors include the biochemical capacity to fix CO_2 (A), and the conductance (g) to CO_2 from the atmosphere to the sites of

carboxylation. Although g includes stomatal conductance (g_s) and mesophyll conductance, we assume the simplified equation from Farquhar *et al.* (1982, 1989) using g_s and c_i are sufficient to model $\delta^{13}C_{plant}$ (Cernusak *et al.*, 2003).

The $\delta^{13}C$ submodel (Wei *et al.*, 2014b) treats the canopy as a big leaf (Farquhar 1989) and combines equations 7 and 8 so $\delta^{13}C_{plant}$ is calculated as:

$$\delta^{13}C_{plant} \approx \delta^{13}C_{air} - a - (b-a)\left(1 - \frac{A}{c_a 0.66g}\right) \quad \text{Eqn 9}$$

To convert $\delta^{13}C_{plant}$ of new photosynthate to $\delta^{13}C$ of tree-ring wood ($\delta^{13}C_{wood}$), a constant offset (ε_{sp}) of 1.99‰ was assumed (Wei *et al.*, 2014b), similar to that observed in other Pinus species (Gessler *et al.*, 2009; Wei *et al.*, 2014a):

$$\delta^{13}C_{wood} = \delta^{13}C_{plant} + \varepsilon_{sp} \quad \text{Eqn 10}$$

This equation was modified to include a constant offset (ε_{wc}) of 1.5‰ observed in *P. ponderosa* (English *et al.*, 2011) between the $\delta^{13}C_{wood}$ and the $\delta^{13}C$ of tree-ring cellulose ($\delta^{13}C_{cell}$):

$$\delta^{13}C_{cell} = \delta^{13}C_{wood} + \varepsilon_{wc} \quad \text{Eqn 11}$$

$\delta^{18}O$ theory and submodel

The $\delta^{18}O$ of plant tissue ($\delta^{18}O_{plant}$) incorporates a signal imparted by the $\delta^{18}O$ value of source water and leaf water, which is mainly influenced by ^{18}O-enrichment at the sites of evaporation within the leaf (Craig & Gordon, 1965; Dongmann *et al.*, 1974). Under steady state conditions:

$$\delta^{18}O_{leaf} = \delta^{18}O_s + \varepsilon* + \varepsilon_k + \left(\delta^{18}O_v - \delta^{18}O_s - \varepsilon_k\right)\frac{e_a}{e_i} \quad \text{Eqn 12}$$

where $\delta^{18}O_{leaf}$, $\delta^{18}O_s$, and $\delta^{18}O_v$ represent the O isotopic composition of leaf water at the site of evaporation, source water, and atmospheric water vapor, respectively. e_a/e_i is the ratio of ambient vapor pressure to saturation vapor pressure within the leaf, ε* is the equilibrium fractionation between liquid water and vapor, and ε_k is the kinetic fractionation factor of vapor diffusion from the leaf to the atmosphere. Mean monthly $\delta^{18}O_s$ values were obtained from WaterIsotopes.org (http://wateriso.utah.edu/waterisotopes/index.html) for January-December. Monthly values were assumed not to change year to year.

Leaf water $\delta^{18}O$ ($\delta^{18}O_{lw}$) heterogeneity can be explained further by the Peclet effect, which describes the ratio between the transpiration-induced mass flow (advection) of unenriched source water to the evaporative sites and the back diffusion of isotopically-enriched water from the sites of evaporation (Farquhar & Lloyd, 1993; Barbour, 2007):

$$\delta^{18}O_{lw} = \delta^{18}O_{leaf}\,\frac{(1-e^{-\wp})}{\wp} \qquad \text{Eqn 13}$$

$$\wp = \frac{E\,L}{C\,D} \qquad \text{Eqn 14}$$

where $\delta^{18}O_{lw}$ is the steady state isotopic enrichment of mean leaf lamina water, $\wp$ is the Peclet number describing the ratio of advection to diffusion, E is the leaf transpiration rate (mol m^{-2} s^{-1}), L is the scaled effective path length (m) for water movement from the veins to the site of evaporation, C is the molar density of water (55.56 10^3 mol m^{-3}), and D is the diffusivity of the heavy water isotopologue ($H_2{}^{18}O$) in water (2.66 x 10^{-9} m^2s^{-1}). L is defined as the product of two components: l, the actual distance of the water pathway from xylem to the evaporative surface, and k, a scaling factor that accounts for the

tortuosity of the path of water through a porous medium (Farquhar & Lloyd, 1993; Barbour *et al.*, 2000).

Isotopic fractionation during the incorporation of the $\delta^{18}O_{lw}$ signal into cellulose of plant tissue is described by the following equation (Farquhar *et al.*, 2000; Barbour, 2007):

$$\delta^{18}O_{cell} = \delta^{18}O_{lw}\,(1 - p_{ex}p_x) + \varepsilon_o \qquad \text{Eqn 15}$$

where p_{ex} is the proportion of oxygen atoms that exchange with source water during cellulose formation (0.42, Roden *et al.*, 2000), p_x is the proportion of unenriched water (xylem water) at the site of cellulose formation, which is equivalent to 1 for wood collected from the main trunk, and ε_o is a fractionation factor of +27‰ associated with the water/carbonyl interactions (Yakir *et al.*, 1990). The $\delta^{18}O$ submodel in 3-PG calculates $\delta^{18}O_{cell}$ with and without the Peclet effect (i.e. substituting $\delta^{18}O_{leaf}$ for $\delta^{18}O_{lw}$ in equation 15). The model was modified so the modeled *E* output is used in the Peclet calculation rather than a fixed *E*.

Parameterization

The model was parameterized using previously reported stand characteristics of the upland trees (Table 5.1). Parameters used in this study are listed in Table 5.2. We used the Wei *et al.* (2014b) version of 3-PG with the $\delta^{13}C$ submodel, and the $\delta^{18}O$ submodel added in this study in Python version 2.7. Parameterization was conducted as in Landsberg *et al.* (2003) and Wei *et al.* (2014b). First, parameters were set to defaults used in previous applications of 3-PG at the Metolius site (Table 5.2). Then, maximum

canopy conductance (g_{cmax}) and the coefficient describing the sensitivity of canopy conductance to VPD (k_g) were calibrated based on previously reported values of *E* and g for *P. ponderosa* at this site (Law *et al.*, 2000, 2001a), and the equation describing the relationship between conductance and VPD (Law *et al.*, 2001a). Next, fertility rating (FR), foliage:stem partitioning ratio of tree diameter of 20 cm (*pfs20*), maximum root partitioning (p_{rx}), maximum tree stem mass likely in mature stands of 1000 trees ha^{-1} (*wSx1000*), and maximum quantum efficiency (α_{cx}) were adjusted to match observed values of LAI, basal area, BAI, stand density, and $\delta^{13}C$. α_{cx} and g_{cmax} were adjusted to match observed $\delta^{13}C_{cell}$ with other parameters held constant (Wei *et al.*, 2014b). *L* was varied to match observed $\delta^{18}O_{cell}$ with Peclet.

To focus on the validity of the model using the observed values of BAI, $\delta^{13}C_{cell}$, and $\delta^{18}O_{cell}$ obtained in this study, these observed metrics were prioritized for parameterization over previously published values and other stand characteristics. The parameterized model was then applied to the riparian trees. To simulate the observed values of riparian trees, water balance parameters including maximum available soil water (ASW), g_{cmax}, and *wSx1000* were adjusted until the simulated BAI, $\delta^{13}C_{cell}$, and $\delta^{18}O_{cell}$ values were the same as or within range of observed values at the riparian site. Because the upland and riparian sites were only <1 km apart, as few parameters as possible were adjusted.

Sensitivity Analysis

We investigated the sensitivity of modeled outputs BAI, LAI, g_c, E, $\delta^{13}C$, $\delta^{18}O_{leaf}$, and $\delta^{18}O_{cell}$ with Peclet, to 20% and 40% changes in the parameters g_{cmax}, k_g, FR, α_{cx}, *pfs20*, p_{rx}, maximum ASW, and *wSx1000*. These parameters were selected because they are known to influence $\delta^{13}C_{cell}$ and biomass allocation (Wei *et al.*, 2014b), but it is unknown how they influence $\delta^{18}O_{cell}$. $\delta^{18}O_{cell}$ with Peclet was used to optimize L. To conduct the sensitivity analysis, one parameter at a time was varied while all other parameters were held constant. The % change in output response was then quantified from the original output value. An output was considered 'sensitive' if a change in parameter resulted in a ≥10% change in output. Only output variables that changed ≥10% and were considered sensitive to shifts in each parameter are shown in figures. Output data are averages for 1895-2002.

5.4 Results

With proper parameterization, the model reasonably simulated observed and previously reported stand characteristics for the upland Metolius site (Figure 5.2). Modeled basal area agreed well with observed basal area of 30 m^2 ha^{-1} and 35 m^2 ha^{-1}. The model accurately predicted BAI, although the model overestimated BAI in recent years 1986-2001. Modeled stand density was lower than observed stand densities of 54 trees ha^{-1} but modeled height matched the observed value of 34 m. Modeled LAI was within range of measured values of 0.9-1.45 m^2 m^{-2}. The model accurately predicted measured NPP of 9.2 tDM ha^{-1} yr^{-1}. Simulated $\delta^{13}C_{cell}$ was within range of observed values, although simulated $\delta^{13}C_{cell}$ exhibited more inter-annual variation than observed

$\delta^{13}C_{cell}$. Simulated *E* was lower than the observed water vapor flux (*LE*) of 50 mm month^{-1} for this site (Figure 5.3).

The addition of the frost modifier in the calculation of g_c caused g_c to become lower compared to that without the frost modifier in fall, winter, and spring months with values reaching 0 in winter (Figure 5.4). This also resulted in increased $\delta^{13}C_{cell}$ in fall, winter, and spring months compared to $\delta^{13}C_{cell}$ without the frost modifier (Figure 5.4). The inhibition of canopy conductance during winter months also coincided with minimal NPP.

The parameterized model was used to compare the upland and riparian sets of trees. Compared to upland trees, measured BAI was consistently greater in riparian trees (Figure 5.5). Riparian trees also exhibited consistently lower $\delta^{13}C_{cell}$ than upland trees with $\delta^{13}C_{cell}$ of the upland trees, ranging from -24.8‰ to -22.3‰ while $\delta^{13}C$ of the riparian trees ranged from -25.3‰ to -23.1‰ (Figure 5.5). While $\delta^{13}C_{cell}$ varied inter-annually by ~2.5‰ for both upland and riparian sets of trees, $\delta^{18}O_{cell}$ varied by over 5‰ for both sets of trees (Figure 5.6, Appendix Figure 5.1). However, the difference in $\delta^{18}O_{cell}$ between upland and riparian trees was smaller than that of $\delta^{13}C_{cell}$. Mean $\delta^{18}O_{cell}$ for 1895-2002 was 28.3‰ in upland trees and 28.9‰ in riparian trees. Due to the lack of difference between sets of trees (Appendix Figure 5.1), $\delta^{18}O_{cell}$ trajectories of both sets of trees were combined (N=10, Figure 5.6). At both sites, $\delta^{18}O_{cell}$ declined between 1992-2002. The $\delta^{18}O$ of river water did not differ from the $\delta^{18}O$ of stem water in either upland or riparian trees (Table 5.3). The $\delta^{18}O$ of stem water and atmospheric water vapor did not differ between upland and riparian trees (Table 5.3).

To simulate the observed BAI, $\delta^{13}C_{cell}$, and $\delta^{18}O_{cell}$ of riparian trees, maximum available soil water (ASW) was increased from 163 mm to 300 mm, maximum canopy conductance (g_{cmax}) was increased from 0.012 m s^{-1} to 0.0135 m s^{-1}, and the maximum tree stem mass likely in mature stands of 1000 trees ha^{-1}(*wSx1000*) was decreased from 45 kg $tree^{-1}$ to 30 kg $tree^{-1}$ (Figures 5.5, 5.6). The model adjusted for the riparian trees simulated the greater BAI and lower $\delta^{13}C$ values observed in riparian trees (Figure 5.5). *L* for both sets of trees combined (Appendix Figure 5.1) was adjusted to 0.022 m based on the equation for $\delta^{18}O_{cell}$ that includes the Peclet effect. Mean observed $\delta^{18}O_{cell}$ of the combined upland and riparian trees for 1895-2002 was 28.7‰, median was 28.9‰, minimum was 25.9‰, and maximum was 30.6‰. Modeled $\delta^{18}O_{cell}$ without the Peclet effect slightly overestimated $\delta^{18}O_{cell}$ where the mean was 29.4‰, median was 29.3‰, minimum was 28.1‰, and maximum was 31.0‰. In contrast, $\delta^{18}O_{cell}$ with Peclet more closely matched observed values, where the mean was 28.8‰, median was 28.9‰, minimum was 27.5‰, and maximum was 29.9‰. Modeled $\delta^{18}O_{cell}$ was within range of observed values except for ~1992-2002 when observed $\delta^{18}O_{cell}$ rapidly declined. The difference between $\delta^{18}O_{cell}$ with and without the Peclet effect declined with time.

The sensitivity analysis showed that BAI, LAI, g_c, and *E* were sensitive to changes in all tested parameters: g_{cmax}, k_g, FR, α_{cx}, *pfs20*, p_{rx}, maximum ASW, and *wSx1000* (Figure 5.7, Appendix Table 5.1). In contrast, $\delta^{13}C$ was only sensitive to changes in g_{cmax} and p_{rx}. The $\delta^{18}O_{leaf}$ was not sensitive to any parameter while $\delta^{18}O_{cell}$ with Peclet was sensitive to k_g, FR, α_{cx}, *pfs20*, and p_{rx}. *L* was optimized using $\delta^{18}O_{cell}$

with Peclet, where *L* of 0.022 resulted in modeled $\delta^{18}O_{cell}$ that best matched observed $\delta^{18}O_{cell}$ (Figure 5.8).

5.5 Discussion

Model Parameterization

Previously reported stand densities ranged from 54-137 trees ha^{-1} (Table 5.1) with a standard deviation of ±36 trees ha^{-1} and a standard error of ±18 trees ha^{-1}. Therefore, although the model underestimated stand density, it is within a reasonable range of the observed values. The range of stand density is consistent with the wide range of measured DBH at this site (55-63 cm, (Law *et al.*, 2001a, 2001b; Youngblood *et al.*, 2004; Warren *et al.*, 2005), which is lower than that of the trees cored in this study (88-112 cm, Table 5.1). Because DBH and stand density are closely related (Meyer, 1938) and 3-PG utilizes this relationship, it is not surprising that the model predicted fewer, larger diameter trees. Further, growth is related to the self-thinning parameter, *wSx1000*, yet adjusting *wSx1000* to match observed stand density would result in underestimating basal area and BAI. Since we prioritized measured BAI over previously reported stand density for model parameterization, this resulted in the accurate prediction of BAI and basal area, and underestimation of stand density. It is also important to note that we did not randomly select trees within the stand but preferentially selected the old, large dominant trees so it could not be expected that the model could accurately estimate all stand attributes when modeling BAI for the selected trees. Growth relationships have been challenging to accurately model in 3-PG (Wei *et al.*, 2014b) likely due to site-

specific and microclimatic conditions such as non-uniform tree spacing not accounted for in a generalizable forest stand model like 3-PG (Waring *et al.*, 2016).

Modeled height and LAI fell within the range of previously reported values. Modeled LAI reached ~2.2 at a stand age of 30 years in 1770 (not shown), consistent with observed values for *P. ponderosa* at that age (Law *et al.*, 2001b), indicating the LAI was well predicted beyond our study period of 1895-2002. Modeled NPP matched previously reported NPP (Law *et al.*, 2000) for *P. ponderosa* (Wei *et al.*, 2014a). Modeled *E* was lower than the water vapor flux (*LE*) values reported by Law *et al.* (2000) but *LE* includes all forms of evaporation from the soil and understory *E* which may explain why *LE* was greater than simulated *E*. In contrast, modeled *E* was within range of 30 mm $month^{-1}$ and 45 mm $month^{-1}$ of water used in the upper 0.8 (Irvine *et al.*, 2002) and 2 m of soil (Warren *et al.*, 2005), respectively for old-growth *P. ponderosa* at the Metolius site. These studies found that *P. ponderosa* utilizes deep sources of water, suggesting that the model may more adequately capture water use in the upper 2 m of soil depth.

The model did not accurately simulate growth with FR values above 0.1 suggesting that tree growth was limited to some extent by soil nutrient availability. FR was lower than FR previously used for this site (0.4 in Law *et al.* 2000), although the soil is volcanic sandy ash that is low in nutrients (Law *et al.*, 2000, 2001a; Warren *et al.*, 2005). FR is also challenging to parameterize in 3-PG due to inadequate soil survey data, the limited ability of models to describe plant responses to nutrition, and our poor understanding of relationships between plant growth and soil chemical properties

(Landsberg, 2003b; Landsberg *et al.*, 2003). The low FR also resulted in somewhat low g_c values (Figure 5.4) compared to observed values (Law *et al.*, 2000).

Modifying the calculation of g_c with the frost modifier to account for inhibited *E* on days with frost reduced g_c in fall, winter, and spring months with values reaching zero during winter months (Figure 5.4). This also caused $\delta^{13}C_{cell}$ to increase compared to $\delta^{13}C_{cell}$ without the frost modifier during fall, winter, and spring months due to reduced discrimination and stomatal conductance limiting CO_2 uptake (Figure 5.4B), coinciding with periods of little or no growth as indicated by low NPP during winter months. This shows that the model weights the periods of little or no growth equally with high NPP periods for estimating $\delta^{13}C_{cell}$ values despite the inhibited gas exchange and carbon assimilation. This modification also had a particularly strong effect on $\delta^{13}C_{cell}$ during fall months, indicating reduced ^{13}C discrimination due to drought-induced stomatal closure following dry summer months when almost no rain occurs (Law *et al.*, 2001a).

The sensitivity analysis showed that $\delta^{13}C_{cell}$ was 'sensitive' (i.e. output changed ≥10% in response to a change in parameter) to fewer parameters than BAI, LAI, g_c, and *E* (Figure 5.7, Appendix Table 5.1). Consistent with Wei *et al.* (2014b), $\delta^{13}C_{cell}$ was sensitive to shifts in parameters relating to gas exchange (e.g. g_{cmax}), supporting that $\delta^{13}C_{cell}$ effectively constrains 3-PG parameterization of gas exchange-related parameters. Unlike Wei *et al.* (2014b), $\delta^{13}C_{cell}$ was not considered 'sensitive' to α_{cx} at the ≥10% level (-7.4%, Appendix Table 5.1), which may be due to the large timespan over which output was averaged for the sensitivity analysis in this study (1895-2002) compared to that in Wei *et al.* (2014) (1991-2007). However, we also found that $\delta^{13}C_{cell}$ was sensitive to

maximum root partitioning (p_{rx}) (Figure 5.7, Appendix Table 5.1), which is likely because p_{rx} affects the amount of below- and aboveground biomass, impacting LAI, g_c, and thus $\delta^{13}C_{cell}$.

Upland vs Riparian: BAI, $\delta^{13}C_{cell}$

The model helped to explain the physiological mechanisms underlying the differences in growth and $\delta^{13}C_{cell}$ between upland and riparian trees. The close proximity of the riparian trees to the Metolius river suggested that their greater BAI was due to the greater water availability and reduced drought stress compared to the upland trees (Orwig & Abrams; Adams & Kolb, 2004). Because drought induces stomatal closure to reduce water loss, the greater water availability also allowed riparian trees to maintain hydraulic function and gas exchange throughout more of the growing season (Panek & Goldstein, 2001), resulting in greater ^{13}C discrimination, thus imparting a lower $\delta^{13}C_{cell}$ signal in tree-rings compared to upland trees (McCarroll & Loader, 2004). This was also supported by the reasonably well-predicted riparian tree BAI and $\delta^{13}C_{cell}$ after increasing maximum ASW and g_{cmax}, and lowering *wSx1000* in the model. These parameter adjustments suggested that the riparian trees had greater water availability as well as greater g_{cmax} because trees modulate stomatal conductance with water availability to maintain hydraulic function. Because g_{cmax} is related to hydraulic properties such as hydraulic conductivity, this is consistent with greater sapwood-specific native conductivity observed in *P. ponderosa* at a riparian site compared to an upland slope site (Stout & Sala, 2003). The greater g_{cmax} of riparian trees was supported by the observed lower

$\delta^{13}C_{cell}$ trajectory of riparian trees indicating greater discrimination due to lower stomatal constraints on *A* (i.e. higher g_{cmax}) and thus greater CO_2 supply. The g_{cmax} values of 0.012 m s^{-1} for upland and 0.0135 m s^{-1} for riparian are within range for this species and site (Law *et al.*, 2000, 2001a; Coops *et al.*, 2005). To maintain the same amount of biomass for each set of trees, the greater BAI of riparian trees resulted in a slightly lower stand density as indicated by the decrease in *wSx1000*. Modeled $\delta^{13}C_{cell}$ was more variable than observed $\delta^{13}C_{cell}$ (Wei *et al.*, 2014b), suggesting that the model may not sufficiently account for mixing of previously stored and fresh assimilates that can mute $\delta^{13}C_{cell}$ in *P. ponderosa* (Sohn *et al.*, 2014; Wei *et al.*, 2014b).

Upland vs Riparian: $\delta^{18}O_{cell}$

Given the greater measured growth and lower $\delta^{13}C_{cell}$ of riparian trees, we also expected $\delta^{18}O$ of the riparian trees to differ from that of the upland trees due to differences in source water and/or in leaf-level physiology given their different proximities to the river. However, $\delta^{18}O_{cell}$ did not substantially differ between the upland and riparian trees (Appendix Figure 5.1, Figure 5.6). To explain the underlying mechanism behind the unexpectedly similar $\delta^{18}O_{cell}$ trajectories between sets of trees, we discuss potential drivers behind patterns in $\delta^{18}O_{cell}$ including differences in relative humidity, leaf-level physiology, and the $\delta^{18}O$ of source water ($\delta^{18}O_s$) (Farquhar *et al.*, 2007; Saugier *et al.*, 2012) with the help of the modeled parameters and outputs.

First, although differences in relative humidity and VPD can alter tree-ring $\delta^{18}O_{cell}$ (Kahmen *et al.*, 2011; Voelker *et al.*, 2014a), we assumed the upland and riparian

trees experienced the same evaporative demand because they were <1 km from each other. Further, we accurately simulated the observed differences in BAI and $\delta^{13}C_{cell}$ in the model using the same climatic inputs for both upland and riparian trees, supporting that the climatic conditions did not significantly differ between sets of trees.

Second, leaf-level physiology may contribute to $\delta^{18}O_{cell}$ patterns. In addition to the differences in growth and $\delta^{13}C_{cell}$ between the sets of trees, the greater modeled g_{cmax} of the riparian trees also suggested that riparian trees had greater water availability and may have different leaf-level gas exchange compared to the upland trees. However, $\delta^{18}O_{cell}$ was not considered sensitive to changes in g_{cmax} in the model (Figure 5.7, Appendix Table 5.1). This suggested that instead the Peclet effect may underlie the expected differences in $\delta^{18}O_{cell}$, although unexpectedly the $\delta^{18}O_{cell}$ trajectories did not differ between sets of trees.

Finally, $\delta^{18}O_s$ is considered to be a primary driver of $\delta^{18}O_{cell}$ (Treydte *et al.*, 2014). In our study, we did not vary source water inputs year to year as the river is spring fed and thought to have a long residence time (Manga, 2001). The difference in proximity of the upland and riparian trees to the Metolius river suggested that they may use different sources of water (Marshall & Monserud, 2006) where riparian trees may rely on river water and upland trees may rely on both river water and precipitation (Stout & Sala, 2003; Kerhoulas *et al.*, 2013). Also, *P. ponderosa* has deep tap roots with evidence that droughted plants develop a larger root system than control plants (Kerr *et al.*, 2015), suggesting that the upland and riparian trees may access water at different depths. However, the similar observed $\delta^{18}O$ signal of the tree-ring cellulose, stem water, and

atmospheric water vapor (Table 5.3) at both sites suggested that upland and riparian trees were likely accessing the same water. In addition, the $\delta^{18}O_s$ from the Metolius river is reflected in the stem water of both upland and riparian trees (Table 5.3). Further, adjusting parameters related to rooting depth and below- and aboveground biomass ratios in the model was not necessary to match observed growth and tree-ring trajectories. Our finding is consistent with Dawson & Ehleringer (1991) who found that proximity to a stream did not influence source water used by mature *Quercus* and *Acer* and instead, mature trees used deeper sources of water while young trees relied on stream water and recent precipitation.

Interestingly, both the upland and riparian sites displayed a decline in $\delta^{18}O_{cell}$ 1992-2002 that is likely related to a change in source water $\delta^{18}O$. This decline was not observed in other central Oregon *P. ponderosa* (Roden & Ehleringer, 2007) likely because the authors examined latewood as opposed to the whole ring as in our study. The presence of this decline imprinted in the growth rings of trees from both sites provided more support that the upland and riparian sites and trees were very similar, as shown by the similar $\delta^{18}O$ of source water (Table 5.3).

$\delta^{18}O$ submodel

The $\delta^{18}O_{leaf}$ without the Peclet effect was not sensitive to any of the tested parameters because it is calculated solely with $\delta^{18}O_s$ and climate inputs including VPD (Equation 12). Therefore, the Peclet effect was crucial for connecting the $\delta^{18}O$ submodel to the rest of the model because $\delta^{18}O_{cell}$ with Peclet was calculated using modeled

transpiration (*E*). Similar to other studies, $\delta^{18}O_{cell}$ without the Peclet effect slightly overestimated observed $\delta^{18}O_{cell}$ providing more evidence that incorporating the Peclet effect may improve $\delta^{18}O_{cell}$ estimates (Barbour *et al.*, 2000; Kahmen *et al.*, 2008; Ripullone *et al.*, 2008; Holloway-Phillips *et al.*, 2016). Interestingly, the difference between $\delta^{18}O_{cell}$ with and without the Peclet effect diminished with time, which was due to the steady temporal decline in *E* (Appendix Figure 5.2). As *E* decreases, $\delta^{18}O_{cell}$ increases (Equations 13, 14, Appendix Figure 5.3) due to the increased back diffusion of enriched water relative to the unenriched stem water, thus increasing the $\delta^{18}O_{cell}$ signal. This temporal decline in *E* led to an underestimation of *E* in 1996 and 1997 compared to measured values by Law *et al.* (2000) (Figure 5.3), which also coincided with the overestimation of $\delta^{18}O_{cell}$ (Figure 5.6). However, 1996 and 1997 was within the 1992-2002 period when we observed the aforementioned unexpected source water-related decline in $\delta^{18}O_{cell}$. This suggests that the potential changes in source water may have influenced the discrepancy between modeled and observed $\delta^{18}O_{cell}$ and *E* during 1992-2002 (Figures 5.3, 5.6).

In addition to *E*, *L* also substantially influenced predictions of $\delta^{18}O_{cell}$ with Peclet (Figure 5.8, Equations 13, 14, (Kahmen *et al.*, 2009). *L* of 0.022 m was within range of previously reported values for *Pinus* species (Song *et al.*, 2013). This study provides support for the use of a well-parameterized model based on observed stand characteristics to estimate *L* since $\delta^{18}O_{cell}$ with Peclet is calculated using the *E* output. This could be a useful way to evaluate the impacts of variation in leaf-level physiology on the stand scale.

To our knowledge, this is the first time a $\delta^{18}O$ submodel has been added to 3-PG. Because the *E* output is used in the calculation of the Peclet number and thus $\delta^{18}O_{cell}$ with Peclet (Equations 13, 14), $\delta^{18}O_{cell}$ provides a new way to constrain 3-PG that differs from $\delta^{13}C_{cell}$. Unlike $\delta^{13}C_{cell}$ that constrains gas exchange parameters before allocation processes (Wei *et al.* 2014), $\delta^{18}O_{cell}$ is calculated "downstream" of other model calculations with output *E*. Thus, $\delta^{18}O_{cell}$ with Peclet was sensitive to parameters that also influence *E* including k_g, FR, α_{cx}, *pfs20*, and p_{rx}. The difference in how $\delta^{13}C_{cell}$ and $\delta^{18}O_{cell}$ constrain 3-PG occurs because $\delta^{13}C_{cell}$ depends primarily on *A* and *g* while $\delta^{18}O_{cell}$ depends on other biophysical factors in addition to *A* and *g* (Roden *et al.*, 2000; McCarroll & Loader, 2004). This was observed with the sensitivity analysis where $\delta^{18}O_{cell}$ was considered sensitive to k_g, FR, α_{cx}, and *pfs20* while $\delta^{13}C_{cell}$ was not. Since *E* and g_c are related and both influence $\delta^{13}C_{cell}$ and $\delta^{18}O_{cell}$, model parameters that influence *E* and g_c would need to be adjusted to match observed values of both $\delta^{13}C_{cell}$ and $\delta^{18}O_{cell}$. In this way, the use of both $\delta^{13}C_{cell}$ and $\delta^{18}O_{cell}$ added a useful modeling constraint to 3-PG.

Conclusion

We used long-term trajectories of observed growth, $\delta^{13}C_{cell}$, and $\delta^{18}O_{cell}$ to represent growth and productivity of old-growth *P. ponderosa* in central Oregon using 3-PG, the $\delta^{13}C_{cell}$ submodel, and the newly added $\delta^{18}O_{cell}$ submodel. The model helped to explain physiological drivers underlying the different tree-ring growth, $\delta^{13}C_{cell}$, and $\delta^{18}O_{cell}$ trajectories measured on the upland and riparian trees. Because $\delta^{18}O_{cell}$ with the

Peclet effect is calculated using stand-level *E* output from the model, *L* and leaf-level physiology may be estimated using a well-constrained model. The $\delta^{18}O$ submodel may improve 3-PG predictions because parameterization based on g_c and *E* must account for both $\delta^{18}O_{cell}$ and $\delta^{13}C_{cell}$, providing a useful and novel way to constrain 3-PG. The application of 3-PG with the $\delta^{13}C$ and $\delta^{18}O$ submodels on the upland and riparian sets of trees indicate the potential of such coupled models to be parameterized for diverse stands using site- and stand-specific information for examining the physiological mechanisms behind forest responses to changes in climate.

5.6 Acknowledgements

The authors would like to thank Dick Waring for help with 3-PG and for commenting on an earlier draft, Liang Wei, Carlos Gonzalez, and Trent Seager for helpful discussions about 3-PG, and Sean Hammond for assistance with Python. This work was supported by the NSF Graduate Research Fellowship Program and NSF grant IOS 11-46746.

5.7 References

Adams HD, Kolb TE (2004) Drought responses of conifers in ecotone forests of northern Arizona: tree ring growth and leaf δ13C. *Oecologia*, **140**, 217–225.

Barbour MM (2007) Stable oxygen isotope composition of plant tissue: a review. *Functional Plant Biology*, **34**, 83–94.

Barbour MM, Schurr U, Henry BK, Wong SC, Farquhar GD (2000) Variation in the Oxygen Isotope Ratio of Phloem Sap Sucrose from Castor Bean. Evidence in Support of the Péclet Effect. *Plant Physiology*, **123**, 671–680.

Bristow KL, Campbell GS (1984) On the relationship between incoming solar radiation and daily maximum and minimum temperature. *Agricultural and forest meteorology*, **31**, 159–166.

Brooks JR, Mitchell AK (2011) Interpreting tree responses to thinning and fertilization using tree-ring stable isotopes. *New Phytologist*, **190**, 770–782.

Cernusak LA, Arthur DJ, Pate JS, Farquhar GD (2003) Water Relations Link Carbon and Oxygen Isotope Discrimination to Phloem Sap Sugar Concentration in Eucalyptus globulus. *Plant Physiology*, **131**, 1544–1554.

Coops N, Waring R, Landsberg J (1998) Assessing forest productivity in Australia and New Zealand using a physiologically-based model driven with averaged monthly weather data and satellite-derived estimates of canopy photosynthetic capacity. *Forest Ecology and Management*, **104**, 113–127.

Coops N, Waring R, Moncrieff J (2000) Estimating mean monthly incident solar radiation on horizontal and inclined slopes from mean monthly temperatures extremes. *International Journal of Biometeorology*, **44**, 204–211.

Coops NC, Waring RH, Law BE (2005) Assessing the past and future distribution and productivity of ponderosa pine in the Pacific Northwest using a process model, 3-PG. *Ecological Modelling*, **183**, 107–124.

Coops NC, Coggins SB, Kurz WA (2007) Mapping the environmental limitations to growth of coastal Douglas-fir stands on Vancouver Island, British Columbia. *Tree physiology*, **27**, 805–815.

Craig H, Gordon LI (1965) Deuterium and oxygen 18 variations in the ocean and the marine atmosphere.

Dawson TE, Ehleringer JR (1991) Streamside trees that do not use stream water. *Nature*, **350**, 335–337.

Dongmann G, Nürnberg H, Förstel H, Wagener K (1974) On the enrichment of H2 18O in the leaves of transpiring plants. *Radiation and environmental biophysics*, **11**, 41–52.

English NB, McDowell NG, Allen CD, Mora C (2011) The effects of α-cellulose extraction and blue-stain fungus on retrospective studies of carbon and oxygen isotope variation in live and dead trees. *Rapid Communications in Mass Spectrometry*, **25**, 3083–3090.

Farquhar G, Lloyd J (1993) Carbon and oxygen isotope effects in the exchange of carbon dioxide between terrestrial plants and the atmosphere. *Stable isotopes and plant carbon-water relations*, **40**, 47–70.

Farquhar GD, Sharkey TD (1982) Stomatal conductance and photosynthesis. *Annual review of plant physiology*, **33**, 317–345.

Farquhar G, O'Leary M, Berry J (1982) On the Relationship Between Carbon Isotope Discrimination and the Intercellular Carbon Dioxide Concentration in Leaves. *Functional Plant Biology*, **9**, 121–137.

Farquhar GD, Hubick KT, Condon AG, Richards RA (1989) Carbon Isotope Fractionation and Plant Water-Use Efficiency. In: *Stable Isotopes in Ecological Research* (eds Rundel PW, Ehleringer JR, Nagy KA), pp. 21–40. Springer New York.

Farquhar G, Barbour M, Styles J *et al.* (2000) Oxygen isotope composition of plant matter reveals physiological and genetic effects on plant water use and crop yields. *Proc Natl Acad Sci USA*.

Farquhar GD, Cernusak LA, Barnes B (2007) Heavy Water Fractionation during Transpiration. *Plant Physiology*, **143**, 11–18.

Forrester DI, Tang X (2016) Analysing the spatial and temporal dynamics of species interactions in mixed-species forests and the effects of stand density using the 3-PG model. *Ecological Modelling*, **319**, 233–254.

Francey R, Allison C, Etheridge D *et al.* (1999) A 1000-year high precision record of δ13C in atmospheric CO2. *Tellus B*, **51**, 170–193.

Gessler A, Brandes E, Buchmann N, Helle G, Rennenberg H, Barnard RL (2009) Tracing carbon and oxygen isotope signals from newly assimilated sugars in the leaves to the tree-ring archive. *Plant, Cell & Environment*, **32**, 780–795.

Gessler A, Ferrio JP, Hommel R, Treydte K, Werner RA, Monson RK (2014) Stable isotopes in tree rings: towards a mechanistic understanding of isotope fractionation and mixing processes from the leaves to the wood. *Tree Physiology*, tpu040.

Gholz HL, Grier C, Campbell A, Brown A (1979) *Equations for estimating biomass and leaf area of plants in the Pacific Northwest*. Corvallis: Forest Research Lab., Oregon State University, School of Forestry.

Hartl-Meier C, Zang C, Büntgen U *et al.* (2015) Uniform climate sensitivity in tree-ring stable isotopes across species and sites in a mid-latitude temperate forest. *Tree Physiology*, **35**, 4–15.

Holloway-Phillips M, Cernusak LA, Barbour M *et al.* (2016) Leaf vein fraction influences the Péclet effect and 18O enrichment in leaf water. *Plant, Cell & Environment*, n/a-n/a.

Irvine J, Law BE, Anthoni PM, Meinzer FC (2002) Water limitations to carbon exchange in old-growth and young ponderosa pine stands. *Tree Physiology*, **22**, 189–196.

Kahmen A, Simonin K, Tu KP *et al.* (2008) Effects of environmental parameters, leaf physiological properties and leaf water relations on leaf water δ18O enrichment in different Eucalyptus species. *Plant, Cell & Environment*, **31**, 738–751.

Kahmen A, Simonin K, Tu K, Goldsmith GR, Dawson TE (2009) The influence of species and growing conditions on the 18-O enrichment of leaf water and its impact on "effective path length." *New Phytologist*, **184**, 619–630.

Kahmen A, Sachse D, Arndt SK, Tu KP, Farrington H, Vitousek PM, Dawson TE (2011) Cellulose δ18O is an index of leaf-to-air vapor pressure difference (VPD) in tropical plants. *Proceedings of the National Academy of Sciences*, **108**, 1981–1986.

Kerhoulas LP, Kolb TE, Koch GW (2013) Tree size, stand density, and the source of water used across seasons by ponderosa pine in northern Arizona. *Forest Ecology and Management*, **289**, 425–433.

Kerr KL, Meinzer FC, McCulloh KA, Woodruff DR, Marias DE (2015) Expression of functional traits during seedling establishment in two populations of Pinus ponderosa from contrasting climates. *Tree Physiology*, **35**, 535–548.

Landsberg J (2003a) Physiology in forest models: history and the future. *FBMIS*, **1**, 49–63.

Landsberg J (2003b) Modelling forest ecosystems: state of the art, challenges, and future directions. *Canadian Journal of Forest Research*, **33**, 385–397.

Landsberg JJ, Waring RH (1997) A generalised model of forest productivity using simplified concepts of radiation-use efficiency, carbon balance and partitioning. *Forest Ecology and Management*, **95**, 209–228.

Landsberg JJ, Waring RH, Coops NC (2003) Performance of the forest productivity model 3-PG applied to a wide range of forest types. *Forest Ecology and Management*, **172**, 199–214.

Law BE, Waring . R. H., Anthoni PM, Aber JD (2000) Measurements of gross and net ecosystem productivity and water vapour exchange of a Pinus ponderosa ecosystem, and an evaluation of two generalized models. *Global Change Biology*, **6**, 155–168.

Law BE, Goldstein AH, Anthoni PM *et al.* (2001a) Carbon dioxide and water vapor exchange by young and old ponderosa pine ecosystems during a dry summer. *Tree Physiology*, **21**, 299–308.

Law B, Van Tuyl S, Cescatti A, Baldocchi D (2001b) Estimation of leaf area index in open-canopy ponderosa pine forests at different successional stages and management regimes in Oregon. *Agricultural and Forest Meteorology*, **108**, 1–14.

Leavitt S, Danzer SR (1993) Method for batch processing small wood samples to holocellulose for stable-carbon isotope analysis. *Analytical Chemistry*, **65**, 87–88.

Loucos KE, Simonin KA, Song X, Barbour MM (2015) Observed relationships between leaf H218O Péclet effective length and leaf hydraulic conductance reflect assumptions in Craig–Gordon model calculations. *Tree Physiology*, tpu110.

Manga M (2001) Using Springs to Study Groundwater Flow and Active Geologic Processes. *Annual Review of Earth and Planetary Sciences*, **29**, 201–228.

Marias DE, Meinzer FC, Woodruff DR *et al.* (2014) Impacts of dwarf mistletoe on the physiology of host Tsuga heterophylla trees as recorded in tree-ring C and O stable isotopes. *Tree Physiology*, **34**, 595–607.

Marshall JD, Monserud RA (2006) Co-occurring species differ in tree-ring delta(18)O trends. *Tree Physiology*, **26**, 1055–1066.

McCarroll D, Loader NJ (2004) Stable isotopes in tree rings. *Quaternary Science Reviews*, **23**, 771–801.

Meyer WH (1938) *Yield of even-aged stands of ponderosa pine*, Vol. 630. US Dept. of Agriculture.

Monteith J (1965) The state and movement of water in living organisms. , pp. 205–234.

Monteith J, Unsworth M (2007) *Principles of environmental physics*. Academic Press.

Nolè A, Law B, Magnani F, Matteucci G, Ferrara A, Ripullone F, Borghetti M (2009) Application of the 3-PGS model to assess carbon accumulation in forest ecosystems at a regional level. *Canadian journal of forest research*, **39**, 1647–1661.

Nolè A, Collalti A, Magnani F *et al.* (2013) Assessing temporal variation of primary and ecosystem production in two Mediterranean forests using a modified 3-PG model. *Annals of forest science*, **70**, 729–741.

Orwig DA, Abrams MD Variation in radial growth responses to drought among species, site, and canopy strata. *Trees*, **11**, 474–484.

Panek JA, Goldstein AH (2001) Response of stomatal conductance to drought in ponderosa pine: implications for carbon and ozone uptake. *Tree Physiology*, **21**, 337–344.

Penman HL (1948) Natural evaporation from open water, bare soil and grass. , Vol. 193, pp. 120–145. The Royal Society.

Ripullone F, Matsuo N, Stuart-Williams H, Wong SC, Borghetti M, Tani M, Farquhar G (2008) Environmental effects on oxygen isotope enrichment of leaf water in cotton leaves. *Plant Physiology*, **146**, 729–736.

Roden JS, Ehleringer JR (2007) Summer precipitation influences the stable oxygen and carbon isotopic composition of tree-ring cellulose in Pinus ponderosa. *Tree Physiology*, **27**, 491–501.

Roden JS, Lin G, Ehleringer JR (2000) A mechanistic model for interpretation of hydrogen and oxygen isotope ratios in tree-ring cellulose. *Geochimica et Cosmochimica Acta*, **64**, 21–35.

Ryan MG, Bond BJ, Law BE, Hubbard RM, Woodruff D, Cienciala E, Kucera J (2000) Transpiration and whole-tree conductance in ponderosa pine trees of different heights. *Oecologia*, **124**, 553–560.

Saffell BJ, Meinzer FC, Voelker SL, Shaw DC, Brooks JR, Lachenbruch B, Mckay J (2014) Tree-ring stable isotopes record the impact of a foliar fungal pathogen on CO2 assimilation and growth in Douglas-fir. *Plant, Cell & Environment*, **37**, 1536–1547.

Saugier B, Ehleringer JR, Hall AE, Farquhar GD (2012) *Stable isotopes and plant carbon-water relations*. Elsevier.

Seidl R, Rammer W, Scheller RM, Spies TA (2012) An individual-based process model to simulate landscape-scale forest ecosystem dynamics. *Ecological Modelling*, **231**, 87–100.

Sohn JA, Brooks JR, Bauhus J, Kohler M, Kolb TE, McDowell NG (2014) Unthinned slow-growing ponderosa pine (Pinus ponderosa) trees contain muted isotopic signals in tree rings as compared to thinned trees. *Trees*, **28**, 1035–1051.

Song X, Barbour MM, Farquhar GD, Vann DR, Helliker BR (2013) Transpiration rate relates to within- and across-species variations in effective path length in a leaf water model of oxygen isotope enrichment. *Plant, Cell & Environment*, **36**, 1338–1351.

Sternberg L da SL (1989) Oxygen and hydrogen isotope ratios in plant cellulose: mechanisms and applications. In: *Stable isotopes in ecological research*, pp. 124–141. Springer.

Stout DL, Sala A (2003) Xylem vulnerability to cavitation in Pseudotsuga menziesii and Pinus ponderosa from contrasting habitats. *Tree Physiology*, **23**, 43–50.

Thornton PE, Running SW, White MA (1997) Generating surfaces of daily meteorological variables over large regions of complex terrain. *Journal of Hydrology*, **190**, 214–251.

Treydte K, Boda S, Graf Pannatier E *et al.* (2014) Seasonal transfer of oxygen isotopes from precipitation and soil to the tree ring: source water versus needle water enrichment. *New Phytologist*, **202**, 772–783.

Voelker SL, Brooks JR, Meinzer FC *et al.* (2014a) Reconstructing relative humidity from plant δ18O and δD as deuterium deviations from the global meteoric water line. *Ecological Applications*, **24**, 960–975.

Voelker SL, Meinzer FC, Lachenbruch B, Brooks JR, Guyette RP (2014b) Drivers of radial growth and carbon isotope discrimination of bur oak (Quercus macrocarpa Michx.) across continental gradients in precipitation, vapour pressure deficit and irradiance. *Plant, Cell & Environment*, **37**, 766–779.

Waring R (2000) A process model analysis of environmental limitations on the growth of Sitka spruce plantations in Great Britain. *Forestry*, **73**, 65–79.

Waring RH, Gao L (2016) Recent reduction in the frequency of frost accounts for most of the increased growth of a high elevation spruce forest in northwestern China. *Trees*, **30**, 1225–1236.

Waring RH, Landsberg JJ, Williams M (1998) Net primary production of forests: a constant fraction of gross primary production? *Tree Physiology*, **18**, 129–134.

Waring R, Landsberg J, Linder S (2016) Tamm Review: Insights gained from light use and leaf growth efficiency indices. *Forest Ecology and Management*, **379**, 232–242.

Warren JM, Meinzer FC, Brooks JR, Domec JC (2005) Vertical stratification of soil water storage and release dynamics in Pacific Northwest coniferous forests. *Agricultural and Forest Meteorology*, **130**, 39–58.

Wei L, Marshall JD, Zhang J, Zhou H, Powers RF (2014a) 3-PG simulations of young ponderosa pine plantations under varied management intensity: Why do they grow so differently? *Forest Ecology and Management*, **313**, 69–82.

Wei L, Marshall JD, Link TE *et al.* (2014b) Constraining 3-PG with a new δ13C submodel: a test using the δ13C of tree rings. *Plant, Cell & Environment*, **37**, 82–100.

Williams AP, Michaelsen J, Leavitt SW, Still CJ (2010) Using tree rings to predict the response of tree growth to climate change in the continental United States during the twenty-first century. *Earth Interactions*, **14**, 1–20.

Xenakis G, Ray D, Mencuccini M (2008) Sensitivity and uncertainty analysis from a coupled 3-PG and soil organic matter decomposition model. *ecological modelling*, **219**, 1–16.

Yakir D, DeNiro M, Gat J (1990) Natural deuterium and oxygen-18 enrichment in leaf water of cotton plants grown under wet and dry conditions: evidence for water compartmentation and its dynamics. *Plant, Cell & Environment*, **13**, 49–56.

Youngblood A, Max T, Coe K; (2004) Stand structure in eastside old-growth ponderosa pine forests of Oregon and northern California. *Forest Ecology and Management*, **199**, 191–217.

Zhang J, Ritchie MW, Maguire DA, Oliver WW (2013) Thinning ponderosa pine (Pinus ponderosa) stands reduces mortality while maintaining stand productivity. *Canadian Journal of Forest Research*, **43**, 311–320.

5.8 Figures & Tables

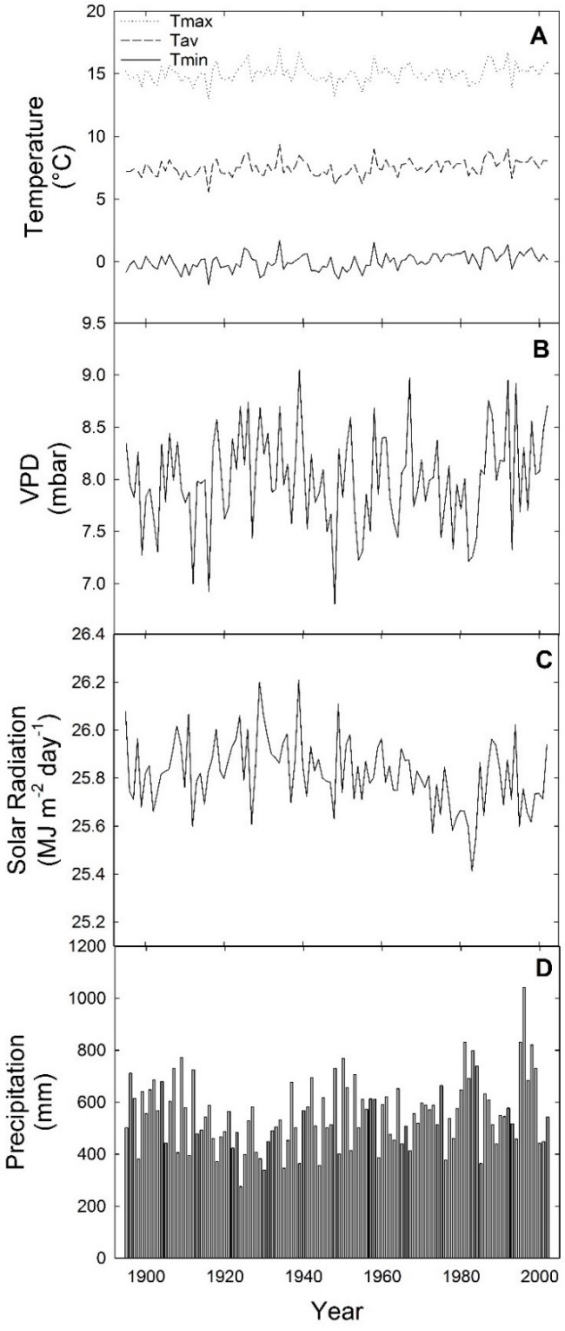

Figure 5.1 Climate inputs from 1895-2002 at the Metolius site: average annual minimum temperature (T_{min}), maximum temperature (T_{max}), average temperature (T_{av}) (A), vapor pressure deficit (VPD, B), solar radiation (C), and precipitation (D) based on the mean monthly values that are used in 3-PG.

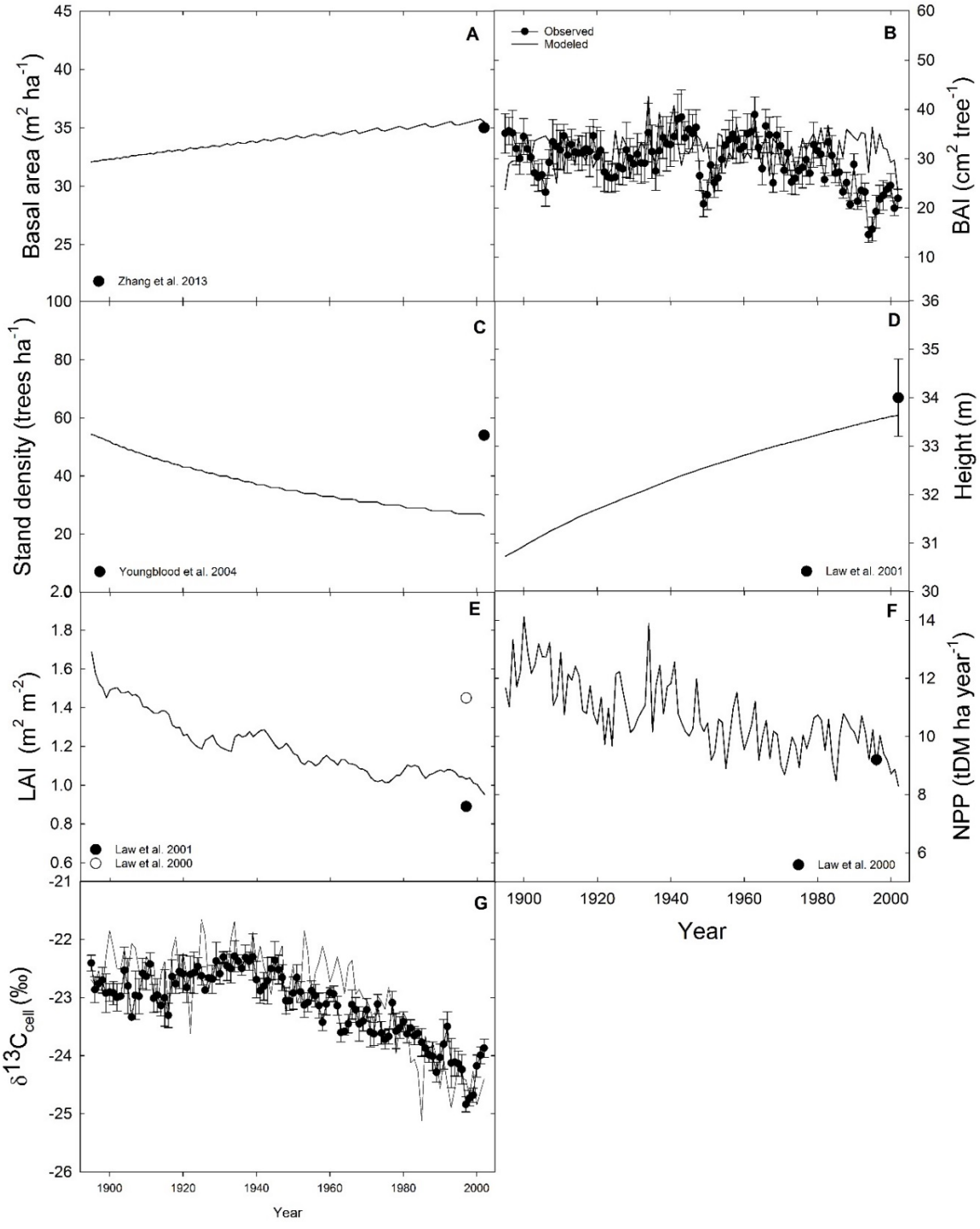

Figure 5.2 Modeled and previously observed basal area (A), basal area increment (BAI, B), stand density (C), height (D), leaf area index (LAI, E), net primary productivity (NPP, F), and $\delta^{13}C_{cell}$ (G) for 1895-2002. For $\delta^{13}C_{cell}$, N=5. Error bars are ± SE. Previously observed values also listed in Table 5.1.

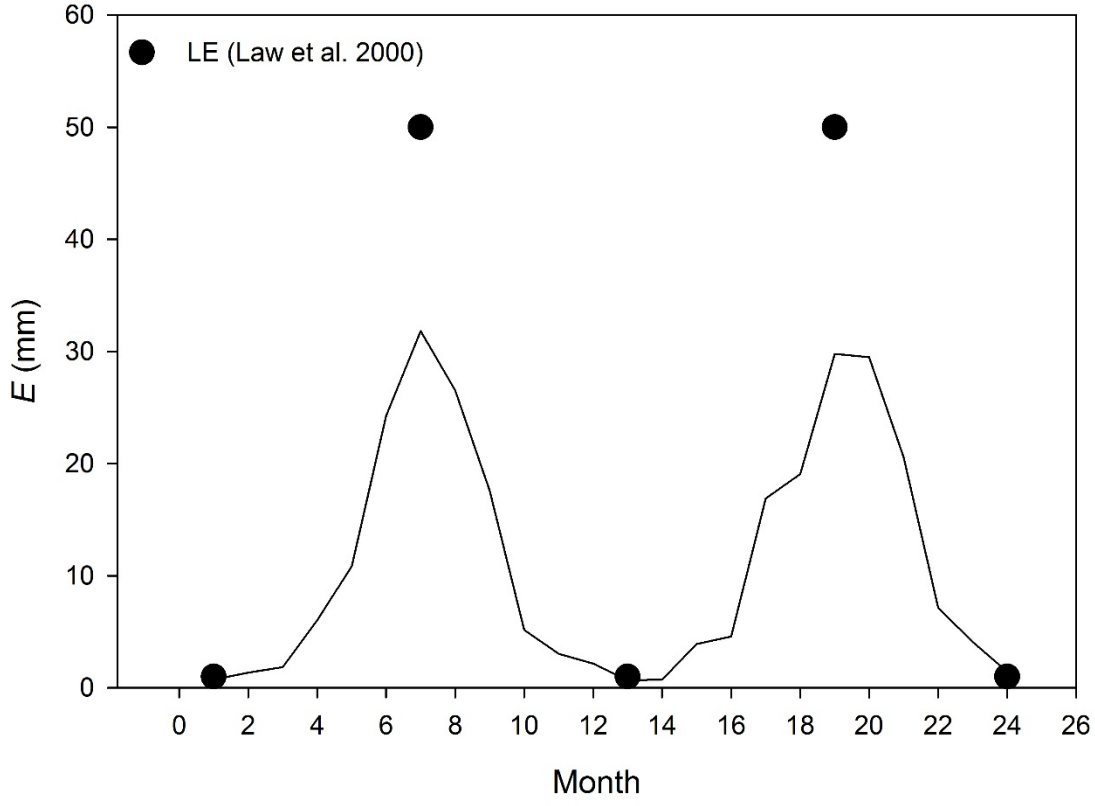

Figure 5.3 Monthly transpiration (*E*, mm month^{-1}) in 2001-2002 predicted by the model compared with previously reported water vapor flux (*LE*) from Law *et al.* (2000).

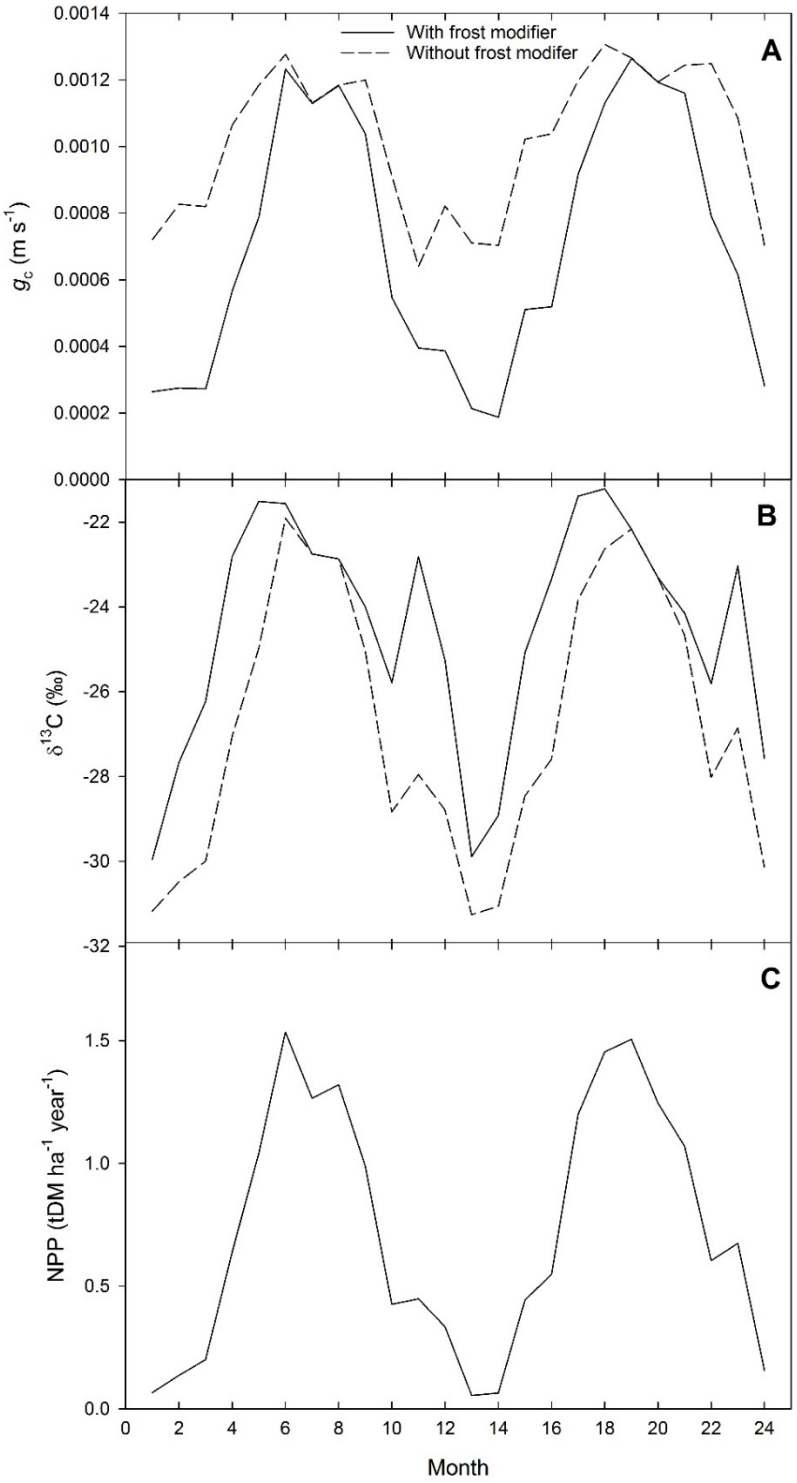

Figure 5.4 The effect of the addition of the frost modifier for calculating canopy conductance (g_c) to account for zero conductance on days with frost (where minimum temperature <0°C) on g_c (A), $\delta^{13}C_{cell}$ (B), and net primary productivity (NPP, B) in 2001-2002.

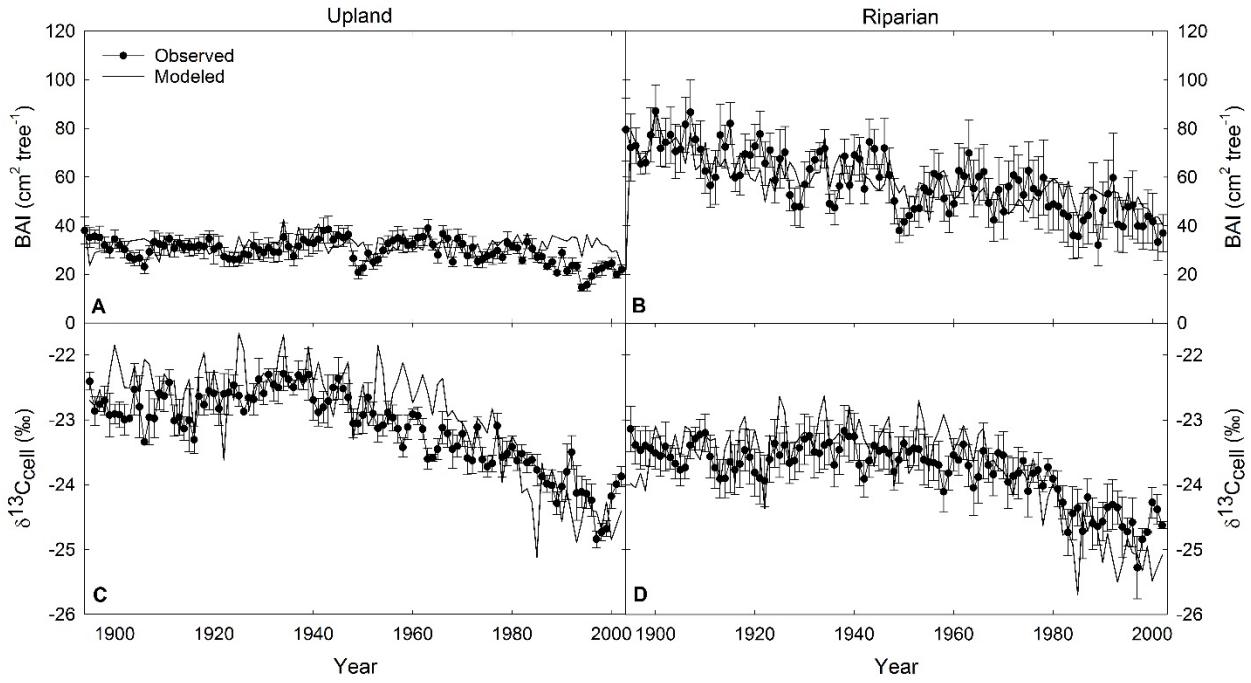

Figure 5.5 Modeled and measured time courses of basal area increment (BAI) and $\delta^{13}C_{cell}$ of upland (A,C) and riparian (B,D) trees. N=5. Error bars are ± SE.

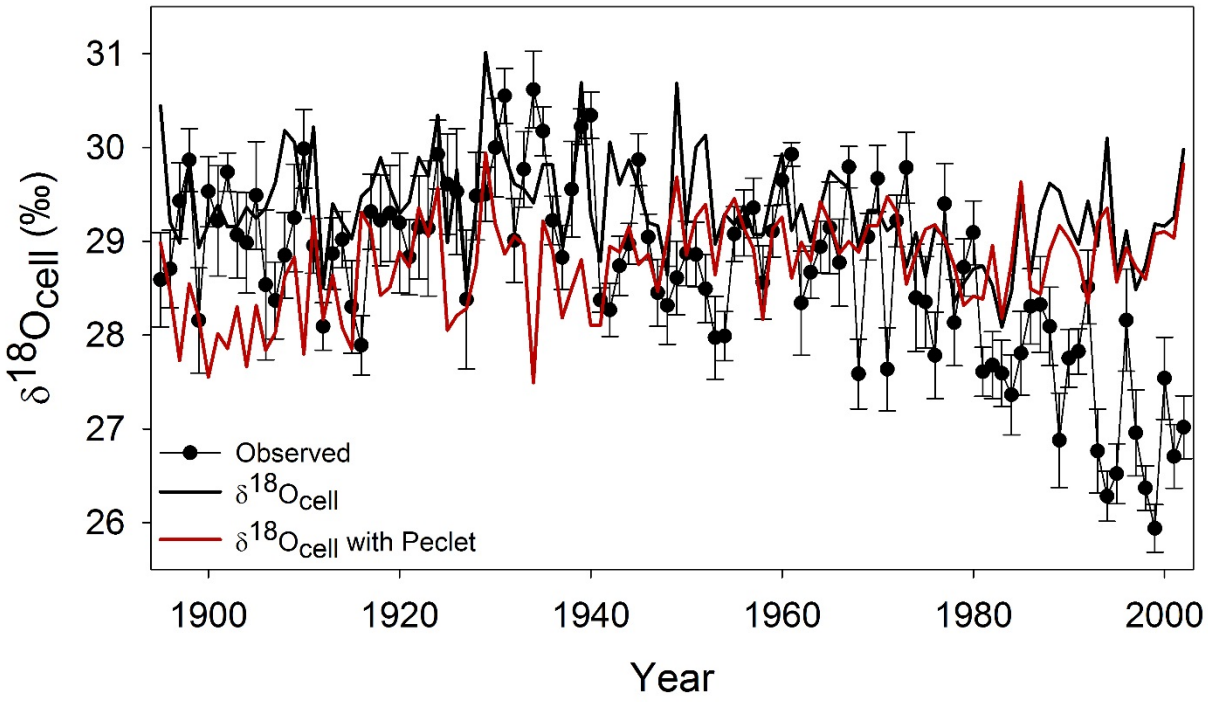

Figure 5.6 Modeled and measured time courses of $\delta^{18}O_{cell}$ and $\delta^{18}O_{cell}$ with Peclet of combined upland and riparian trees. N=10. Error bars are ± SE.

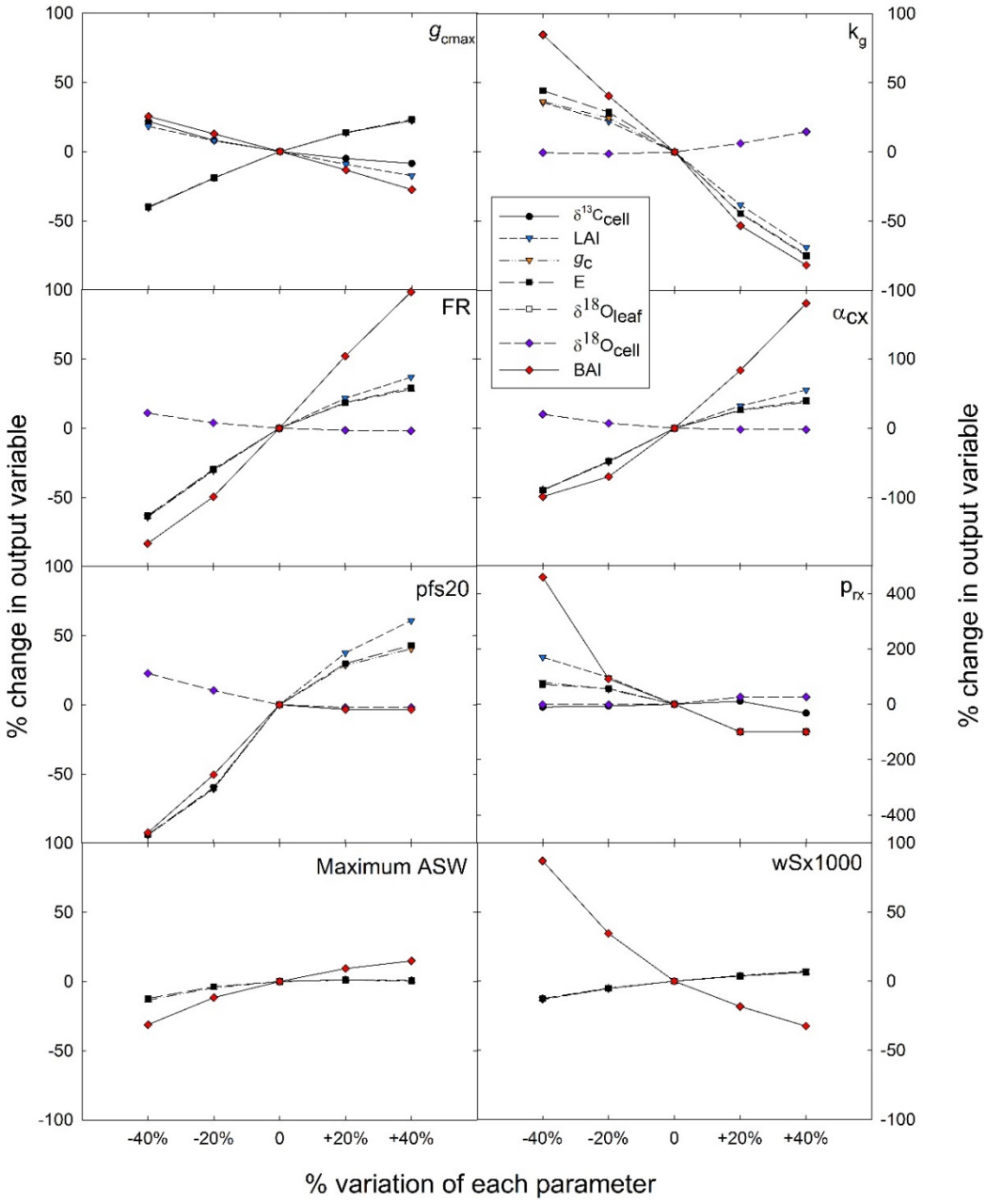

Figure 5.7 Sensitivity analysis results examining the effect of parameters: maximum canopy conductance (g_{cmax}), sensitivity of canopy conductance to VPD (k_g), fertility rating (FR), maximum quantum efficiency (α_{cx}), foliage:stem partitioning ratio for tree diameter of 20 cm (*pfs20*), maximum root partitioning (p_{rx}), maximum available soil water (ASW), and maximum tree stem mess in mature stands of 1000 trees ha^{-1} (*wSx1000*) on output variables: $\delta^{13}C_{cell}$, basal area increment (BAI), leaf area index (LAI), canopy conductance (g_c), transpiration (E), $\delta^{18}O_{leaf}$, and $\delta^{18}O_{cell}$ with Peclet. Only output variables that changed ±10% and were considered 'sensitive' to shifts in each parameter are shown. Appendix Table 5.1 shows complete sensitivity analysis values. Note the different y-axis ranges for α_{cx} and p_{rx}.

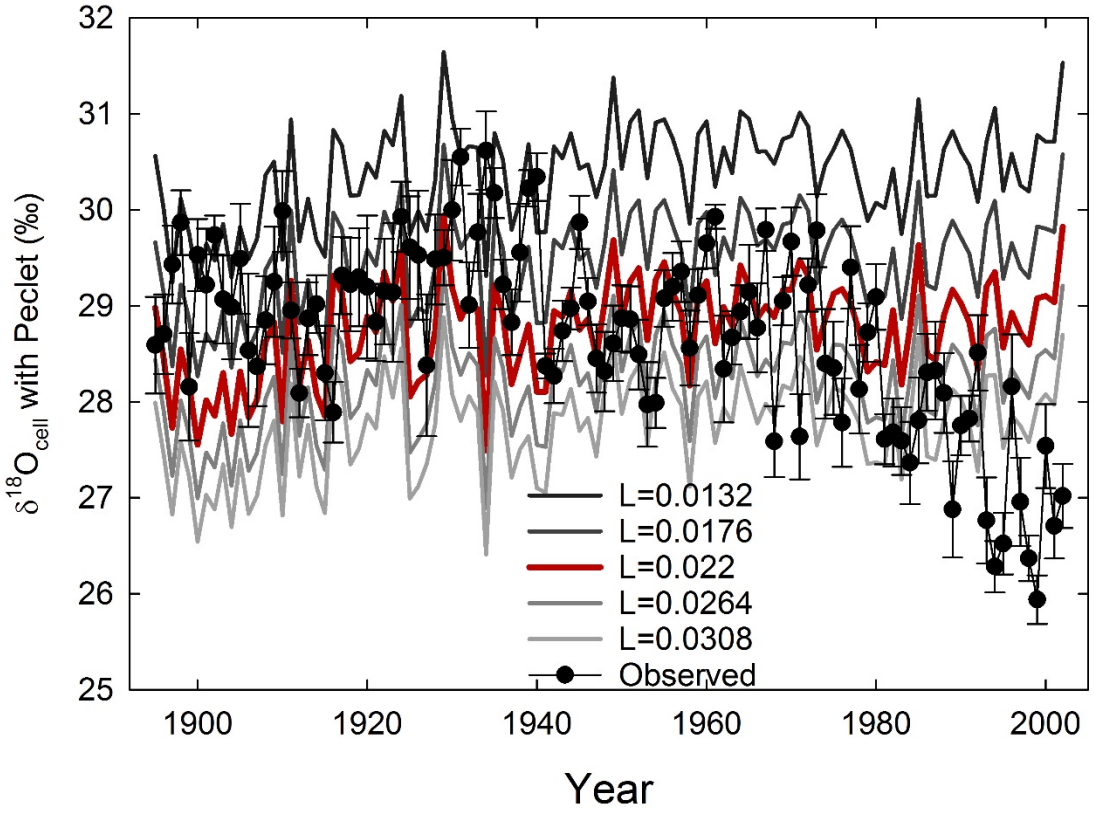

Figure 5.8 Optimization of L using $\delta^{18}O_{cell}$ with Peclet. L values are ±20% and ±40% of the optimized L=0.022 m.

Table 5.1 Stand characteristics for old-growth *P. ponderosa* at the Metolius AmeriFlux site used to parameterize the model.

Tree height (m)	30.9 ± 0.93	(Youngblood *et al.*, 2004)
	33.5 ± 1.26	(Law *et al.*, 2001b)
	34 ± 0.8	(Law *et al.*, 2001a)
Age (years)	~260	This study
DBH (cm)	Upland: 87.8 ± 3.9	This study
	Riparian: 112.3 ± 8.2	This study
$\delta\,^{13}C_{cell}$ (‰)	-	This study
$\delta^{18}O_{cell}$ (‰)	-	This study
LAI	<1.0	(Ryan *et al.*, 2000)
($m^2\ m^{-2}$)	0.89-1.6	(Law *et al.*, 2001b)
	1.1-1.8	(Law *et al.*, 2000)
	2.1	(Irvine *et al.*, 2002)
Basal area	30	(Youngblood *et al.*, 2004; Warren *et al.*, 2005)
($m^2\ ha^{-1}$)	35	(Zhang *et al.*, 2013)
	45	(Meyer, 1938)
Stand density	54	(Youngblood *et al.*, 2004)
(trees ha^{-1})	72	(Law *et al.*, 2001a; Warren *et al.*, 2005)
	84	(Law *et al.*, 2001b)
	137	(Meyer, 1938)
NPP	9.2	(Law *et al.*, 2000)
(tDM $ha^{-1}\ year^{-1}$)		
Transpiration	30	(Irvine *et al.*, 2002)
(mm $month^{-1}$)	45	(Warren *et al.*, 2005)
	50	(Law *et al.*, 2000)

Table 5.2 Parameters for old-growth *Pinus ponderosa* at the Metolius site, Oregon. Default values from 3PGpjs vsn 2.7, 2010.

Parameter	Units	Abbreviation	Value	Reference
Initial conditions				
Initial foliage biomass	kg ha^{-1}	InitialWF	1.5	(Wei *et al.*, 2014a)
Initial root biomass	kg ha^{-1}	InitialWR	1.4	(Wei *et al.*, 2014a)
Initial stem biomass	kg ha^{-1}	InitialWS	0.9	(Wei *et al.*, 2014a)
Initial stocking	trees ha^{-1}		550	(Warren *et al.*, 2005)
Initial available soil water	mm	InitASW	30	Default
Maximum available soil water	mm	Maximum ASW	163	(Law *et al.*, 2000)
Allometric relationships and partitioning				
Foliage:stem partitioning ratios for D=2 cm	-	*pfs2*	1.2745	Coops *et al.* 2005
Foliage:stem partitioning ratios for D=20 cm	-	*pfs20*	0.77	Calibrated
Stem constant	-	S_c	0.0561	Equation 5
Stem Power	-	S_p	2.488	Equation 5
Maximum root biomass partitioning	-	p_{rx}	0.95	Calibrated
Minimum root biomass partitioning	-	p_{rn}	0.25	Default
Modifiers for photosynthesis and NPP/GPP				
Maximum temperature	°C	T_{max}	40	Law *et al.* (2000)
Minimum temperature	°C	T_{min}	-2	
Optimum temperature	°C	T_{opt}	20	Law *et al.* (2000)
Days production lost per frost day	days	k_F	1	Default
Assimilate use efficiency	-		0.47	Default
Soil water and fertility				
Soil type	-		Sandy loam	(Law *et al.*, 2000)
Fertility rating	-	FR	0.1	Calibrated
Value of ‘fN’ when FR=0	-	fN_0	1	Default
Value of m when FR = 0	-	m_0	0	Default
Age modifier (f_{age})				
Maximum age	years	MaxAge	500	

Power of relative age in function for f_{age}	-	n_{Age}	4	Default
Relative age to five f_{age}=0.5	-	r_{Age}	95	Default
Litterfall and root turnover				
Maximum litterfall rate	$month^{-1}$	γ_{Fx}	0.021	Default
Coefficients in litterfall rate at t=0	$month^{-1}$	γ_F	0.001	Default
Age at which litterfall rate has median value	month	$t_{\gamma F}$	36	Default
Root turnover rate	$month^{-1}$	γ_R, Rttover	0.04	Default
Conductance				
Maximum canopy conductance	$m\ s^{-1}$	g_{cmax}	0.012	Calibrated
LAI required for maximum canopy conductance	-	LAI_{gcx}	3.3	Default
Response of canopy conductance to VPD	$mbar^{-1}$	k_g	0.05	Calibrated
Canopy boundary layer conductance, assumed constant	$m\ s^{-1}$	BL_{cond}	0.2	(Law *et al.*, 2000)
Stem mortality				
Maximum stem mass (kg) likely in mature stands of 1000 trees ha^{-1}	$kg\ tree^{-1}$	*wSx1000*	45	Calibrated
Power in self-thinning law	-	thinPower	1.5	Default
Leaf mortality fraction	-	m_F	0.0	Default
Root mortality fraction	-	m_R	0.2	Default
Stem mortality fraction	-	m_S	0.2	Default
Branch & bark fraction at age 0	-	$frac_{BB0}$	0.15	Default
Branch & bark fraction for mature trees	-	$frac_{BB1}$	0.15	Default
Stand age for fracBB = (fracBB0+fracBB1)/2	years	t_{BB}	1.5	Default
Canopy structure and processes				
Specific leaf area for mature trees (m^2/kg)	$m^2\ kg^{-1}$	SLA_1	4.2	(Law *et al.*, 2000)
Stand age (years) for SLA = (SLA0+SLA1)/2	$m^2\ kg^{-1}$	t_{SLA}	2.5	(Law *et al.*, 2000)
Age at full canopy cover (years)	years	fullCanAge	15	Default
Radiation extinction coefficient	-	*k*	0.5	Default
LAI required for maximum rainfall interception	-	LAImaxIntcptn	5	Default
Max proportion of rainfall intercepted by canopy	-	MaxIntcptn	0.1	Default
Canopy quantum efficiency	mol C (mol PAR)$^{-1}$	α_{cx}	0.04	Calibrated
Power term used for describe the trajectory of canopy closure	-	CanPower	1	Default

Added parameter for tree height	-	HtC_0	4.85	Calibrated
Added parameter for tree height	-	HtC_1	-7.0	Default
Basic wood density	t m^{-3}		0.4	Default
$\delta^{13}C$ submodel				
Conductance CO2 to water	-	RGcGW	0.66	Default
$\delta^{13}C$ difference of modeled tissue and new photosynthate	‰	δ^{13}CTissueDif	1.7	(Wei *et al.*, 2014b)
Fractionation against ^{13}C in diffusion through air	‰	aFracDiffu	4.4	(Farquhar & Sharkey, 1982)
Enzymatic fractionation by Rubisco	‰	bFracRubi	27	(Farquhar & Sharkey, 1982)
Temperature modifier for g_c:k_2	-	TK_2	0.244	(Wei *et al.*, 2014b)
Temperature modifier for g_c:k_3	-	TK_3	0.0368	(Wei *et al.*, 2014b)

Table 5.3 $\delta^{18}O$ of source river water, stem water, and atmospheric water vapor at the upland and riparian sites in 2002 and 2004. N=1-4 ± SE.

Location	**Sample Type**	**Date**	**$\delta^{18}O$ (‰)**
Metolius River	river water	29 Aug 2002	-13.9
		13 Jul 2004	-14.2
Upland	stem water	29 Aug 2002	-13.3 ± 0.1
		13 Jul 2004	-14.6
	water vapor	13 Jul 2004	-26.0
Riparian	stem water	13 Jul 2004	-14.22
	water vapor	13 Jul 2004	-25.3

5.9 Appendices

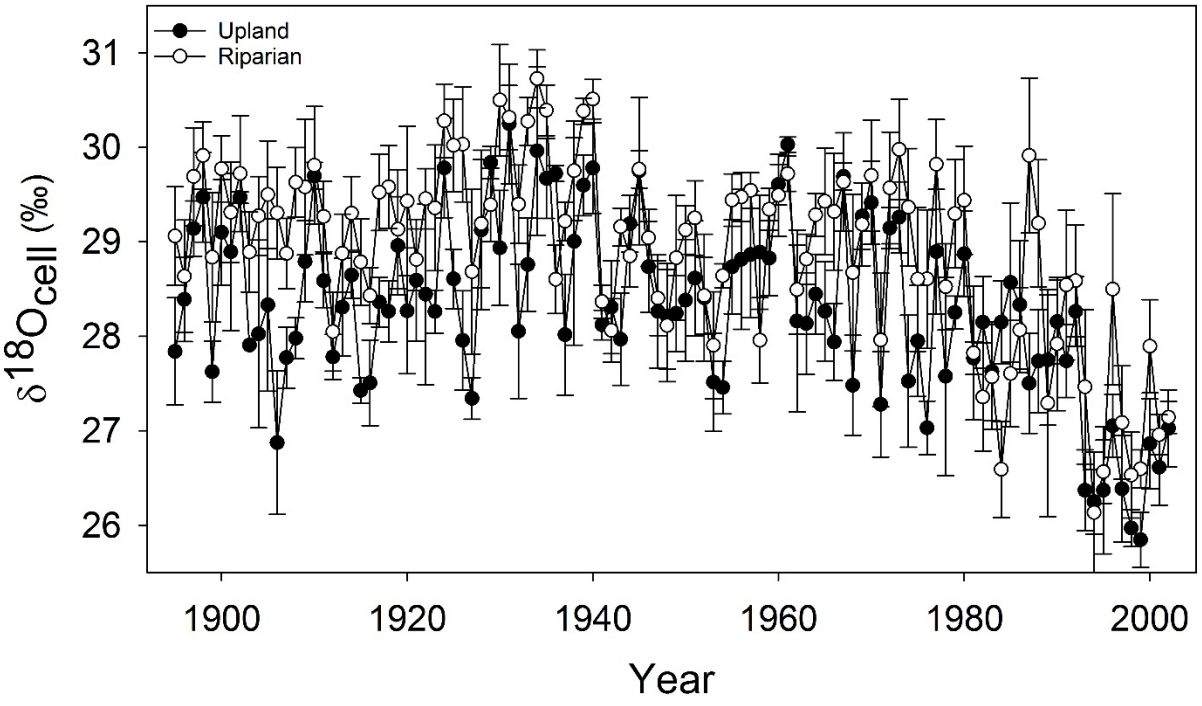

Appendix Figure 5.1 Time courses of $\delta^{18}O_{cell}$ measured in upland and riparian trees. N=5. Error bars ± SE.

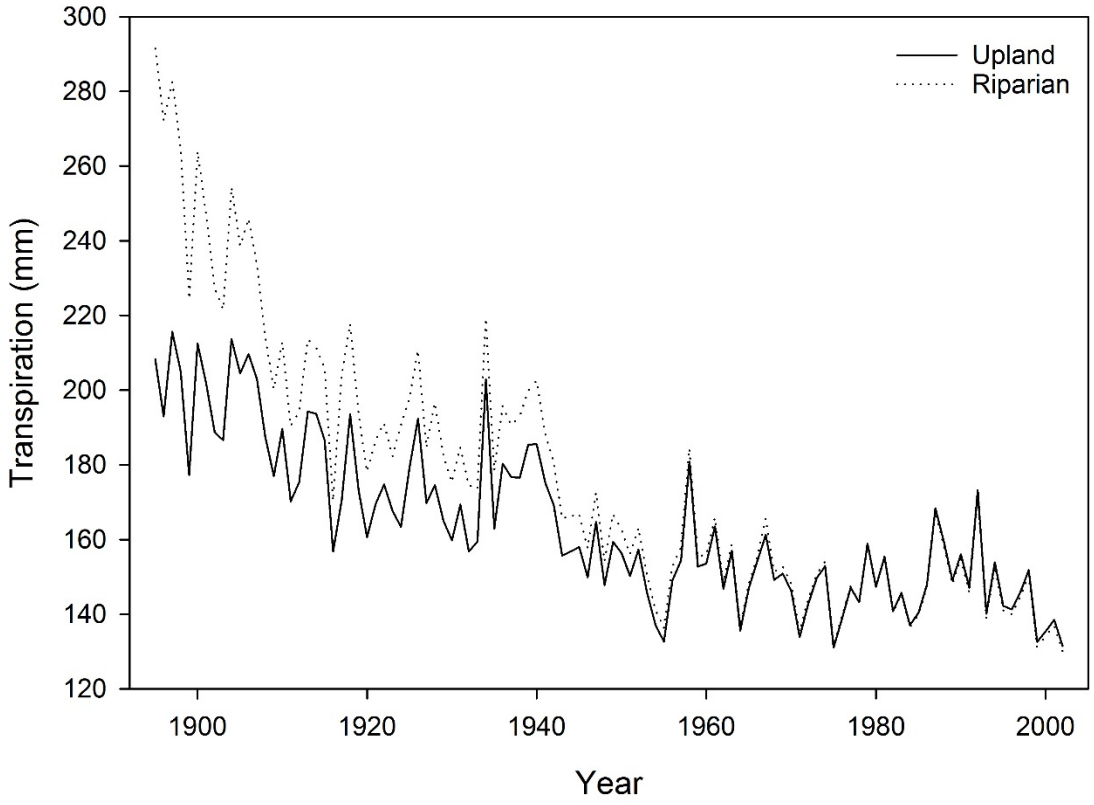

Appendix Figure 5.2 Modeled transpiration (mm year^{-1}) for upland and riparian trees.

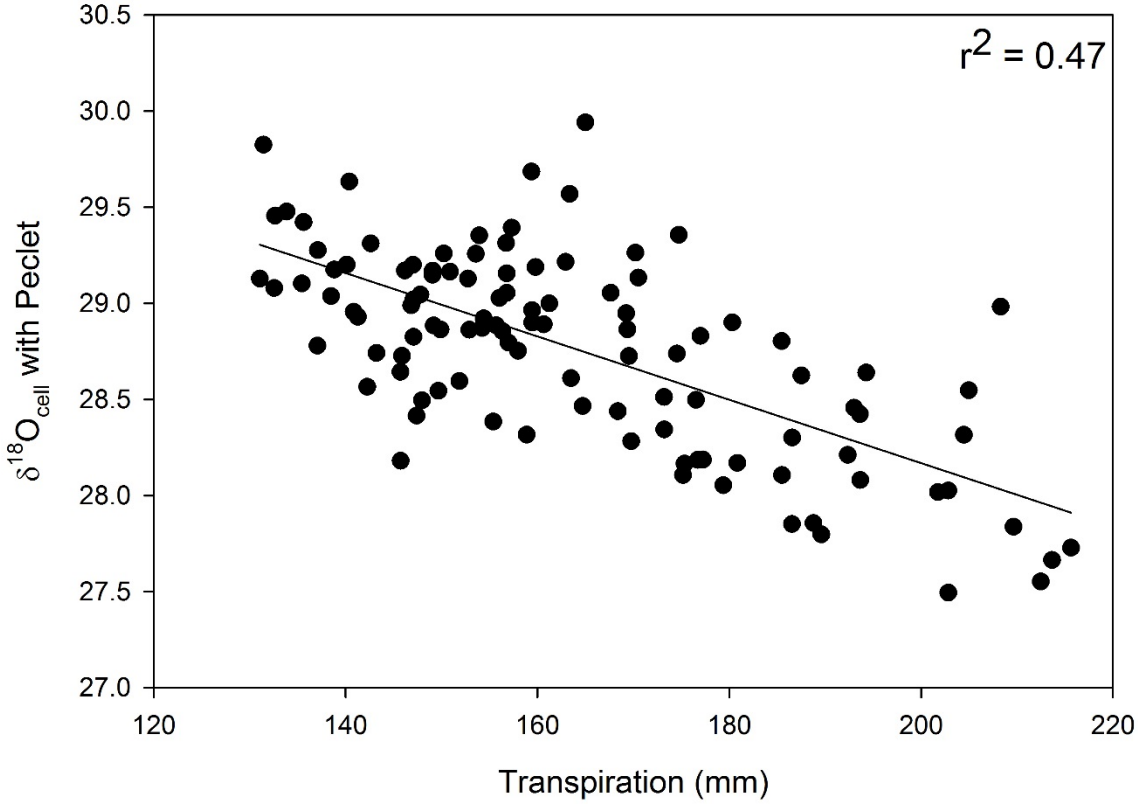

Appendix Figure 5.3 Modeled $\delta^{18}O_{cell}$ with the Peclet effect was negatively related to annual transpiration for each year 1895-2002.

Appendix Table 5.1 Sensitivity analysis evaluating the effect of ±20% and ±40% changes in parameters on outputs. Bolded outputs are those that changed ≥10%, are considered 'sensitive,' and are depicted in Figure 5.7.

Parameter	*Output*	*-40%*	*-20%*	*+20%*	*+40%*
g_{cmax}	**$\delta^{13}C_{cell}$**	21.7	8.0	-5.1	-8.6
	BAI	25.4	12.7	-13.4	-27.6
	LAI	18.2	7.8	-9.3	-17.5
	g_c	-40.5	-19.2	13.5	22.4
	E	-40.1	-18.9	13.8	23.1
	$\delta^{18}O_{leaf}$	0.0	0.0	0.0	0.0
	$\delta^{18}O_{cell}$ with Peclet	5.6	2.3	-1.2	-1.7
k_g	$\delta^{13}C_{cell}$	-2.8	-1.7	3.5	6.7
	BAI	84.7	40.6	-53.2	-81.7
	LAI	35.8	22.0	-38.3	-69.0
	g_c	36.4	24.7	-43.8	-74.3
	E	44.3	28.8	-44.4	-75.0
	$\delta^{18}O_{leaf}$	0.0	0.0	0.0	0.0
	$\delta^{18}O_{cell}$ with Peclet	-0.5	-1.3	6.3	14.7
FR	$\delta^{13}C_{cell}$	6.0	2.7	-1.7	-2.8
	BAI	-83.3	-49.5	52.1	98.5
	LAI	-64.2	-30.6	21.7	37.0
	g_c	-63.7	-30.0	18.2	28.2
	E	-63.2	-29.6	18.6	29.4
	$\delta^{18}O_{leaf}$	0.0	0.0	0.0	0.0
	$\delta^{18}O_{cell}$ with Peclet	11.1	3.9	-1.5	-2.0
α_{cx}	$\delta^{13}C_{cell}$	-7.4	-2.9	3.4	7.0
	BAI	-98.4	-69.6	83.3	179.7
	LAI	-89.2	-48.4	32.3	55.1
	g_c	-89.0	-47.8	25.4	37.7
	E	-88.8	-47.3	26.3	40.0
	$\delta^{18}O_{leaf}$	0.0	0.0	0.0	0.0
	$\delta^{18}O_{cell}$ with Peclet	20.2	7.2	-1.9	-2.0
pfs20	$\delta^{13}C_{cell}$	9.9	5.8	-2.9	-4.6
	BAI	-92.5	-50.5	-3.5	-19.6
	LAI	-94.2	-60.8	37.4	60.8
	g_c	-94.0	-60.3	28.5	40.3
	E	-93.9	-59.8	29.7	42.9

	$\delta^{18}O_{leaf}$	0.0	0.0	0.0	0.0
	$\delta^{18}O_{cell}$ with Peclet	22.7	10.2	-2.0	-2.0
wSx1000	$\delta^{13}C_{cell}$	1.1	0.5	-0.3	-0.6
	BAI	86.9	34.5	-18.3	-32.6
	LAI	-13.3	-5.5	4.0	7.1
	$\boldsymbol{g_c}$	-12.7	-5.2	3.6	6.4
	$\boldsymbol{E}$	-12.6	-5.1	3.6	6.5
	$\delta^{18}O_{leaf}$	0.0	0.0	0.0	0.0
	$\delta^{18}O_{cell}$ with Peclet	1.4	0.5	-0.4	-0.6
p_{rx}	**$\delta^{13}C_{cell}$**	-10.6	-7.0	10.7	-32.4
	BAI	458.8	91.5	-100.0	-100.0
	LAI	169.5	96.8	-100.0	-100.0
	$\boldsymbol{g_c}$	78.8	54.3	-99.9	-99.9
	$\boldsymbol{E}$	71.6	56.3	-100.0	-100.0
	$\delta^{18}O_{leaf}$	0.0	0.0	0.0	0.0
	$\delta^{18}O_{cell}$ with Peclet	-1.2	-1.7	26.3	26.3
Maximum ASW	$\delta^{13}C_{cell}$	0.9	0.3	-0.1	0.0
	BAI	-31.2	-11.7	9.3	14.8
	LAI	-9.2	-2.9	0.6	-0.1
	$\boldsymbol{g_c}$	-13.5	-4.5	1.3	0.7
	$\boldsymbol{E}$	-12.3	-3.9	1.0	0.4
	$\delta^{18}O_{leaf}$	0.0	0.0	0.0	0.0
	$\delta^{18}O_{cell}$ with Peclet	1.9	0.6	-0.2	-0.1

6. CONCLUSION

Climate change will have substantial impacts on vegetation worldwide (Allen *et al.*, 2010; Intergovernmental Panel on Climate Change, 2014). However, predicting how vegetation will respond to future shifts in climate regimes is challenging for many reasons. Firstly, there is great uncertainty related to the amount and extent of climate change so research approaches have to encompass a wide range of temperatures, precipitation regimes, and combinations of stressors. Further, the extent of climate change will not be uniform around the globe. Biomes will be differentially impacted so understanding adaptations of different plant functional types improves our ability to predict how future changes in climate will impact diverse vegetation types. Finally, responses to climate will not only vary by plant functional type, but also species, populations within species, and growth stages. Therefore, it is vital that we focus our research efforts on a broad range of functional types, species, and growth stages with both modeling and physiological approaches.

By utilizing multiple approaches on broadleaf and coniferous species from the seedling through old-growth developmental stages, this dissertation highlights the advantages and limitations of observational, experimental, greenhouse, field, and modeling methodologies. This dissertation provides strong support for the use of multiple, diverse approaches to effectively and comprehensively address how vegetation will respond to changes in climate.

In Chapter 2, I evaluated the heat tolerance of detached leaf discs from *Coffea arabica* saplings using chlorophyll fluorescence and electrolyte leakage methods. An

advantage of measuring heat tolerance with these methods is that they are well-established and widely used (Flint *et al.*, 1967; Bilger *et al.*, 1984; Larcher, 1995; Maxwell & Johnson, 2000; Baker & Rosenqvist, 2004), allowing comparisons with other species and functional types. However, Chapter 2 showed that standardizing the methodology is crucial for accurately evaluating heat tolerance, as the greater recovery time of 24 h yielded more accurate heat tolerance assessments than the 15 min recovery time. I also showed that photochemistry as measured with chlorophyll fluorescence is more sensitive to heat stress than cell membranes as measured with electrolyte leakage, emphasizing the importance of considering the plant function being assessed for heat tolerance (Teskey *et al.*, 2015). *C. arabica* heat tolerance also increased with leaf age, an evolutionary adaptation that protects older leaves of evergreen species from irreversible damage (Yamada *et al.*, 1996; Zhang *et al.*, 2012). Thus, the time between temperature exposure and measurement, tissue type, and leaf age should be considered to accurately quantify heat tolerance, a crucial component for understanding vegetation responses to high temperature stress. This chapter also highlighted that heat tolerance is only one metric and that surviving heat stress requires whole-plant strategies that cannot be characterized using detached leaf discs. For instance, evaporative cooling through stomatal conductance mitigates heat stress but is not considered on detached leaf discs.

To address this limitation, in Chapter 3 I exposed whole *C. arabica* plants to a simulated heat wave and monitored physiological responses *in situ*. This enabled me to monitor physiological recovery and capture whole-plant strategies for mitigating heat stress. I also demonstrated that the increase in heat tolerance with leaf age measured on

leaf discs in Chapter 2 generally held on whole plants as shown in Chapter 3. However, this study was conducted on potted saplings in a greenhouse. This enabled us to grow tropical *C. arabica* year round in the Pacific Northwest, without confounding effects of competing vegetation or variable soil conditions. However, greenhouse conditions such as temperature and relative humidity were regulated (~18°C, ~64%, respectively) and did not necessarily mimic field conditions. Photosynthetically active radiation in the greenhouse was also lower than that in field conditions, limiting the scope of inference of this study. We also were only able to impose experimental heat stress using a relatively small growth chamber as opposed to growing plants at elevated temperatures or using a more gradual rise in temperature regime. Thus, the jump in temperature (18°C to 49°C) may appear to be extreme but aseasonal fluctuations in temperature and the sudden onset of heat waves are expected to increase in frequency. Our approach enabled us to investigate the impacts of heat waves on leaf temperatures, which far exceed temperatures to which *C. arabica* was adapted. Because leaf temperatures can be ~20°C greater than air temperature, especially in outer canopy leaves in sun-grown *C. arabica* (DaMatta & Ramalho, 2006; Alvim & Kozlowski, 2013), a heat wave resulting in leaf temperatures of 49°C is realistic in field grown *C. arabica*, as shown by the leaf energy balance model. I also observed that even a 45 min heat wave can substantially influence physiology and inhibit flowering, and that the duration of a heat wave has substantial impacts on physiological recovery, non-structural carbohydrate dynamics, and gas exchange. In a real world context, elevated temperatures and heat waves are often accompanied by drought as in the coffee-growing regions of Mexico, Central America,

and Vietnam (The Climate Institute, 2016). To explore this further, I used the leaf energy balance model to more accurately predict leaf temperatures in response to drought-induced stomatal closure. The combination of observational gas exchange measurements and the leaf energy balance model enabled me to estimate the effects of drought during a heat wave on leaf temperatures and the extent to which drought may exacerbate heat stress. The potential for drought to accompany increased temperatures emphasizes the value of combining physiological and experimental approaches with modeling. However, it is important to acknowledge that other regions that grow *C. arabica* such as Colombia, Brazil, Tanzania, and Ethiopia are expected to become warmer and wetter (The Climate Institute, 2016). This variability in temperature and precipitation regimes emphasizes the importance of understanding the effects of both abiotic stressors on physiology. Regardless of the precipitation shifts, the "Bean Belt" where *C. arabica* is grown is experiencing elevated temperatures (Davis *et al.*, 2012; Bunn *et al.*, 2014), further highlighting the importance of investigating the impacts of high temperatures on *C. arabica* physiology.

Shifts in climate impact vegetation worldwide (Allen *et al.*, 2010) and not just tropical regions. Further, the *C. arabica* plants studied in Chapters 2 and 3 were ~1 m tall, but heat stress impacts smaller, younger plants such as germinant seedlings much differently. This is because seedlings are found close to the soil surface where they experience reduced wind and turbulent eddies compared to taller plants, making seedlings highly susceptible to temperatures that commonly reach between 40°C and 50°C or higher in exposed sites (Alexander, 1987; Kolb & Robberecht, 1996). Because seedling

establishment has huge impacts on species' distributions in response to climate regimes (Johnson *et al.*, 2011), examining the effects of heat stress on seedlings is essential for understanding species' responses in a warmer world. To address this, in Chapter 4 I investigated the physiological responses to heat stress of *Pinus ponderosa* (PIPO) and *Pseudotsuga menziesii* (PSME) seedling populations from contrasting climates. Unexpectedly, PSME was more heat tolerant than PIPO when measured on detached needles, again highlighting the limitation of heat tolerance assessments on detached leaves. This also emphasized the importance of considering whole plant strategies such as rooting depth, capacity for evaporative cooling, and seasonal shifts in heat tolerance when evaluating mechanisms to cope with heat stress among species. Although this study was also conducted on potted seedlings in the greenhouse with the same limitations as those in Chapter 3, growing populations from climates with contrasting temperature and precipitation regimes in the same controlled environment was advantageous because it allowed us to examine the extent to which phenotypic plasticity and ecotypic variation influenced mechanisms underlying population-specific resistances to high temperature and drought, respectively (Daas *et al.*, 2008; Gimeno *et al.*, 2009; Du *et al.*, 2014; Matías *et al.*, 2016). Interestingly, heat stress responses exhibited phenotypic plasticity and reflected the conditions under which the plants were grown (Knight & Ackerly, 2002), whereas intrinsic water use efficiency, a measure of potential drought resistance, reflected ecotypic differentiation and the climates from which the seedlings originated (Kerr *et al.*, 2015). This suggests that these populations may more readily adapt to elevated temperatures, but less drought-adapted populations may not mitigate drought

stress as effectively as more drought-adapted populations. This sheds light on plant responses to environmental stress and how species with large geographic ranges such as PSME and PIPO may persist under future shifts in climate.

Although drought is expected to accompany high temperature stress in some regions, heat is less studied than drought (Sevanto & Dickman, 2015), underscoring the importance for studies such as Chapters 2, 3, and 4 that focus on physiological responses to heat stress. Isolating the effects of heat waves on physiological responses will help us better understand the dynamic interactions between heat and other abiotic stressors such as drought, pests, disease, and increasing atmospheric [CO_2], elements expected to shift with climate change. For example, heat damage may reduce pathogen resistance in *C. arabica* (Chen *et al.*, 2003). I also saw in Chapter 3 that heat stress will be exacerbated by drought, expected to occur in certain tropical regions where *C. arabica* is grown (The Climate Institute) and temperate regions where PSME and PIPO grow (Allen *et al.*, 2010). We are still trying to understand the impacts of increasing ambient [CO_2] and high temperature stress on vegetation (Curtis & Wang, 1998) as elevated [CO_2] may induce stomatal closure and thus increase leaf temperatures and exacerbate heat stress (Surano *et al.*, 1986). However, elevated [CO_2] may mitigate the impacts of heat stress in *C. arabica* (Rodrigues *et al.*, 2016). In contrast, high temperature stress may negate the increased growth caused by elevated atmospheric [CO_2] in other species (Lewis *et al.*, 2015). Elevated [CO_2] also may differentially impact growth and intrinsic water use efficiency in PIPO and PSME (Soulé and Knapp 2015). Therefore, by intensively examining heat stress effects from the leaf to whole plant scale, we improve our understanding of the

interacting effects of high temperature stress with other abiotic stressors on physiology and growth.

To achieve a more comprehensive understanding of vegetation responses to environmental stress, in Chapter 5 I employed the 3-PG process-based model on old-growth PIPO in central Oregon to provide growth and physiological information at larger temporal and spatial scales, as well as at a different developmental stage. This chapter highlighted the advantages of predictive physiological process-based vegetation models such as 3-PG that extend physiological processes beyond the whole-tree level to larger spatial and temporal scales without destructive sampling to predict vegetative growth and productivity (Kerns & Peterson, 2014). Chapters 3 and 4 were useful for examining current *in situ* responses to environmental stress on seedlings and saplings while Chapter 5 highlighted the use of tree-ring growth and stable isotopes for reconstructing past physiological responses of old-growth trees to environmental stress. This study was a unique application of 3-PG because 3-PG was applied to over a century rather than only a few years (Law *et al.*, 2000) to understand physiological drivers behind observed growth patterns. Although tree-ring growth and stable isotope analyses provide information on longer time scales than *in situ* physiological measurements, these studies are still relatively limited to individual trees. Thus, the combination of tree-rings, stable isotopes, and a generalizable forest stand model such as 3-PG enabled me to estimate stand-level responses of upland and riparian trees with contrasting soil water availability. 3-PG is also advantageous because it allowed me to estimate stand-scale physiological responses without the challenges that accompany sampling old-growth trees. For example, I

investigated the effect of heat stress on leaf non-structural carbohydrates in Chapters 3 and 4, which is valuable for quantifying how carbon allocation is influenced by heat stress. However, destructive sampling of old-growth canopies and roots is challenging because they are often inaccessible. Therefore, well-established allometric equations used in 3-PG are valuable for estimating carbon dynamics and allocation at the stand level without intensive destructive sampling. Both empirical and modeling approaches have advantages and disadvantages so understanding and utilizing both is crucial.

Process-based models like 3-PG are widely used and applied to diverse species because they utilize simple equations to describe physiological processes and incorporate species-specific characteristics under changing environmental conditions. This is an improvement over other types of models that use plant functional type to make predictions (Lauenroth *et al.*, 1993; Bodegom *et al.*, 2014), which does not accurately describe how vegetation characteristics vary across different sites. This transferability and flexibility of 3-PG combined with the abundance of observed stand characteristics and physiological measurements on this species at the Metolius site in Oregon allowed me to parameterize the model with reasonable accuracy and use it to investigate the physiological mechanisms underlying the differences in observed tree-ring growth, carbon stable isotope ($\delta^{13}C$), and oxygen stable isotope ($\delta^{18}O$) trajectories between the upland and riparian sets of trees. This was also the first time a $\delta^{18}O$ sub-model was utilized in conjunction with a $\delta^{13}C$ sub-model in 3-PG, providing a novel way to constrain the model and estimate leaf-level physiological characteristics using stand characteristics.

Although 3-PG is useful for long-term stand-scale forest data sets, 3-PG has its own set of limitations. 3-PG is optimized for even-aged, single-species stands when many forests are mixed-age and -species, although attempts have been made to accommodate this (Forrester & Tang, 2016). 3-PG also uses simplistic equations which makes it easy to manipulate but can be overly simplistic for accurately predicting reality. This was observed when stand density was underestimated to accurately estimate basal area increment (BAI) in upland trees, for example. Tree-ring stable isotopes are useful for reconstructing tree physiological responses to climate but the analyses are costly and time-consuming. These challenges further emphasize the importance of utilizing multiple approaches to examine the effects of environmental stress on physiological responses.

This dissertation employed creative approaches to monitor a suite of physiological parameters to understand the comprehensive effects of environmental stress on *C. arabica* saplings and PSME and PIPO seedlings, and old-growth PIPO. Although it is clear that environmental stress such as increased temperature and drought are expected to increase in duration and frequency throughout the 21st century, it is unclear how vegetation will respond, complicating predictions of and impacts on plant species distributions (Allen *et al.*, 2010; Intergovernmental Panel on Climate Change, 2014). In this dissertation, the combination of physiological and modeling methods applied to multiple species and growth stages informs our knowledge of plant physiological responses to environmental stress. These types of experimental and observational studies combined with process-based modeling inform predictions of species distributions by providing insight into species-, population-, and growth stage-specific physiological

responses to heat and drought stress. Combining scales and methods to create innovative and multifaceted approaches is necessary to adequately address the challenge of understanding the effects of future climate change on vegetation.

6.1 References

Alexander RR (1987) *Ecology, Silviculture, and Management of the Engelmann Spruce--Subalpine Fir Type in the Central and Southern Rocky Mountains*. U.S. Dept. of Agriculture, Forest Service, 144 pp.

Allen CD, Macalady AK, Chenchouni H *et al.* (2010) A global overview of drought and heat-induced tree mortality reveals emerging climate change risks for forests. *Forest ecology and management*, **259**, 660–684.

Alvim P de T, Kozlowski TT (2013) *Ecophysiology of Tropical Crops*. Elsevier, 517 pp.

Baker NR, Rosenqvist E (2004) Applications of chlorophyll fluorescence can improve crop production strategies: an examination of future possibilities. *Journal of Experimental Botany*, **55**, 1607–1621.

Bilger H-W, Schreiber U, Lange OL (1984) Determination of leaf heat resistance: comparative investigation of chlorophyll fluorescence changes and tissue necrosis methods. *Oecologia*, **63**, 256–262.

Bodegom PM van, Douma JC, Verheijen LM (2014) A fully traits-based approach to modeling global vegetation distribution. *Proceedings of the National Academy of Sciences*, **111**, 13733–13738.

Bunn C, Läderach P, Rivera OO, Kirschke D (2014) A bitter cup: climate change profile of global production of Arabica and Robusta coffee. *Climatic Change*, **129**, 89–101.

Chen Z, Ribeiro A, Silva M *et al.* (2003) Heat shock-induced susceptibility of green coffee leaves and berries to Colletotrichum gloeosporioides and its association to PR and hsp70 gene expression. *Physiological and Molecular Plant Pathology*, **63**, 181–190.

The Climate Institute (2016) A Brewing Storm: the climate change risks to coffee.

Curtis PS, Wang X (1998) A meta-analysis of elevated CO2 effects on woody plant mass, form, and physiology. *Oecologia*, **113**, 299–313.

Daas C, Montpied P, Hanchi B, Dreyer E (2008) Responses of photosynthesis to high temperatures in oak saplings assessed by chlorophyll-a fluorescence: inter-specific diversity and temperature-induced plasticity. *Annals of Forest Science*, **65**, 1.

DaMatta FM, Ramalho JDC (2006) Impacts of drought and temperature stress on coffee physiology and production: a review. *Brazilian Journal of Plant Physiology*, **18**, 55–81.

Davis AP, Gole TW, Baena S, Moat J (2012) The impact of climate change on indigenous arabica coffee (Coffea arabica): predicting future trends and identifying priorities. *PLoS One*, **7**, e47981.

Du B, Jansen K, Junker LV *et al.* (2014) Elevated temperature differently affects foliar nitrogen partitioning in seedlings of diverse Douglas fir provenances. *Tree Physiology*, **34**, 1090–1101.

Flint H, Boyce B, Beattie D (1967) Index of injury-a useful expression of freezing injury to plant tissues as determined by the electrolytic method. *Canadian Journal of Plant Science*, **47**, 229–230.

Forrester DI, Tang X (2016) Analysing the spatial and temporal dynamics of species interactions in mixed-species forests and the effects of stand density using the 3-PG model. *Ecological Modelling*, **319**, 233–254.

Gimeno TE, Pías B, Lemos-Filho JP, Valladares F (2009) Plasticity and stress tolerance override local adaptation in the responses of Mediterranean holm oak seedlings to drought and cold. *Tree Physiology*, **29**, 87–98.

Intergovernmental Panel on Climate Change (2014) IPCC Fifth Assessment Synthesis Report. *IPCC 5th Assessment Synthesis Report*.

Johnson DM, McCulloh KA, Reinhardt K (2011) The Earliest Stages of Tree Growth: Development, Physiology and Impacts of Microclimate. In: *Size- and Age-Related Changes in Tree Structure and Function*, Vol. 4 (eds Meinzer FC, Lachenbruch B, Dawson TE), pp. 65–87. Springer Netherlands, Dordrecht.

Kerns B, Peterson DW (2014) An Overview of Vegetation Models for Climate Change Impacts. U.S. Department of Agriculture, Forest Service, Climate Change Resource Center.

Kerr KL, Meinzer FC, McCulloh KA, Woodruff DR, Marias DE (2015) Expression of functional traits during seedling establishment in two populations of Pinus ponderosa from contrasting climates. *Tree Physiology*, **35**, 535–548.

Knight CA, Ackerly DD (2002) An ecological and evolutionary analysis of photosynthetic thermotolerance using the temperature-dependent increase in fluorescence. *Oecologia*, **130**, 505–514.

Kolb PF, Robberecht R (1996) High temperature and drought stress effects on survival of Pinus ponderosa seedlings. *Tree Physiology*, **16**, 665–672.

Larcher W (1995) Photosynthesis as a Tool for Indicating Temperature Stress Events. In: *Ecophysiology of Photosynthesis* (eds Schulze PDE-D, Caldwell PDMM), pp. 261–277. Springer Berlin Heidelberg.

Lauenroth W, Urban D, Coffin D, Parton W, Shugart H, Kirchner T, Smith T (1993) Modeling vegetation structure-ecosystem process interactions across sites and ecosystems. *Ecological Modelling*, **67**, 49–80.

Law BE, Waring . R. H., Anthoni PM, Aber JD (2000) Measurements of gross and net ecosystem productivity and water vapour exchange of a Pinus ponderosa ecosystem, and an evaluation of two generalized models. *Global Change Biology*, **6**, 155–168.

Lewis JD, Phillips NG, Logan BA *et al.* (2015) Rising temperature may negate the stimulatory effect of rising CO2 on growth and physiology of Wollemi pine (Wollemia nobilis). *Functional Plant Biology*, **42**, 836.

Matías L, Gonzalez-Díaz P, Quero JL, Camarero JJ, Lloret F, Jump AS (2016) Role of geographical provenance in the response of silver fir seedlings to experimental warming and drought. *Tree Physiology*, tpw049.

Maxwell K, Johnson GN (2000) Chlorophyll fluorescence—a practical guide. *Journal of experimental botany*, **51**, 659–668.

Rodrigues WP, Martins MQ, Fortunato AS *et al.* (2016) Long-term elevated air [CO2] strengthens photosynthetic functioning and mitigates the impact of supra-optimal temperatures in tropical Coffea arabica and C. canephora species. *Global change biology*, **22**, 415–431.

Sevanto S, Dickman LT (2015) Where does the carbon go?—Plant carbon allocation under climate change. *Tree physiology*, **35**, 581–584.

Surano K, Daley P, Houpis J, Shinn J, Helms J, Palassou R, Costella M (1986) Growth and physiological responses of Pinus ponderosa Dougl ex P. Laws. to long-term elevated CO2 concentrations. *Tree Physiology*, **2**, 243–259.

Teskey R, Wertin T, Bauweraerts I, Ameye M, McGuire MA, Steppe K (2015) Responses of tree species to heat waves and extreme heat events. *Plant, cell & environment*, **38**, 1699–1712.

Yamada M, Hidaka T, Fukamachi H (1996) Heat tolerance in leaves of tropical fruit crops as measured by chlorophyll fluorescence. *Scientia Horticulturae*, **67**, 39–48.

Zhang J-L, Poorter L, Hao G-Y, Cao K-F (2012) Photosynthetic thermotolerance of woody savanna species in China is correlated with leaf life span. *Annals of Botany*, **110**, 1027–1033.